UNIVERSITÀ DEGLI STUDI DI TRIESTE

XXVII CICLO DEL DOTTORATO DI RICERCA IN

NANOTECNOLOGIE

DNA ORIGAMI ACTUATION AS A POWERFUL DYNAMIC AND TUNABLE ARCHITECTURE FOR PLASMONIC STRUCTURE

Settore scientifico-disciplinare:

FIS/07

DOTTORANDO
LUCA PIANTANIDA

COORDINATORE
PROF. LUCIA PASQUATO

SUPERVISORE DI TESI
DR. MARCO LAZZARINO

ANNO ACCADEMICO 2013 / 2014

Contents

Abstract

In this thesis I present my research work of PhD in Nanotechnology. This study is focused on DNA nanotechnology as a tool for nano-bio-objects construction and gold particles functionalization. Gold nanoparticles (AuNPs) have been largely investigated and their peculiar properties have been exploited for important applications, such as Raman spectroscopy, biological sensing or medical therapy. AuNPs are characterized by well defined plasmon optical resonance and scattering properties and well established protocols exists for their chemical functionalization. Among the latter, DNA self assembly was demonstrated to be an excellent way to assemble nanoparticle structures with controlled shape and dimensions. This approach was applied for optical properties engineering, plasmonic hot spot in AuNP aggregates, and molecular ruler in AuNP dimers in which the inter-particle gap was controlled with nm precision. In this study I compare two effective strategies toward the efficient formation of gold nanoparticles dimer using DNA hybridization. Using one of them I reached a dimer yield as high as 26% of the overall initial amount of AuNP, the highest reported in literature, also with DNA sequences as short as 11 nucleotides (nts).

In the second part of my thesis, I combined the LSPR properties of gold particles with DNA origami structure in order to create hybrid systems. Using this combination I introduced an original approach for plasmon resonance tuning which, in perspective, are the starting point for the development of innovative biosensors. In particular, continuous and reversible LSPR tuning using a DNA origami actuation to modulate the nanometric separation of two gold nanoparticles has been demonstrated. The actuation mechanism is based on DNA hybridization, in particular three different DNA sequences were shown to induce resonance shift up to 6 nm. The proposed design is suitable to investigate DNA hybridization configurations, or could be used as tunable plasmonic platform for enhanced Raman applications.

Abstract

(italian)

In questa tesi presento il mio lavoro di ricerca di Dottorato in Nanotecnologie. Questo studio è concentrato sull'uso di nanotecnologia a DNA come strumento per la creazione di strutture nano-biologiche e funzionalizzazione di particelle d'oro. Le nano-particelle d'oro sono state largamente studiate e le loro proprietà sono state sfruttate per importanti applicazioni come la spettroscopia Raman, la rilevazione biologica e la terapia medica. Queste nano-particelle sono caratterizzate da una risonanza ottica plasmonica e proprietà di dispersione della luce ben definite ed esistono numerosi protocolli di provata efficienza per la loro funzionalizzazione chimica. Tra questi, il protocollo di auto-assemblaggio di DNA si è dimostrato eccellente nel comporre strutture di nano-particelle con dimensioni e forma controllate. Questo approccio è stato impiegato per l'ingegnerizzazione di proprietà ottiche, per la creazione di "*hot spot"* nel campo plasmonico in aggregati di nano-particelle e anche per la formazione di righelli plasmonici con dimeri di nano-particelle nei quali la loro spaziatura è controllata con precisione nanometrica. In questo studio confronto due strategie per la formazione di dimeri di nano-particelle d'oro usando l'ibridizzazione del DNA. Una di queste strategie mi ha permesso di raggiungere una al resa del 26% di formazioni di dimeri rispetto al totale delle AuNP, senza ulteriori procedure di filtrazione, dato che rappresenta il valore più alto riportato in letteratura; inoltre questo dato è stato replicato utilizzando sequenze di DNA molto corte, fino ad 11 nucleotidi, condizione che normalmente riduce l'efficienza del processo.

Nella seconda parte della mia tesi, ho combinato le proprietà plasmoniche delle nano-particelle d'oro con strutture a DNA origami in modo da creare sistemi ibridi tra di loro. Questa combinazione mi ha permesso di esplorare architetture innovative per la il controllo della plasmonica con la prospettiva di essere un punto di partenza per lo sviluppo di biosensori. Ho sviluppato una strategia per un controllo innovativo, reversibile e continuo della risonanza plasmonica usando un'attuazione basata su DNA origami. Il meccanismo di attuazione è basato sull'ibridizzazione del DNA, in particolare si è visto uno spostamento del picco di risonanza fino a 6 nm utilizzando tre sequenza di DNA diverse. Il sistema proposto è potrà essere utilizzato per lo studio dei meccanismi di ibridazione di DNA in condizioni di stress controllato, oppure potrà essere usato come piattaforma per un controllo continuo della posizione della risonanza plasmonica o in spettroscopia Raman.

Chapter 1

The DNA functional structure

1.1 DNA structural subunits

The structure of the DNA was known to be a long polymer composed by a set of four subunits. In the 1950s from the X-ray diffraction analysis, Franklin-Watson-Crick proposed a double filament DNA structure linked together by simple hydrogen bonds. The subunits involved in the two filaments or strands are composed by three specific units: a sugar, a phosphate group and a base. A pentose sugar in the form of β-D-2-deoxyribose is joined to a tri-phosphate group (mono- in case of DNA backbone) and is joined to the base by a N-glycosilic bond. While the sugar and phosphate are the same throughout the whole molecule, the bases are the only components that can change. The bases are nitrogen-containing ring compounds that are divided in purine and pyrimidine. The purine are composed by one hexagon linked to a pentagon ring and are: guanine (G) and adenine (A). The pyrimidine are composed by only one hexagon and are uracil (U), cytosine (C) and thymine (T) (Figure 1.1).

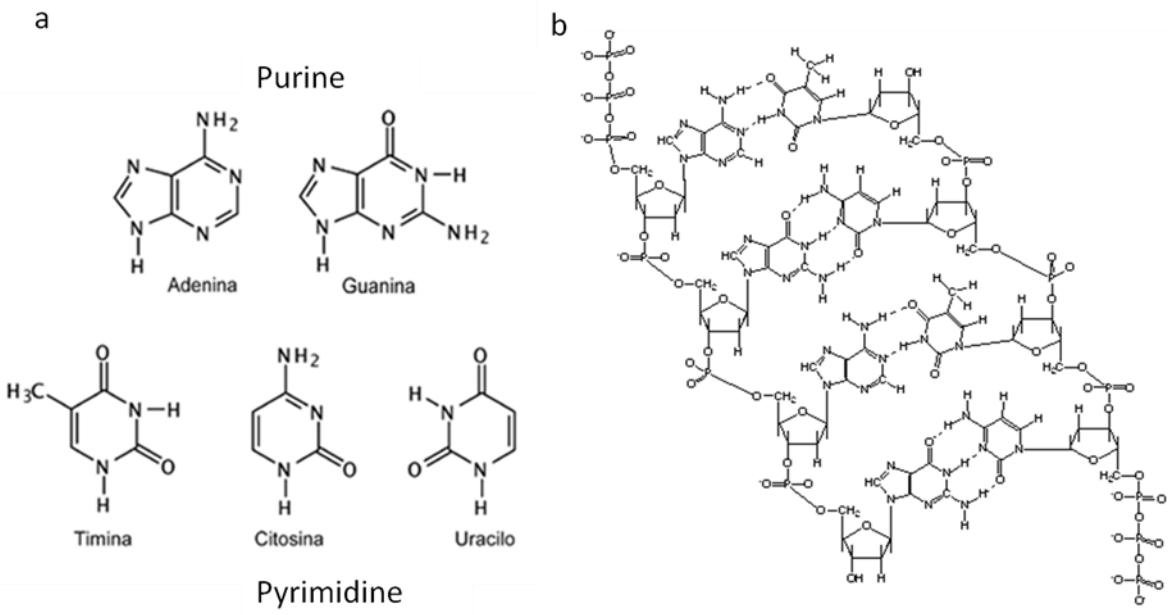

Figure 1.1 (a) Chemical structure of the DNA/RNA bases and (b) of the DNA base-pairing between the A-T and C-G nucleotides.

The association between sugar and base is called nucleoside and become nucleotide in presence of the phosphate group. The uridine nucleoside replace the thymidine in the RNA structure thus, the DNA and RNA subunits are always four. The different combinations

between the DNA nucleotides follow the A-T and G-C connection rule, basic for carrying the genetic information. These base-base interactions generate three hydrogen bonds between G-C and two between A-T that confer an equal distance between the two sugars in both configurations. The double filaments DNA structure is directional because the phosphodiester bonds involve different carbon positions on the sugar ring. In particular, the phosphodiester bond links the 5' carbon to the 3' carbon of the next sugar ring defining a direction in both the filaments (Figure 1.2). Thus, after their complementary hybridization, the two paired strands point in opposing directions.

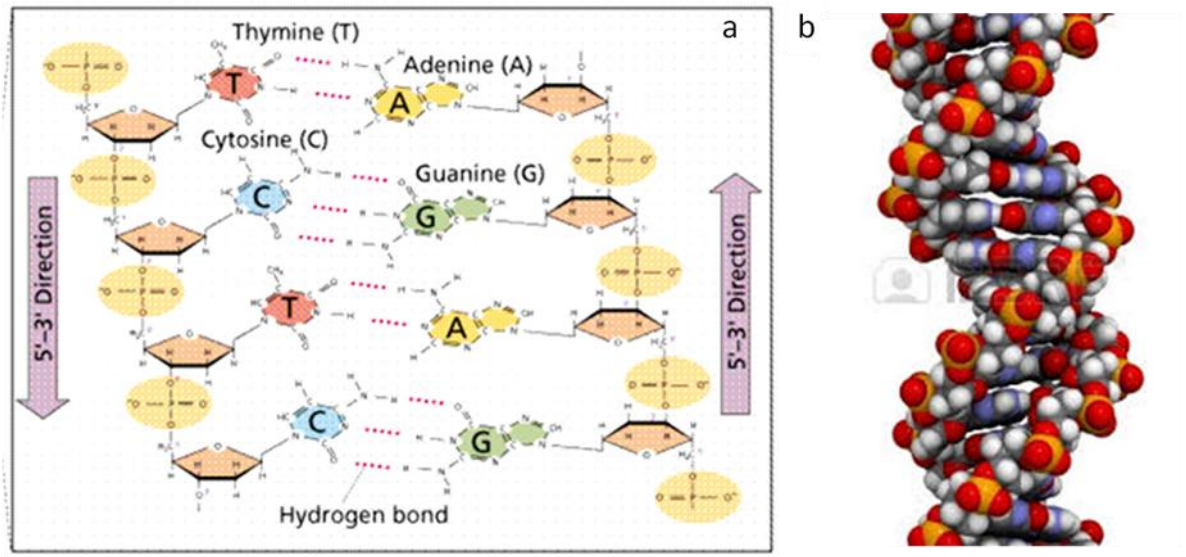

Figure 1.2 (a) Representation of the antiparallel configuration caused by two strands hybridization. (b) DNA B form atomistic model where are visible the major and minor groove.

The complementary base-pairing enables the base pairs to be packed in the energetically most favorable arrangement. To maximize the base pair packing, the two sugar-phosphate backbones wind around each other to form a double helix. Since the filaments have antiparallel directions, the winding around each other in the helical configuration generates two grooves one wider than the other: the major and the minor groove (Figure 1.2). This is the DNA form most present in nature, is called "B form", and is well characterized by a few geometrical parameters. The helical diameter is around 2-2.2 nm and the helix make a complete turn every 10.4-10.5 base pair or 3.5 nm giving a length of 0.34 nm per nucleotide (nt). In nature, the DNA is present also with other less common, forms: the A form that presents larger helical pitch and it is observed in not physiological conditions (dehydration) and the form Z that presents a small helical pitch and diameter; it is typical of the chemical modified sequence (methylation)[1].

1.2 Functional DNA chemical structure

The DNA double stranded configuration not only minimize the energy in case of base pairing possibility but possesses also other specific functionalities. The transfer of the genetic information expressed by the central dogma of biology is assured by the replication of one and/or more DNA sequences. The DNA duplication is permitted by the enzymatic separation of the two filaments where one of them acts like template strand for the newly synthesized one. The enzymes can break the hydrogen bonds of the bases while the covalent linkage between the sugars assures the filament structural stability. The double stranded configuration gives the possibility to use one of them as mold for the elongation of the other one that is perfectly exploited in the replication process otherwise not permitted with only one filament. Moreover, the nucleotides can be seen as bricks in the DNA strand and this modular structure confers high plasticity also in the longitudinal axis. This properties is exploited in the process of ligation and elongation of the DNA filament. The creation of phosphodiester bonds between single nucleotide sugars is driven by enzymatic action that are like builders of a rail line that have to repair injuries or increase the line length. Another great example of the DNA chemical structure functionalities is the backbone framework along which, a phosphate group is exposed every nucleotide. In pH physiological conditions the phosphates present a localized negative charge on the free oxygen that makes the single DNA filament a negative charged polyelectrolyte. After the hybridization of the two filaments, every base pair, the backbone negative charge is double and a great ionic force is needed to keep hybridized the two strands. This negative charge is fundamental in the DNA packing inside the eukaryotic cell. Although the DNA length is extremely high, in the cell it is organized and packed in order to occupy the less space possible. This is facilitated by multimer assembled protein called hystones that exploit the negative charged backbone and major-minor groove alternation to bend and roll the double stranded filaments on their own creating a sort of highly packed buttons chain that compose the chromatin.

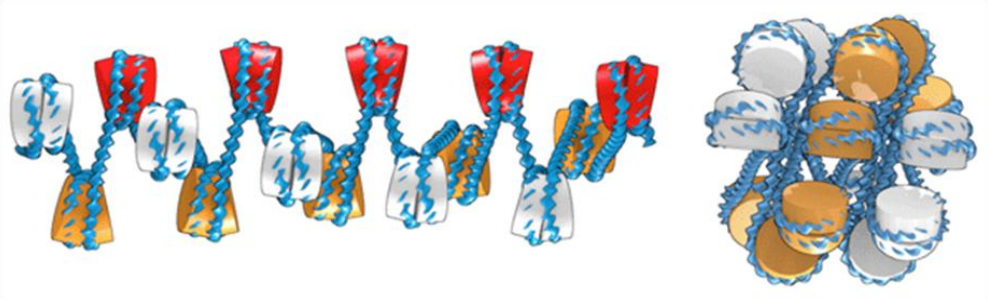

Figure 1.3 Drawing of the DNA packing around the hystones proteins: the chromatin.

Chapter 2

DNA Nanotechnology

2.1 Linear DNA junctions as structural building blocks

The DNA is one of the most powerful molecule as a building block for molecular engineering: mechanical properties, recognition affinity, programmability are key ingredients at the base of nanotechnology. The extraordinary bending and rearranging properties of the nucleotides chemical bond structure enable the formation of different known forms of the DNA molecule such as A, B and Z with which is possible the formation of single, double and even triple, quadruple strand. This structural versatility discloses the great role of DNA as architecture molecule.

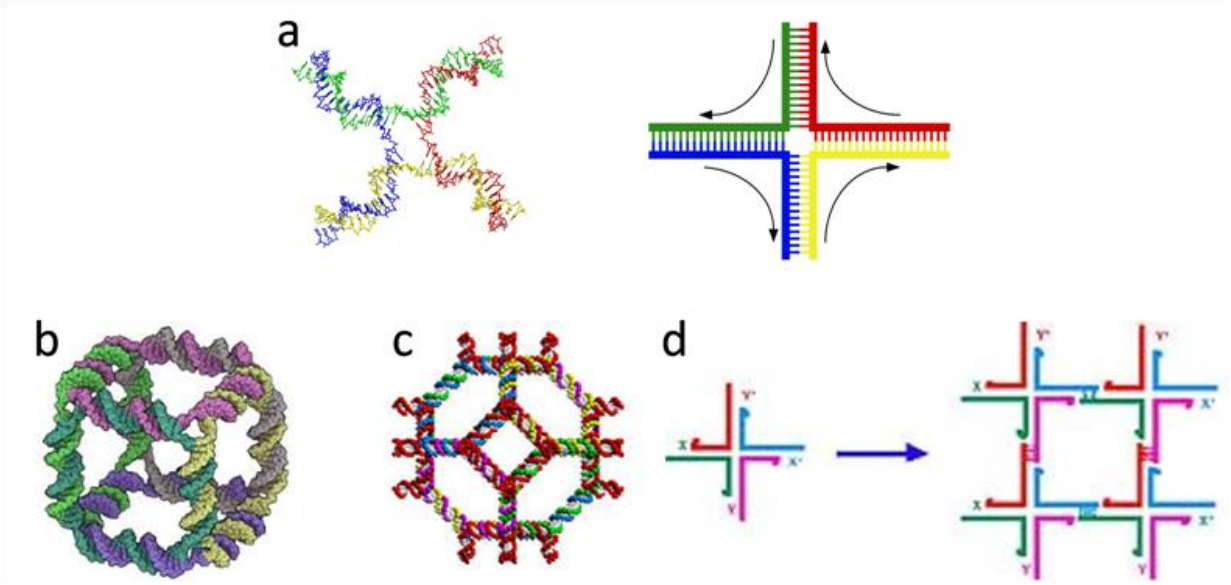

Figure 2.1 (a) Structure and scheme of the Holliday junction. Schematic representations of the (b) DNA cube, (c) truncated octahedron and (d) 2D lattice based on the Holliday junction as building block.

The DNA molecular plasticity as strands connection was first seen by Robin Holliday in 1965 in the homologous recombination. The particular the exchange of genetic information is provided by a four DNA strands junction (Holliday junction) that can be reassumed in a X form where all the duplex pairing are in the classical B form. The junction itself is formed by a few changes in the backbone conformation, the two arms are right-hand twisted with an angle between them of ~40°; this particular conformation allows a sliding between the two double helix that promotes the genetic exchange[2, 3] (Figure 2.1a).

The extraordinary interconnection property of DNA was analyzed by replicating the naturally junctions in laboratory producing different fixed conformations. Luo and coworkers for the first time demonstrated dendrimer-like structures assembly via sticky end cohesion from DNA units Y-shaped, that can be arranged also in X shape making a good candidate as DNA building block[4]. An undeniable effort on this has been provided by Nadrian C. Seeman that basically exploited the synthetic formation of Holliday junctions as building block for the creation of larger structures. Seeman's group reported the construction of a closed DNA cube, a truncated octahedron and a 2D lattice inserting a sticky end cohesion in each of the four branches of Holliday junctions[5-8] (Figure 2.1b-c-d).

Following the idea of non-sliding DNA junctions as structural repetitive unit, many DNA building blocks have been designed and analyzed experimentally. Seeman's group presented the construction of a double-crossover (DX) consisting in two Holliday junctions connected by two double helical arms. Their orientation could be parallel or antiparallel depending on the orientation of the helical axis and they analyzed the stability by different number (even or odd) of double-helical half turns between two crossovers[9] (Figure 2.2a). Moreover Seeman and coworkers reported the creation of triple crossovers (TX) consisting in three double helices connected by four immobile crossovers and assembled them into 2D lattices providing larger space for gaps in which were inserted hairpin strand points visible with atomic force microscopy (AFM)[10] (Figure 2.2b).

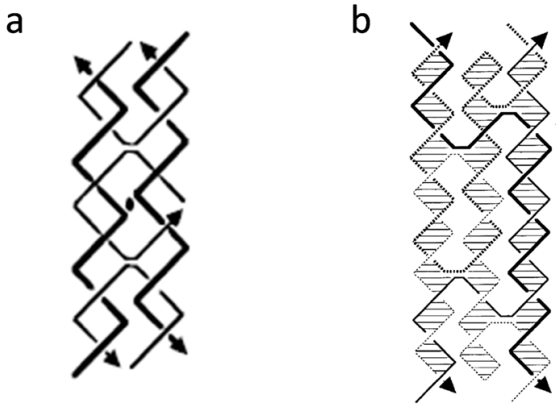

Figure 2.2 Schematization of (a) double crossover DX and (b) triple crossover TX.

A forward step in the DNA architecture was provided by the assembly of these double and triple crossover structures in larger planar lattices in which the connections complexity could even increase. Multiple helices DNA tiles have been also formed promoting the periodicity of planar shapes and grids where is possible to insert DNA-linked molecule. This leads to the

creation of a planar substrate to address computed patterns[11-13] (Figure 2.3). All these structures have a defined size and can be used to build up even more complex system just exploiting the DNA self assembly process.

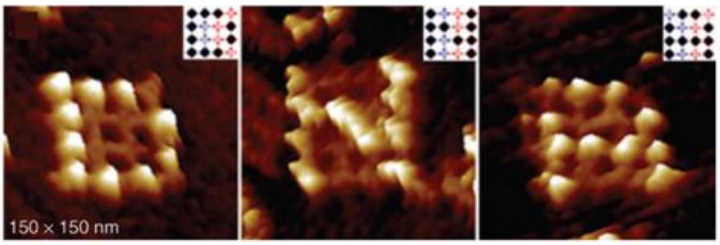

Figure 2.3 DNA tiles arrays decorated with proteins in the shape of the letters "D", "N", "A".

2.2 Scaffolded assembly: DNA origami technology

The design and combination of different DNA strands into complex structures basically exploit a self assembly process driven by temperature. The cooling ramp from ~90° to 4° allows the correct folding of above mentioned crossovers structures. An innovative forward step on the DNA nanotechnology has been provided by the "scaffolded assembly" where a long DNA strand is used as a molecular scaffold.

The pioneering work made by Paul Rothemund in 2006 have gave the light to the DNA origami technology. He exploited the scaffolded assembly in a new method which enabled addressing simple and complex shapes made only by DNA. He used a 7.2 Kb single circular strand bacteriophage genome (M13 phage) as scaffold and some hundreds of DNA oligonucleotides. The process is driven by the univocal hybridization between the short strands and the scaffold in order that DNA origami can be regarded as a large composite of DX motifs. The short DNA strands, acting like "staples", are able to bend and model the scaffold in a pre-designed structure[14].

The first step in developing a DNA origami is to decide on the folding path to generate the desired shape. The scaffold strand is allocated to run back and forth as if the whole area of our shape should be painted without detaching the brush from the paper. The desired shape is possible thanks to the formation of a "seam" that allows the circularity of the scaffold strand path that, in most of the cases, produces an eyelet connecting the two parts of the seam. The seam is placed, usually, in the center of the structure to keep high stability but could be shifted in accord to the shape complexity (Figure 2.4).

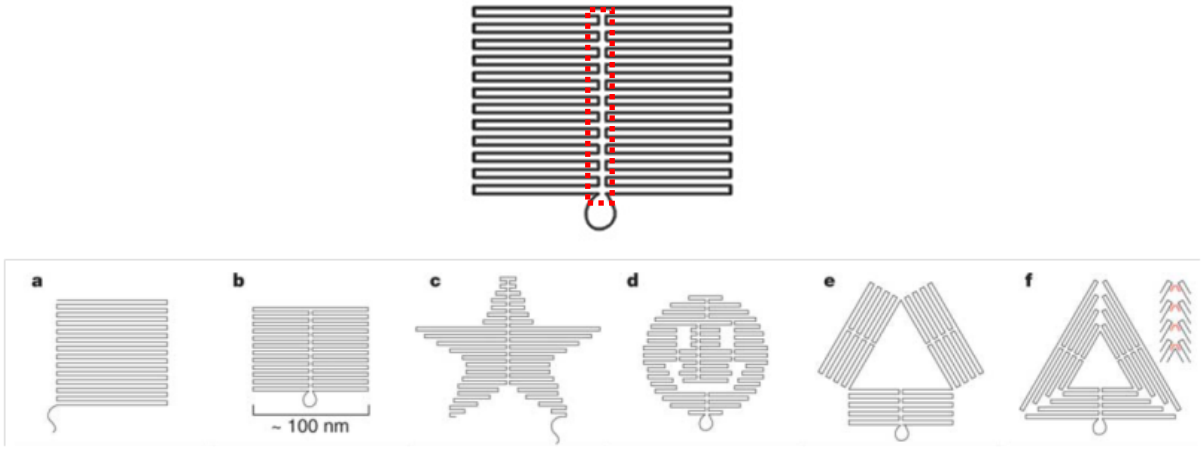

Figure 2.4 Drawings of different Rothemund's DNA origami shapes. The seam is highlighted in dotted red. The seam (a) is absent in the square, (b,c) is centered in the rectangular and star, (d,e,f) is shifted in the more complex shapes. The circularity is maintained by an eyelet of scaffold strand only in (b,d,e,f).

The structure of the scaffold, the position of the crossovers and the geometry of the staples hybridization should be designed considering the following parameters. The diameter of standard DNA B form is 2.2-2.6 nm and there is one helical turn every 10.5 nucleotides (nts) or 3.4 nm (0.33 nm/nt). The structural design of a DNA origami as introduced by Rothemund, is based on slightly stretched parameters. In particular the helical turn is approximated to 10.67 nts (3.5 nm) and so it is possible to insert one helical crossover at minimum length of 16 bp (5.2-5.3 nm) or 1.5 turns. The result is a crossover that starts from one helix, switch to the following helix and ends in the next adjacent (or third) helix. Having possible crossovers positions every an odd number of half turns all the newly formed double helices lay in a single plane. Conversely, if we look at the crossovers that start from one helix, switch to the following and return on the previous visited helix we have possible positions at even number of half turns between, still maintaining the full structure in a single plane (Figure 2.5a). These geometrical constraints are necessary because only at those locations where the scaffold is placed at a tangent point between two adjacent helices, the crossover is possible. Moreover the crossovers direction is determined by the angular twisting of the filament progression that after 1.5 turns is tangent with the above helix and after 3 turns come back tangent to initial helix.

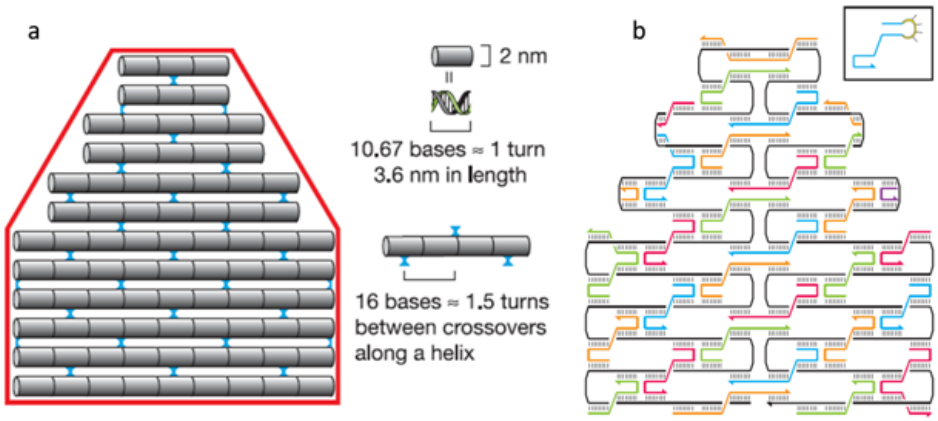

Figure 2.5 Schematization of a simple DNA origami structure where (a) are represented the approximated helical parameters and the spacing between crossovers (blue ticks). In (b) are highlighted the staples strands (colored) that forms crossovers between the parallel helices and between anti-parallel helices to bridge the seam. Some staples could be engineered to carry a 4-T loop to prevent stacking interaction (b-inset).

Since parallel helices in DNA lattices present electrostatic repulsion between them are not rigid packed. Rothemund illustrated that the inter-helix spacing, that is 1-1.5 nm approx., is changing depending on the crossovers spacing (1.5 or 2.5 turns) determining the "y resolution". The approximated parameters used in programming a DNA origami were chosen empirically and consequentially to the electrostatic repulsion phenomenon between helices[14, 15].

Once placed the positions for the crossovers the staples can be designed along and crossing the helices of the structure. The length is a multiple number of 16 nts when the crossovers spacing is 1.5 turns resulting in a typical length of 32 nts. Shorter oligonucleotides are also possible but the univocally hybridization stability can be affected while for larger sequences is not a problem, but in this case an exaggerated length could affect its diffusion and interaction rate in the self assembly process. An optimal length ranges between 20 and 50 nts. Conversely, the length is a multiple of 26 nts when the crossover spacing is 2.5 turns and the typical length is 52 nts. In his pioneeristic work Rothemund chose the optimal crossovers spacing of 1.5 turns[14].

If a circular scaffold strand for the structure is chosen will be generated an inter-structural seam between two different areas of the shape as mentioned previously (Figure 2.4). The presence of a seam could generate a weaker line or section that introduces a certain degree of fragility to the whole DNA structure. For this reason Rothemund inserted extended crossovers along the seam line, in such a way that one staple strand, instead to switch to the adjacent helix, continues the progression on the parallel helix crossing the seam (Figure 2.5b). The

latter extended staples hold the areas separated by the seam providing an increased solidity. The pairing of the parallel helices is maintained by the multiple crossing back and forth of the so modified staple strands (Figure 2.5b). DNA origami shapes with straight edges have high probability to stick together at the edges since the DNA base-pairs exposed at the edge are highly hydrophobic and tend to stack to each other. To prevent this phenomenon the staples strands placed on the edges of the scaffold could be modified with 4 thymines sequence (4-T loop) that forms a non interacting loop (Figure 2.5b). The DNA loop structure can be exploited also to insert some points as dots for patterning the structure that are detectable by the height difference with atomic force microscopy. The latter modification firstly opens the possibility to decorate the DNA substrate.

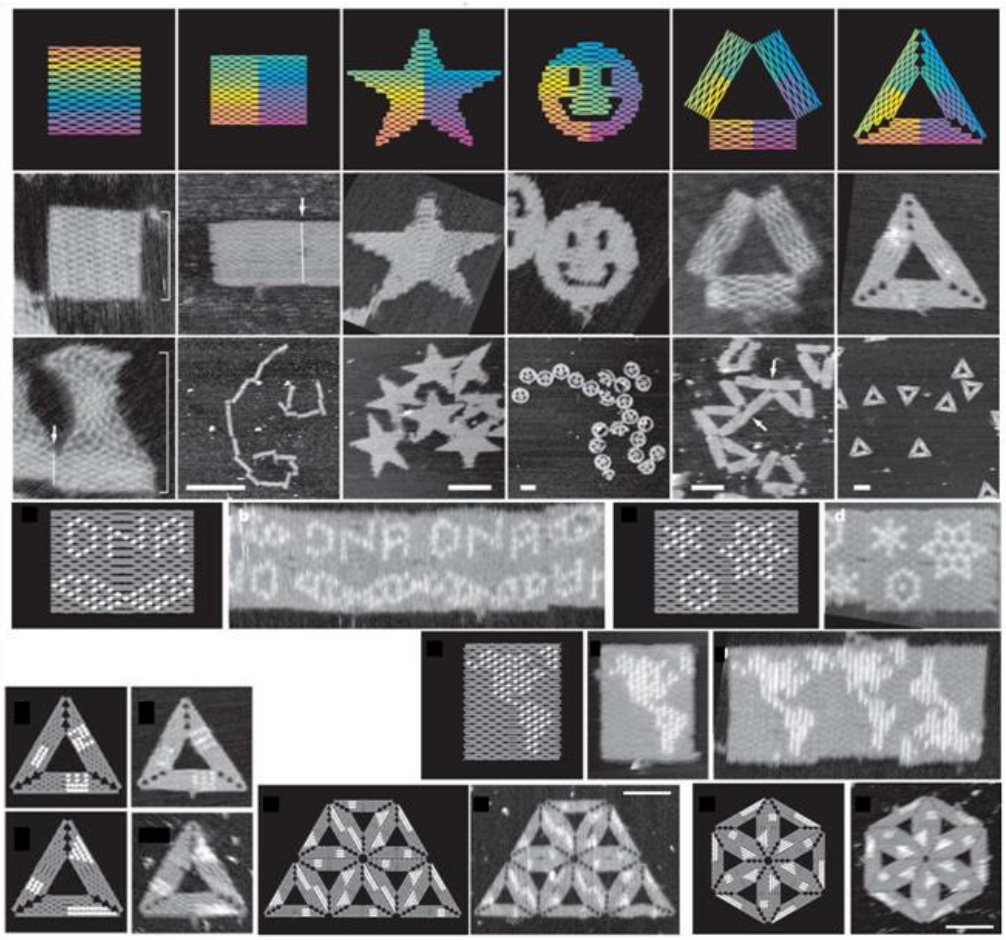

Figure 2.6 Examples of 2D DNA origami structures from Rothemund's study, where he used the M13 scaffold. Are visible the design and representative AFM images of each type of shape.

Once the DNA origami design is complete, the staples are defined corresponding to the scaffold sequence inserted. The origami structure can now be obtained by a simple self assembly process where the scaffold and staples strands are mixed together in a buffered solution allowing them to anneal (Figure 2.6).

2.3 Multilayer lattices and curved folding: 3D DNA origami structures

DNA origami technology was born as a technique to obtain arbitrary 2D nanostructures but there were no fundamental limitations to extend this approach to the construction of more complex 3D architectures. As the helices can be packed in *x,y* as illustrated before, with a further rotation they can be piled one over the other also in the *z* direction, providing a 3D DNA building strategy. Following this concept lattice structures composed by several 2D layers of helices, can be created. Yan and Shih presented for the first time a squared lattice DNA origami composed by piled helices bound together by, so called, anti-parallel crossovers[16]. Looking at the 1.5 turns spacing we have two crossovers every 16 base pairs (bp) or 32 bp on different or the same helix but only along one axis of the hypothetical helical cylinder. In their work Shih and colleagues inserted a modified crossovers spacing of 8 bp, generating a crossover every 0.75 helical turns, thus, every 8 bp the staple is positioned to link one adjacent helix. If we look at the helix cylinder at its orthogonal view choosing 0.75 turns spacing, the staples complete a clockwise rotation after 32 bp that generates positions at 0°/90°/180°/270° and 0/0.75/1.5/2.25 turns respectively. The structure can be simplified as a folding of planes of parallel helices producing parallel crossovers (along the plane) and orthogonal crossovers (crossing the plane).

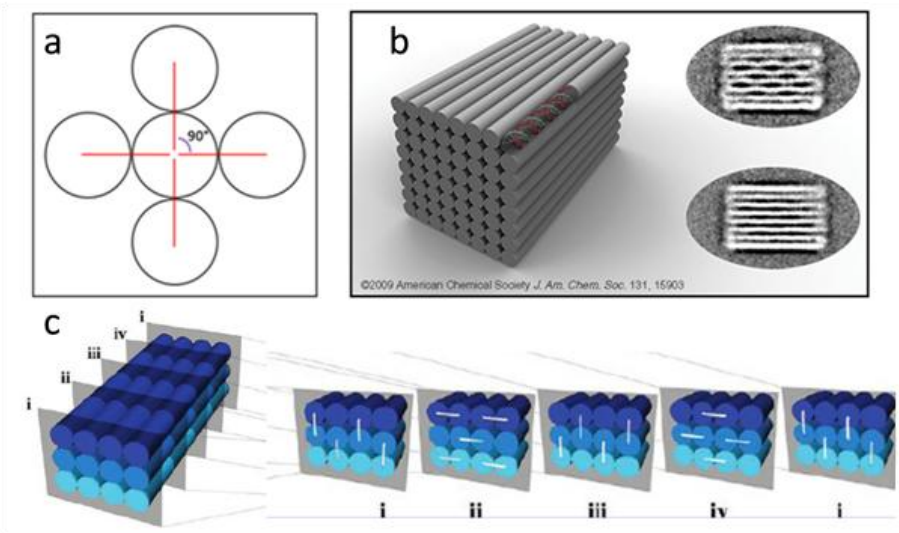

Figure 2.7 (a) Drawing of the possible crossovers positions with a 8 bp spacing. The rings represents the helices in the orthogonal view. The red lines represents the four positions where the staple completes 0.75 turns (8bp) step and is tangent to the adjacent helix at 0°/90°/180°/270° in clockwise rotation or 0/0.75/1.5/2.25 turns respectively. (b,c) Representations of the squared lattice (c) where are highlighted the crossovers planes (i-iv) determined by the four angles repetitions.

This particular configuration leads to the crossovers alignment in periodic intersection or panels crossing the lattice determined by the four different possible rotations of the staple

strand; thus, two crossover planes will be generated by parallel crossovers and two by the anti-parallel crossovers resulting in an entire cycle after four planes (Figure 2.7). The 8 bp spacing is permitted by the 10.67 nts/turn approximation, this initially imposed double-helical twist generates a slightly underwinding compared to the canonical 10.5 nts/turn; this underwinding would be predicted to lead a compensatory global right-handed twist of the entire structure[16]. This squared packing allows the formation of DNA lattices with vary dimensions depending on the number of helices involved and limited to the scaffold length.

Shih and colleagues have studied further the possible structural modifications acting on the crossover spacing till to develop bended helices that allowed curved structures[17]. The key element that allow to modify directionality of the helices is always the variable spacing between the crossovers. Modifying the spacing at 7 bp Shih and colleagues forced the staple to twist to the adjacent helix every ~0.67 turns (10.67 bp/turn) generating a complete period of 21 bp in which are possible 3 crossovers to return to the initial helix position. Thus, in a orthogonal view, the staple crossover with the adjacent helix is possible at 120° producing a shift from the axis of 30° between every helix. The repetitions of latter configuration in an array of antiparallel helices provides an "honeycomb" structure. This design can be exploited to create 3D structure as bundles of six helices that allow higher level of shape complexity[18].

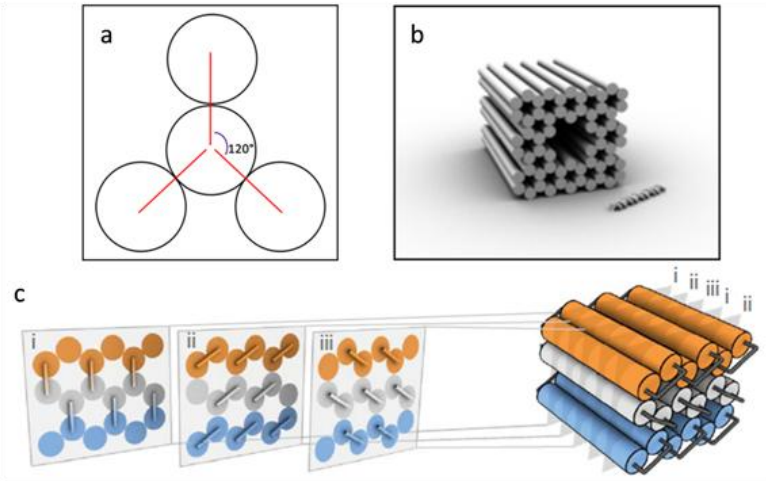

Figure 2.8 (a) Drawing of the possible crossovers positions with a 7 bp spacing. The rings represents the helices in the orthogonal view. The red lines represents the three positions where the staple completes 0.67 turns (7bp) step and is tangent to the adjacent helix at 0°/60°/120° in complete clockwise rotation (21 bp) or 0/0.33/0.67 turns respectively. (b,c) Representations of the honeycomb lattice and six helix bundles. (c) Are highlighted the crossovers planes (i-iii) determined by the three angles repetitions.

The crossovers between adjacent helices are restricted every two-thirds of a turn so, the density of Holliday junctions is increased respect to the previous examples. This raises the

necessity to control finely the positions of scaffold crossovers in order to place all the crossovers (scaffold and staples) in an arrangement most uniform as possible. To resolve this problem Shih and colleagues permit scaffold crossovers at positions displaced upstream or downstream of the corresponding staple-crossover point by 5 bp or half a turn. Moreover, staple crossover are added at all permitted positions that are not 5 bp away from a scaffold crossover; this rule keeps low the crossover density along helix-helix interface (~1 per 21bp). Shih's group analyzing the DNA lattices at transmission electron microscopy (TEM) revealed a diameter of 2.1-2.4 nm per individual double helix observed and a inter-helical gap of 0.1-0.4 nm. The discrepancy with the inter-helical gap of 1 nm estimated by Rothemund can be conferred by the higher density of crossovers present in the honeycomb-plated origami[18]. In all these DNA origami lattices a large use of 4-T loops can be done to minimize undesired multimerization or, if structure multimerization is desired can be left unpaired scaffold bases at the end of the helices to link different structural parts of a multimeric composed shapes. Hierarchical assembly of DNA-origami nanostructures can be also created programming staple strands to bridge separate scaffold strands[18].

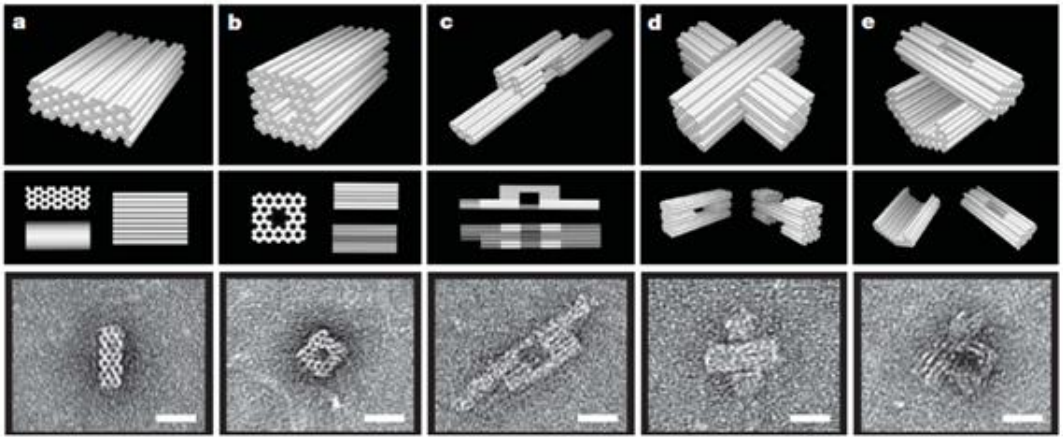

Figure 2.9 CaDNAno graphical designs and TEM characterization of different complex structures obtained with the honeycomb helices array. In (c,d,e) are showed 3D structures with hierarchical multimeric assembly.

Developing a graphical-interface-based called caDNAno to design so complex structures Shih and colleagues developed two different interfaces: a squared and an honeycomb array of helices. This computer-aided-design includes all the parameters, above described, to allow simple drawing of complex DNA structures making it largely user friendly.

Dietz and colleagues went beyond the simple squared and honeycomb linear structures described above and created bended regions on the bundles of helices[17]. They developed interesting twisted and curved structures only playing with the elongation or shortening of the

period between crossovers. They started from the honeycomb array defined by 7 bp spacing, complete period of 21 bp and a relative rotation of 240° (0.67 turns) of the helical path. Focusing on the 7 bp as structural unit, if the number of bases is decreased (< 7) it will be obtained an overwinding and a tensile strain of the fragment, which force it to exert a left-handed torque and a pull of the helices close to its neighbors. The latter overwind strain will be balanced by a compensatory global left-handed twist of the bundle, while the tensile strain of the fragment will be balanced by a compensatory global bend of the bundle. Conversely, if the number of bases is increased (> 7) it will be obtained an underwinding and a compressive strain of the fragment, which force it to exert a right-handed torque and a push of the helices far to its neighbors. The latter underwind strain will be balanced by a compensatory global right-handed twist of the bundle, while the compressive strain of the fragment will be balanced by a compensatory global bend away of the bundle[17] (Figure 2.10).

The key point of the construction of bended/twisted 3D origami is the result of the different forces exerted by the global interaction of multiple modified fragment units along the bundle and the whole structure. In fact, if only deletions or only insertions are placed along a lattice we will have only the compensatory global twist and absence of the bending. While a gradient distribution of deletions and insertions through a bundle cross section can cancel the global twist and reinforce the compensatory global bend. Using these calculations Dietz and colleagues built up a straightlattice of 10 by 6 bundle and two modified lattices with tensile (10 bp/turn) and compressive (11 bp/turn) fragments developing only global twist (left and right-handed). Moreover, they were able to combine different gradients of insertions/deletions in order to create different degrees of bending along a 3 by 6 bundle. They implemented gradients with extreme deviation from B native form till to generate a bundle cross section with one side of 6 bp/turn twist density and the other side with 15 bp/turn twist density. They considered DNA as a continuum rod with elastic bending, stretch compression and twist stretch coupling in order to calculate with iterative optimization procedures different gradients that produce bend angles from 30° to 180° with 30° steps with a radius of curvature that can reach 6 nm. In addition of bended bundles or twisted lattices Dietz and colleagues created circular objects; using hierarchical assembly of small parts a complete gear were developed as well as a toothed gear, six parts spiral, and a spherical wireframe. The spiral is essentially a continuum gradient with increasing radius of curvature of circle sections assembled[17] (Figure 2.10).

The spherical wireframe consists in six interconnected vertices each composed by two crossed six-helices bundles, but a real sphere was missing. In 2011 Yan and co-workers filled this gap

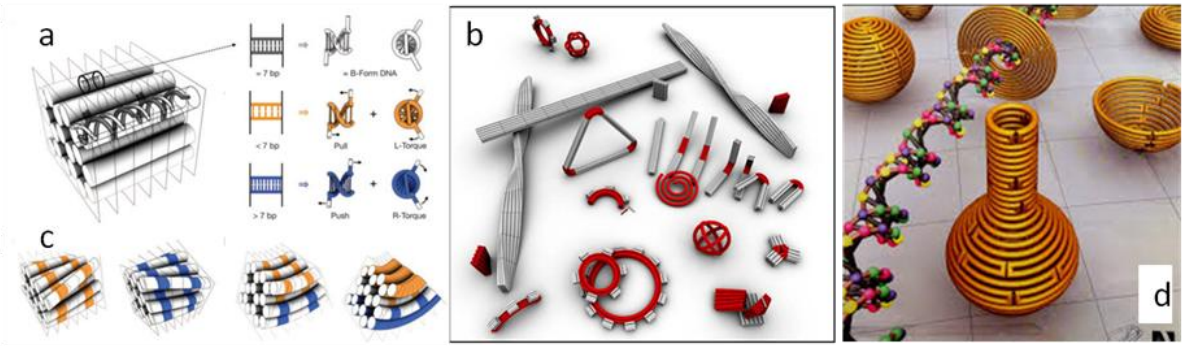

Figure 2.10 (a) Deletions (<7 bp) or insertions (>7 bp) produce a relative tensile or compressive force in the fragment between two crossovers exerting specific forces along the bundle. The tensile and compressive forces generate a left-handed and a right-handed torque relatively. (c) The presence of only insertions or deletions provides only global twist in the structure. Conversely a gradient of insertions/deletions through a bundle cross section cancel the twist and provides a global bend. (b) These modifications allowed to create several curved shapes like gears, toothed gears, triangles, spirals etc. (d) Drawing of the spherical shells, ellipsoidal shells and narrowed nanoflask.

and completed the architectural possibilities of the curved 3D DNA origami creating a real spherical surface[19]. Concentric rings of DNA were used to generate in-plane curvature while, out-of-plane curvature is introduced by adjusting the particular position and pattern of crossovers between adjacent DNA double helices, whose conformation often deviates from the natural B-form twist density and increasing the base pairs number. Adjusting the piling of these concentric rings incredible structures were developed such as spherical shells, ellipsoidal shells and narrowed nanoflask.

2.4 DNA origami functionalization: pointed and array decoration

The DNA origami is extremely powerful and versatile technique not only for the architectural peculiarities but also for the simplicity of functionalization. The easiness of synthetization of DNA oligonucleotides modified with some reactive chemical groups or even small molecules is the starting point to make DNA origami a functional object instead a structural only. The staple strands synthetization step allows to insert a modified DNA oligonucleotide simply mixing it in the self assembly process and, designing the position properly, a selective deposition of the molecule can be achieved. Theoretically DNA origami can be modified with nucleotides resolution, but even if the real resolution is bigger (~6 nm) it can be considered as a promising platform for the precise arraying of nanomaterials.

Yan and co-workers used a rectangular DNA origami platform to demonstrate the recognition of different RNA targets strands[20]. In their work the hybridization between DNA probes and RNA targets was exploited to functionalize specific points of the platform. Multiple DNA

probes complementary to the RNA targets were placed on the structure free to be hybridized and, in order to recognize the directionality and to identify the target, DNA hairpins were introduced as index onto the DNA origami. Imaging the structures with AFM the ridges provided by the linked strands were visible and, after the hybridization, the RNA targets could be identified from the specific hairpin markers on the DNA origami (Figure 2.11).

The selective deposition of a nucleic acid onto a DNA origami structure is simply provided by the addition of the strand in the mixed solution for the self assembly process. On the contrary, the selective binding of a protein is more complex since we need a linker between the DNA and reactive groups of the protein. One solution is using DNA sequences known as aptamers that bind naturally a specific protein. Yan and colleagues demonstrated the selective patterning of two types of aptamers on a 2D DNA origami analyzing them with AFM[21]. Nevertheless a selective linker in protein immobilization was searched to get a wider binding possibility. One example of reversible protein-DNA conjugation was reported using the histidine (His)-tag and Ni-nitrilotriacetic acid (NTA)[22]. The His-tag is a tail of 6-10 residues of histidines attached to the end of a protein backbone. Since the NTA and two histidines can bind a nickel ion and the tag can be easily replaced by addition of imidazole, this system is used in affinity chromatography to purify the tagged proteins. Norton and co-workers presented a method to directly patterning proteins using the NTA and histidine-tag metal linked interaction. They created a circular shape of DNA origami as platform where staples modified with NTA were placed thus, after the addition of His-tag protein both were clearly imaged with AFM[23].

The DNA origami and protein binding has been reported not only with tags linkers but also with more common components like antigen-antybody[24, 25] or predominantly biotin-streptavidin (STV) interactions. Niemeyer and colleagues demonstrated the decoration of a DNA origami with multiple different proteins. They designed a human face origami shape where several binding sites were placed. Using two different protein-tag interactions and the biotin-STV strong couple, they were able to selectively "switch on" different points of the face that were clearly visible with AFM analysis[26] (Figure 2.11).

An interesting strategy to immobilize protein on a DNA origami substrate was reported by Komiyama's group in which, a robust quadrilateral DNA origami well was built[27]. The well was sized to allocate only one STV protein and in order to do that, two biotins proteins were inserted in the well via a triethylene glycol (TEG) linkers. Since a periodically array of DNA origami wells was formed, when excess streptavidin was added to the solution exactly one STV molecule was captured in each well producing a streptavidin nanoarray (Figure 2.11).

Moreover, the STV molecules trapped in the wells presented higher stability in comparison with those trapped on the origami surface or those captured in the wells but attached by only one biotin.

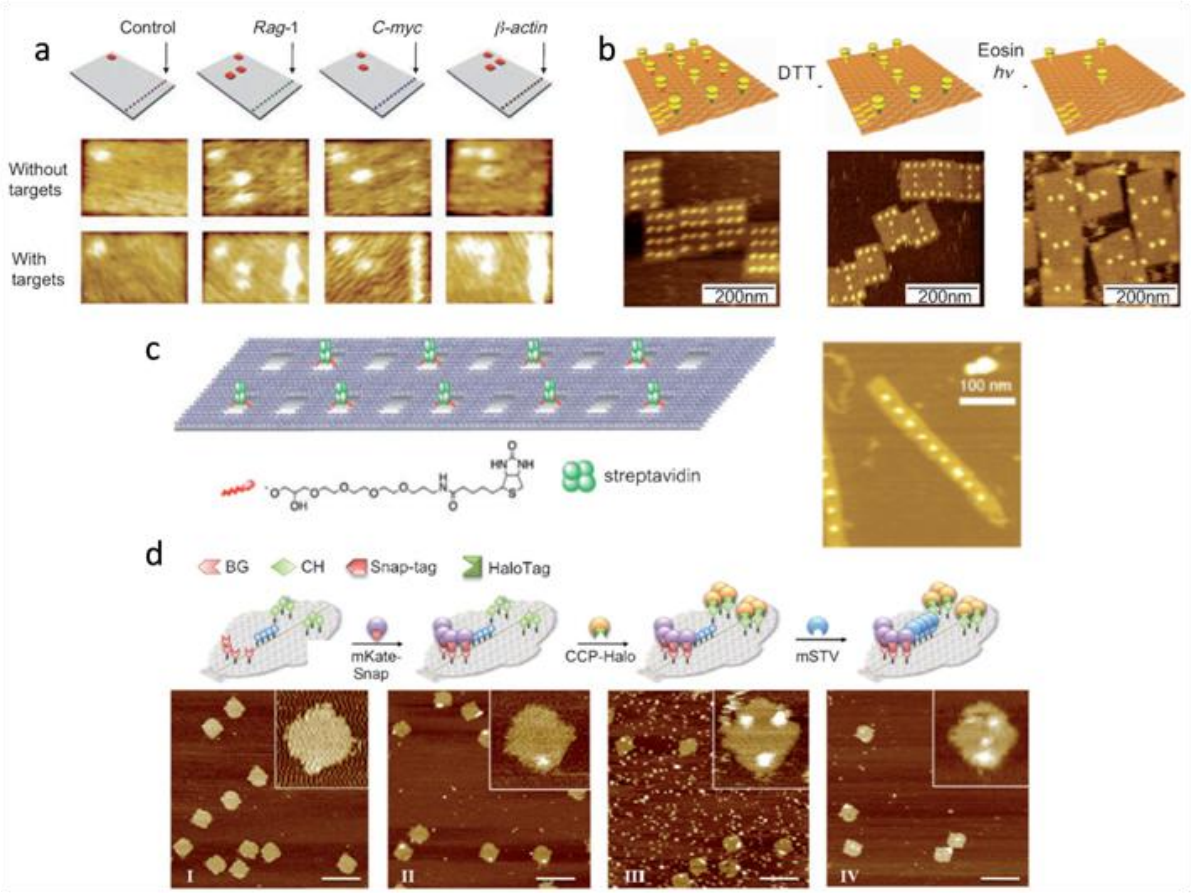

Figure 2.11 (a) Selective depositions via hybridization of different RNA targets. The asymmetric index made of DNA hairpins helps to identify the annealed RNA target. (b) Example of chemical reaction on a DNA origami surface. The addition of different reagents produces the displacement reactions of the biotins in a selective manner. (c) Single STV molecules are trapped in a DNA origami well by the action of two TEG linkers. The dimensions of the well are fundamental to capture the protein and the periodic nanoarray is imaged by AFM. (d) The selective protein binding is well demonstrated with two protein tags and biotin-streptavidin strong interaction using a human face DNA origami substrates and AFM characterization.

The rectangular shape of DNA origami has been exploited also to carry on molecular reactions. Single molecule reactions were reported by Gothelf's group on the origami surface exploiting the displacement of DNA-bound biotins[28]. They placed 12 binding sites in the structure modifying staples with biotins but they used three different linkers in asymmetric positions, in order to recognize the type of molecular reaction. Two different linkers were selective reactive with two reagents (Dithiothreitol and Eosin) and one linker was not reactive so, were generated a control, first reaction and second reaction. After each step of reagent

addition AFM imaging analysis was carried out resulting in a complete coverage (12 sites) after the STV addition and increasingly asymmetric deletions after addition of dithiothreitol (DTT) and Eosin (Figure 2.11).

2.5 Selective arrangement of DNA origami: towards nanodevices creation

The selective deposition of DNA origami structures on a desired location on a substrate is the starting point to create hybrid devices linking self assembly and top-down fabrication. Combining conventional nanofabrication techniques and self assembly of bio-molecules we can confer new properties that can overcome the limits of a not hybrid structures generating innovative devices.

Törmä and colleagues studied a way to trap a DNA origami at a desired site applying a dielectrophoresis technique[29]. Gold electrodes with a relative gap close to the dimensions of the origami shape were fabricated on a SiO_2 substrate using electron beam lithography (EBL). They used the well known covalent interaction between surface gold atoms and thiol chemical groups that were placed at the two extremities of the origami structure to attach it to the electrodes after the trapping. Once optimized the voltage, the trapped DNA origami structure was clearly visible however, the single origami trapping yield was pretty low (5-10%).

Usually the substrates employed to deposit the DNA is mica surface because is highly electronegative and forms a stable salt bridge in presence of cations. In order to find an alternative substrate to firmly placing DNA molecules and that can be employed in nanofabrication is necessary to search a surface modified material that could provide the required electro-negativity. Following this concepts self assembled monolayers (SAM) were used to modify the material surface to link the nanofabricated surfaces and the bio-molecules in water solution. The SAM is generated by the self-organization of thiolated molecules covalently bound to the material surface; the same molecules can carry a specific chemical termination on the opposite side, in order trigger a further reaction at the surface. The final reactive group of these molecules can be designed allowing good possibilities of binding nucleic acids, protein and even other materials. Yan-Soh and colleagues created a pattern of a SAM on a gold polished surface deposited by electron-beam evaporation[30]. They used two types of molecules: one terminated with carboxyl group that can bind Mg^{2+} and create efficient salt bridges while the other molecule (6-mercaptohexanol) was not able to bind Mg^{2+}. The selective deposition of DNA origami on the carboxyl surface was demonstrated by introducing a gold disk pattern modified only with carboxyl groups.

One example that exploits the salt bridge linking without SAM formation is the work of Wallraff and colleagues where they created sticky patches in the shape and size of a triangular DNA origami using EBL and dry-oxidative etching[31]. They succeeded in single origami deposition on the binding site with a fairly orientation however, it was necessary a ten times higher concentration of Mg^{2+} to achieve a binding of the structures (Figure 2.12).

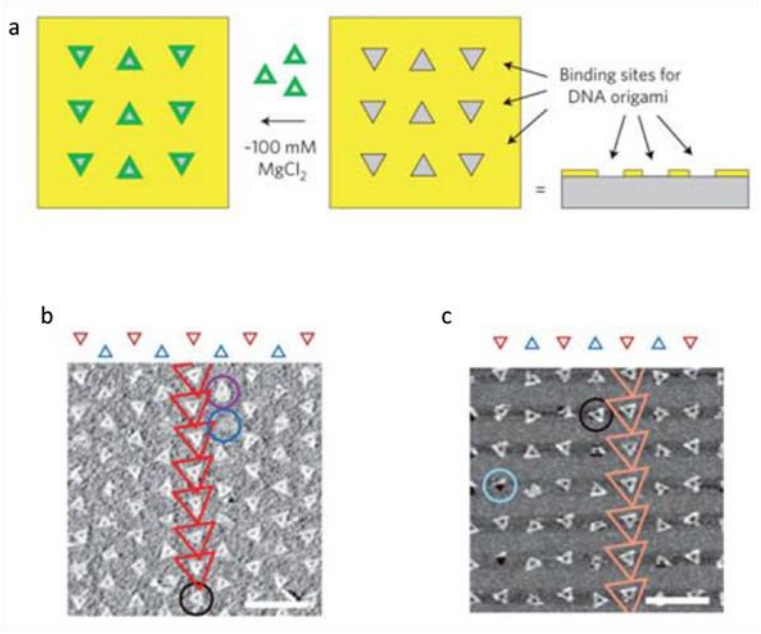

Figure 2.12 (a) The scheme of the patterning for the selective deposition of triangles DNA origami structures. (b,c) AFM images that show the single origami deposition in each binding sites with different orientations.

2.6 Nanomaterial incorporation in DNA origami structure

The arrangements of molecules and proteins onto DNA origami structures gave the possibility to think at hybrid structures with several functional scopes. Inorganic nanomaterial objects are important components for physical and engineering applications because combining them with bio-materials, new levels of manufacturing can be achieved. Surface-Enhanced Raman Spectroscopy (SERS) and Localized Surface Plasmon Resonance (LSPR) are two applications that can gain main advantages from the combination of bio and inorganic materials. In order to enhance the physical properties of inorganic materials for their applications a precise arrangement on DNA origami structures is needed. Nowadays, through chemical synthesis, a large variety of nanoparticles can be obtained: nano-spheres, cubes, rods, triangles, stars etc.. These structures can be different in size, shape and material to achieve the desired functional properties. However is possible the synthesis with various metals such as gold, silver, copper, iron, the most used one is gold because can form a chemical bond with thiol (-SH) group that

has a strength close to the covalent bond[32]. Moreover, gold is inert material in water solution conferring it a good stability in biological medium.

Yan and Liu reported for the first time, a selective deposition of gold nanoparticles (AuNP) on a DNA origami structure[33]. 10 nm gold nanoparticles were functionalized with a thiolated DNA oligonucleotide, and they were purified by agarose gel electrophoresis to collect only the 1:1 AuNP- DNA conjugates. The latter were used as staples in the self assembly process to incorporate directly the AuNP into the DNA origami structure. The rectangular origami with one or two inserted nanoparticles were successful imaged with AFM providing a yield around 90% (Figure 2.13a). The same group was also able to encapsulate a nanoparticle in a DNA origami open cage decorating precisely the structural faces[34] (Figure 2.13b).

Subsequently, Bokor and colleagues presented a fine deposition of gold nanoparticles with different diameters onto a triangular DNA origami shape[35]. In this case they used a slightly different strategy to link AuNPs and DNA substrate, because six position were created on the triangle surface with protruding staples strands with different sticky ends for each nanoparticle diameter. The spacing between nanoparticles was controlled by the positions of the sticky ends. Then, 15, 10 and 5 nm AuNP were functionalized with three different thiolated DNA sequences complementary to the catchers strands protruding from origami surface. The hybrid structure was analyzed and purified by agarose gel electrophoresis and the successful arrangements of the six AuNPs was demonstrated by Scanning Electron Microscopy (SEM) imaging where precise and complete placement of nanoparticles is clearly visible (Figure 2.13c). This chained structures produced several order of magnitude of field enhancement in the inter-particle gap, thanks ot the precise AuNP positioning offered by DNA structure.

Whit a similar strategy, Yan and Liu used a triangular DNA origami design to place silver nanoparticles (AgNP) of different diameters with an architecture where the distance between nanoparticles and their number was fined controlled[36]. In this study also heterodimer structure of AuNP and AgNP was also arranged onto the DNA origami.

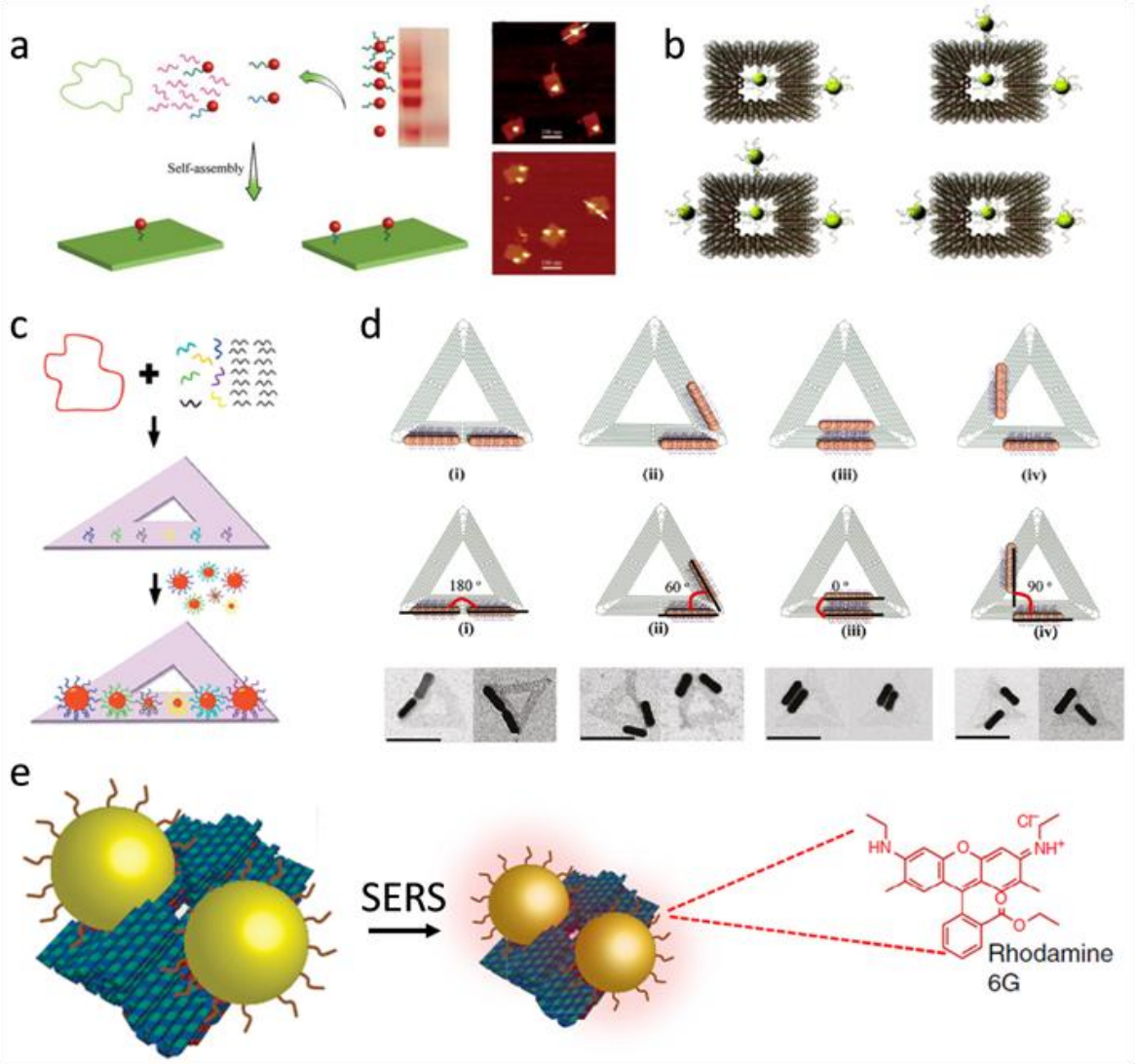

Figure 2.13 (a) 5 nm gold nanoparticles are functionalized *via* thiol modification to some staples strands to directly be inserted in a rectangular DNA origami platform. (b) Example of AuNP encapsulation in a DNA origami cage open structure. (c) Deposition of a chain of six AuNPs with different diameters in a triangular origami. (d) Precise arrangements of gold nanorods dimers onto a triangular origami with defined angles between them: 180°(i), 60°(ii), 0°(iii), 90° (iv) with relative TEM images. (e) Drawing of the nanoparticles dimer antenna to create an hot spot between them exploitable for SERS analysis with Rhodamine 6G and other molecular dyes.

Moreover, to generate unique plasmonic properties, the same group presented a well-ordered architecture of gold nanorod placed on the same triangular origami shape[37]. The gold nanorods (AuNR) are linked to origami surface with the same strategy i.e. using some protruding catchers strands allowing the placement of single but also dimer of AuNRs. The catchers were placed in order to confer different nanorods positions and orientations producing several angles between them with a relative high precision. To study the properties of anisotropic plasmonic structures also hybrid AuNP/AuNR heterodimer were arranged,

demonstrating the programmability of DNA direct assembly and ability to create asymmetric metallic nanostructures (Figure 2.13d).

As mentioned above, particular architectures of nanoparticles can highly enhance the local electromagnetic (EM) field. When a single molecule is placed with nanometer accuracy in the position where the local field is enhanced, its optical response, for instance, fluorescence is also greatly amplified. However to have a significant effect, the nanostructures, such as AuNP and AuNR should be positioned with sub-nm resolution, a requirement extremely challenging in nanolitography technology[38]. DNA origami technology, on the other hand, represents an effective way to address these issues, namely both the positioning of the AuNP to form a resonant structure and the the molecule of interest exactly between the nanoparticles. Tinnefeld and co-workers successfully created a nanoantenna structure using two gold nanoparticles of 80 or 100 nm focusing the incident light in the hot spot in the nanoparticles gap[39]. In order to hold together the AuNP dimer and precisely address a molecule of interest, they constructed a DNA origami pillar with catchers staples to bind all the three components. They exploited their antenna structure to enhance the fluoresce of a molecular dye placed between the DNA oligonucleotides covering the NPs and the DNA origami pillar; in this way they registered a 117-fold fluorescence enhancement in the case of 100 nm AuNPs dimer.

The strategy of nanoparticles dimer has been exploited also to enhance the Raman scattering (SERS). Keyser and colleagues employed a particular DNA origami structure to create a strong plasmonic coupling in a 3-4 nm gap between two 40 nm gold nanoparticles[40]. They demonstrated the high field enhancement analyzing the SERS properties of Rhodamine 6G that was inserted precisely in the nanoparticles gap thanks to the origami linking. The SERS analysis was carried on also using other small number of dyes molecules as well as short single strand DNA (ssDNA) oligonucleotide demonstrating the high versatile properties of DNA origami also as SERS-active nanoparticles assembly platform (Figure 2.13e).

Rationally designed DNA origami structures enable the precise arrangement of metal nanoparticles that provides plasmonic properties. Noble metal nanoparticles exhibit localized surface plasmon resonance (LSPR), which is dependent on the incident light. Chiral molecules preferentially interact with left- or right- polarized light and produce an optical response known as circular dichroism, but natural chiral molecules only exhibit a circular dichroism in the UV range. The combination of precise DNA structure with plasmonic nanoparticles allows a sub-nm precision positioning of the plasmonic structure thus, controlling and eventually tuning their optical response. The development of particular

architectures of plasmonic nanoparticles could allow the investigation of chiral properties also in the visible light range thus, the chiral optical response can be engineered[41]. If AuNPs are arranged with asymmetrical geometries and small interparticle distances, the plasmon coupling could induced the circular dichroism effect.

Since the DNA origami can provide a solid template to arrange AuNP in a stable and fixed way with high precision, Ding and colleagues organized four gold nanoparticles using a rectangular shape DNA origami linked to the catchers strands[42]. Placing three AuNPs on the top and one on the opposite surface of the origami they produced left- and right- handed plasmonic structures demonstrated by the circular dichroism profile analysis (Figure 2.14).

The metal nanoparticles assembly in chiral shapes has been clever interpreted by Ding's group firstly and then followed by Liedl and colleagues. The clever idea of the first group was to arrange two lines of gold nanoparticles on the surface of a rectangular DNA origami modified at the longer sides with protruding strands in several positions. These strands are complementary to some DNA oligonuleotides that can be inserted after the self assembly of the hybrid structure triggering the rolling up of the rectangle in the shape of a nano-tube that exposes the AuNP on the external part. In this way an helical geometry with chiral properties is produced[43].

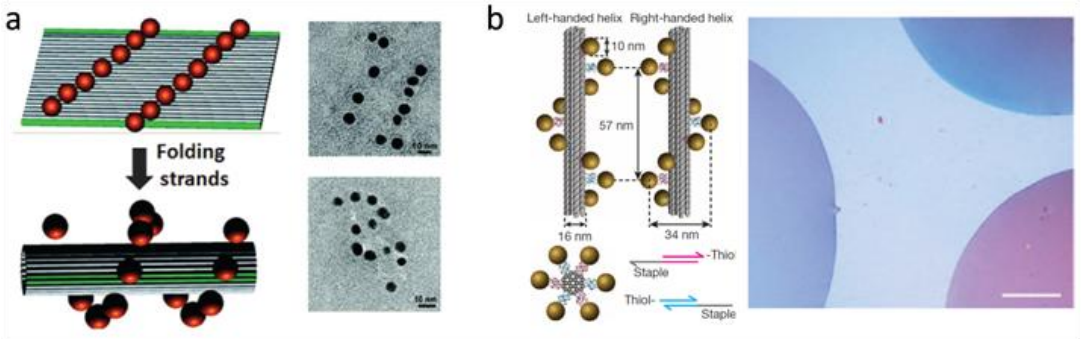

Figure 2.14 (a) DNA origami rectangular sheet rolling up after addition of folding strands generating 15 AuNPs helical structure with chiral properties. (b) DNA origami rigid tubular structure is decorated with 9 AuNPs in a left- and right- handed assembly with accurate helical pitch. Droplets of solutions of the two opposite chiral structures provide different colors under polarized light illumination .

Conversely, Liedl and colleagues designed a 3D DNA origami with tubular shape composed by honeycomb bundles of helices[44]. Nine binding sites were placed along the tube to allocate nine AuNPs with left- and right- handed behavior. The rigid origami with accurate helical pitch were imaged with TEM and the chiral properties were demonstrated by circular dichroism profiles. Moreover, they grew an alloy shell on the 10 nm AuNP seeds using a mixture of gold and silver ions to enhance the chiral effect in order to see optically droplets of

the sample solution with different colors produced by the different plane changing of polarized visible light (Figure 2.14).

2.7 Movable DNA origami.

DNA origami technology, in principle, has little limitations in term of available shape design and since 2006 many different structures for several purposes have been developed. Among all these examples particularly interesting are those capable of conformational changes after the addition of specific stimulus ascribing a movable interaction to the structure architecture.

Kjems and colleagues reported, for the first time, an example of flexible DNA origami structure[45]. They created a curious dolphin-shaped origami using SARSE program starting from a dolphin picture and optimizing the crossovers. They inserted the seam along the horizontal axis of the dolphin leaving the tail section without crossovers between the two parts of the seam. In this way, the tail results linked to the dolphin body through an highly flexible linker which allows the caudal fin to flap. Several coexisting tail conformation angles were observed in the AFM characterization and interestingly, the analysis of a new design with complete crossovers along the seam revealed much smaller angles variations. In a thin and small DNA origami portion like a dolphin tail the seam crossovers confer higher stability so, the origami structure can be engineered to introduce desired flexible properties (Figure 2.15).

The same group studied how the flexibility of DNA structures can be exploited to allow movements of parts of DNA origami structures. In their work a DNA box was created by interconnections of many rectangular DNA origami shapes assembled together. The structure was characterized by AFM and Cryo-TEM to verify the actual formation of a 3D structure[46]. The box faces sizes were close to 40x30 nm and the scaffold strand hold the faces by passing through a vertex of each ones implying a long self assembly process to construct the complete 3D box. The so connected box faces presented a weaker and flexible link along the sides that was exploited to allocate a structural motion dependent on a stimulus addition. They inserted two DNA oligonucleotides on the top face that were partially complementary with other two strands on the bottom face, in order to use them hybridization like a lock system for the box lid. Then, they used the same DNA base pairing to open the lid by the addition of two key DNA strands fully complementary to the linked oligonucleotides. The demonstration of successful opening movement of the box lid after the key DNA strands addition was performed by placing a FRET couple between the lid and the bottom face, recording the

emission of donor when the box is closed and the emission of the acceptor when the box lid is open. The box, once open, did not close, also when the key was removed: the shape change was not reversible[46] (Figure 2.15). The same Kjems's group reported the construction of similar DNA origami box with smaller dimensions and using the same lock-key system they presented a reversible opening of the box lid[47].

The conformational changes into DNA origami have been exploited also for more specific functions. Komiyama's group developed DNA origami levers that can be used as single-molecule beacons for the detection of biomolecules[48]. They designed two long lever domains (170 nm) joined together in a specific pivot point by a non-sliding Holliday junction. The flexibility of the structure allows three possible forms between the two levers, all of them observed by AFM: cross, parallel and antiparallel. In this study the detection of target molecules is permitted by a concavity in each lever where a molecular ligand can be linked. Three independent mechanisms were identified: pinching, zipping and unzipping. The pinching mechanism is when a molecular target is recognized by the two ligands and clamped between the two levers; zipping mechanism is the multiple detection of target molecules thanks to the insertion of multiple recognition elements along the two levers and finally unzipping is the opposite mechanism after the target addition. The opening and closing movements of the DNA origami pliers were monitored in real time by the placement of two dyes molecules and a quencher on the two levers and observing which dye reacts with the quencher and thus is switched off[48] (Figure 2.15).

The applications of structural changes of DNA origami are wider than just molecular sensors. Sugiyama and colleagues used a DNA origami tube to regulate the gene transcription. They used a six helices bundle origami to hide inside a double strand DNA (dsDNA) which includes the promoter region for a DNA polymerase[49]. The dsDNA strand is prolonged out of the tube, but the promoter region remains hidden inside the tube. When the tube is opened using a DNA strand complementary to a closing staple, the promoter region is exposed and the polymerization can be initiated. The success of dsDNA transcription was confirmed by the PCR (Polymerase Chain Reaction) amplification product (Figure 2.15).

Once proven, the motility of a DNA origami was exploited to design a drug delivery systems using the origami like a cargo container. A conformational change is needed to distinguish the open and closed state of the cargo. Church and colleagues best interpreted the concept of the molecular cargo; they created a sort of DNA origami nano-barrel where is possible to allocate a specific payload[50]. Two concave origami parts were connected, on one side, with DNA linker strands; and on the opposite side it with a DNA aptamer-based lock mechanism that can

be open by the binding of specific antigen as key. The internal faces of the origami were modified with twelve binding sites with 3' extensions strands so that, different cargo objects like 5 nm AuNPs and antibody fragments, were functionalized with the complementary strands and used in different experimental tries. Upon the aptamer recognition of the antigen, the origami opens like a bivalve and exposes the cargo objects.

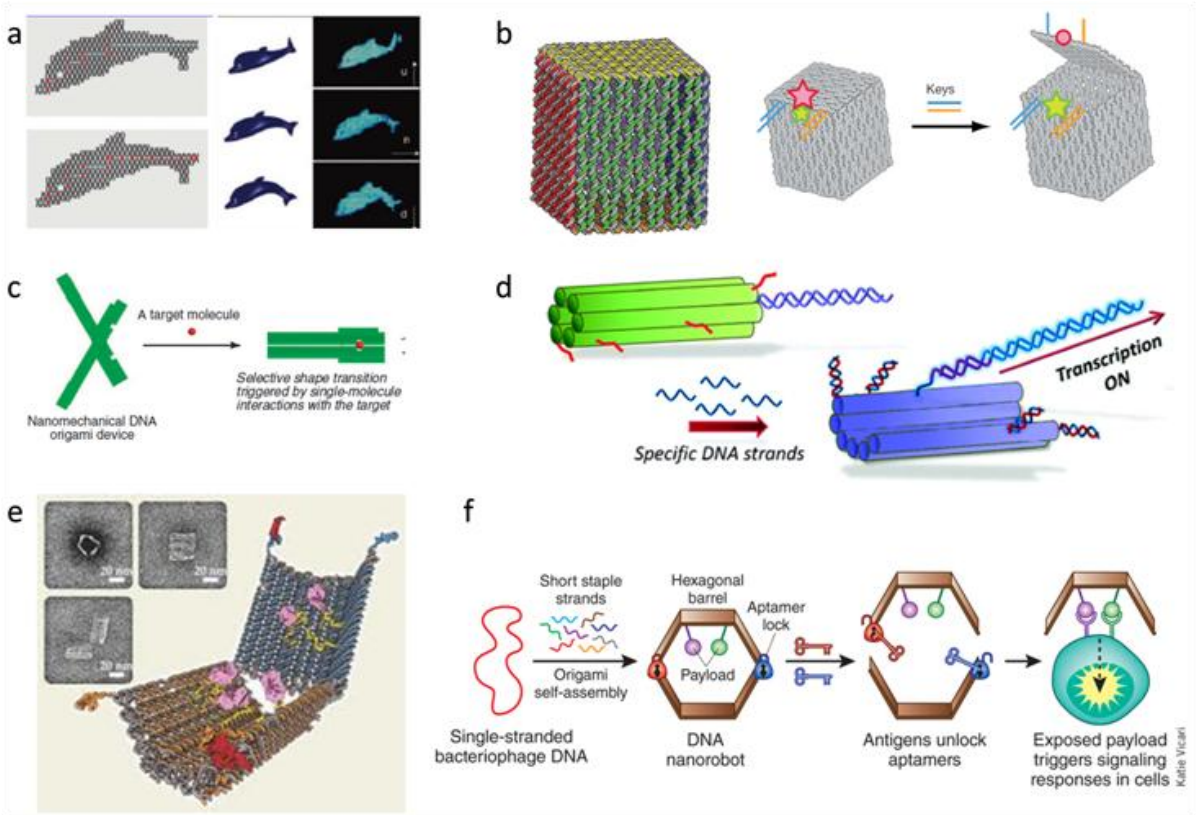

Figure 2.15 (a) DNA origami dolphin shape: the absence of seam crossovers provides the tail flexibility. (b) DNA origami box with a DNA lock system, the addition of key-strands enable the lid opening. (c) The DNA origami levers that can pinch as tweezers the molecule of interest. (d) Tubular DNA origami composed by six helices in which is located a promoter dsDNA region. The opening of the tube allows the starting of DNA polimerase action. (e,f) DNA origami barrel with binding sites in the internal part for specific cargo molecules. (d) The aptamer-antigen recognition regulates the opening of the structure and so the exposition of its cargo to the cell receptors.

In addition to the TEM images of the open and closed structure the researchers also analyzed the barrel specific interaction with several types of cells only playing with aptamer specificity to insert logic operations in the origami opening. A fluorescent labeled antibody fragment specific to leukemia human cells (membrane receptor) was loaded into the barrel; then two different aptamers were placed on the lock system in order to create different AND gates tested in different antigens combinations[50] (Figure 2.15).

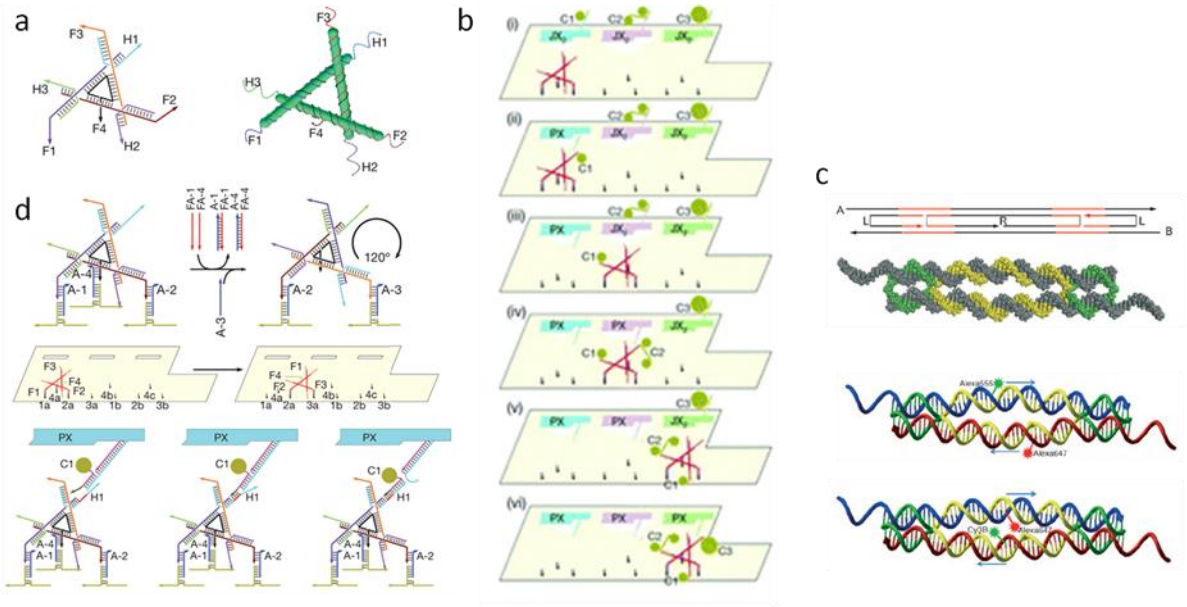

Figure 2.16 (a,b,d) Programmable DNA origami robot composed by: (a) the DNA walker with four feet and three hands, the three machines cassette and (b) the tile where are patterned the three machines and the track for the walker transit. The mechanism of rotation of the walker structure is based on the hybridization with DNA catchers protruding from the track and the AuNP release from the machines (PX) is based on the proximity of the strands. In (b) is clearly visible the progression along the assembly line of the walker collecting all the cargo AuNPs. (c) DNA origami actuator composed by two pistons filaments A-B and the roller that is fixed in eleven discrete states by the lock strands L. The cyclic proximity of two fluorophores allows to detect the different states by FRET analysis.

The DNA origami switching between two states has been exploited also to create a DNA nano-robot programmed to collect cargos in a sort of assembly line. The complex structure was engineered by Seeman and co-workers using a DNA origami tile on which were allocated three DNA machines and a track that provides the movements of a DNA "walker" structure[51]. The DNA machines can toggle between two states and depending on them they can "donate" (PX) or "do not donate" (JX_2) a cargo. In the published example the cargo objects were: 5 nm AuNP, couple of 5 nm of AuNP and 10 nm AuNP on the first, second and third machine respectively. The interestingly walker structure is a triangular DNA structure that exposes three strands as hands and four strands as feet; the hands are able to take the cargo and feet are able to link and walk on the pre-programmed track on the origami tile. The AuNP functionalized DNA cargo strands recognize by base pairing the hands and vice versa, in this way the walker can proceed on the track and dependent on the machines switching state, can collect all the AuNPs cargo. This study is an impressive example of the complexity that can be addressed simply using DNA complementarity[51] (Figure 2.16).

In the wake of the programmed DNA robot construction Gothelf and colleagues presented a DNA actuator that undergoes to a sliding type motion and is able of eleven discrete states[52]. The simple concept of Holliday junction was exploited to place a DNA actuator strand (roller) in between two other main DNA filaments (pistons). Thanks to the complementarity of the roller to pistons sequence regions the roller strand can slide in between. The insertion of lock strands that are half complementary to these pistons regions allows to fix the roller in eleven discrete states. These states are detectable by FRET thanks to the insertion of two fluorophores in specific positions along the two pistons DNA filaments (Figure 2.16).

Chapter 3

Nano-metrical detection

3.1 Nano-actuation detection techniques: scanning electron microscopy

The DNA origami actuation produces a movement or conformational change of the structure in the nanometer range of distances: in order to observe it a detection technique able to operate on a molecular scale is needed. The scanning electron microscopy is often employed in the characterization of nanometrical structures due to its easiness of use and high resolution. An highly focused (1.5nm) beam of accelerated electrons (1-30 kV) interact locally with the sample producing a cloud of scattered electrons, whose energy and intensity depends on the sample geometry and composition. The electron beam is raster scanned on the substrate, the scattered electrons are collected and amplified with the aid of detectors positioned at fixed angles, their intensity is associated to the position of the primary beam in the sample, and finally the image is reconstructed point by point. The best resolution can be as good as 2-4 nm but not all the type of samples can be imaged with that precision (Figure 3.1). The highest resolution can be achieved with sample materials that are good scatterers (typically heavy metals) but it decreases a lot when biological sample are imaged due to their poor scattering cross section (Figure 5.30 and 5.31). Moreover, the imaging condition requires a vacuum chamber to enable the electrons to fly so that the biological samples have to be dried and fixed.

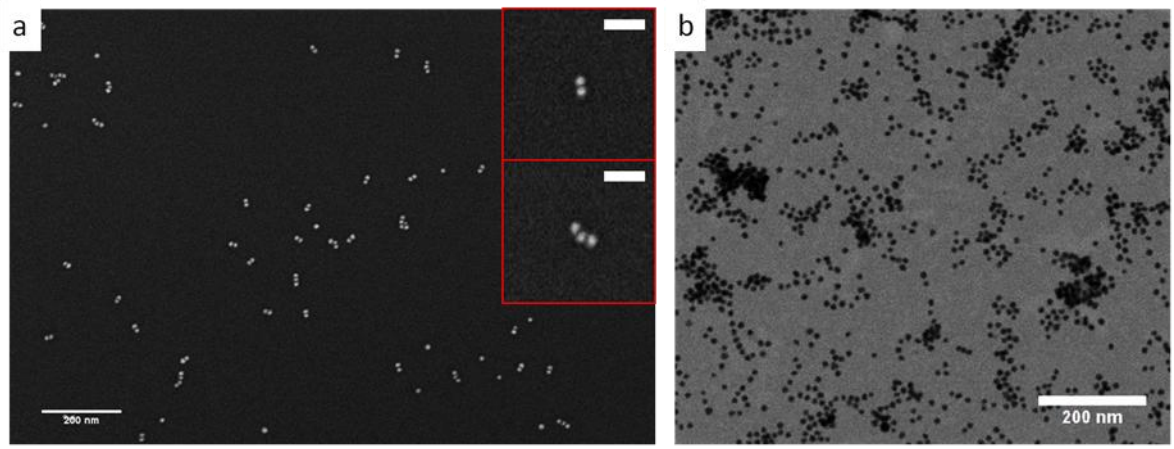

Figure 3.1 Gold nanoparticles of 20 nm diameter imaged in (a) SEM and (b) STEM configuration. The contrast is different for the different configuration, while the resolution does not change dramatically, even if in image (b) the NP borders are better appreciable. (a) The red insets scale bars are 50 nm.

This implies that biological samples are imaged in a "frozen" and not normal liquid phase condition. In addition, the low pressure tends to distort the soft sample pushing and forcing it to adhere at the substrate. For this reasons the SEM is a good technique to image metal nanoparticles but is not suitable to see a conformational change like in the case of a target-driven actuation especially if, like in my case, the actuation is producing a 3D complex change.

In order to have better contrast and so achieve better resolution, we can use the SEM in transmission configuration (STEM). A of copper grid, that is transparent to electrons, is used as sample substrate and only electrons which are not deflected by the sample are recorded. This approach allows the use of high energy, and thus smaller beam size, without charging effects, and slightly improved spatial resolution. The two techniques provide two images with opposite contrast, because in SEM the signal is higher where the scattering cross section is higher, while in STEM the signal is maximized where all the electrons are transmitted and no-one is scattered by the sample. In Figure 3.1 I report an example of 20 nm gold nanoparticles imaged with both the configurations, in which we can see the different contrast but no clear gap of resolution is appreciable comparing the two images.

3.2 Nano-actuation detection techniques: atomic force microscopy

Atomic force microscopy is widely used especially for its suitability to image biological sample in liquid phase. The AFM tip acts as a nano-metrical phonograph. The movement of the AFM tip (probe) is dependent on the sample surface morphology. The tip is positioned at the end of a flexible cantilever. An infrared (IR) laser is aligned on the top of the tip cantilever thus, its movements are registered by the use of a four quadrant detector, in this way the image is then reconstructed. Since, in this instrument, the probe is a nano-dimensional metal tip the resolution is dependent on the radius of curvature of the tip apex (typical 5-20 nm). For this reason, compared with electron microscopy, the achievable resolution is much lower in *x-y* axis but is sub-nano-metrical in *z* axis. Although the sample can be imaged in its normal biological liquid phase and so, no limitations are introduced in its potential workability, the tip interaction with the soft sample surface can distort the 3D structure morphology (Figure 3.2)[53]. Moreover, the scanning movement associated with the contact or non contact interaction of the tip can drag and move the samples objects especially which ones can roll like nanoparticles. For these reasons is not suitable to image metal nanoparticles especially

big ones in liquid condition but is largely effective in imaging of planar DNA origami even if the 3D actuation can be distorted by the continuous or intermittent contact with the tip.

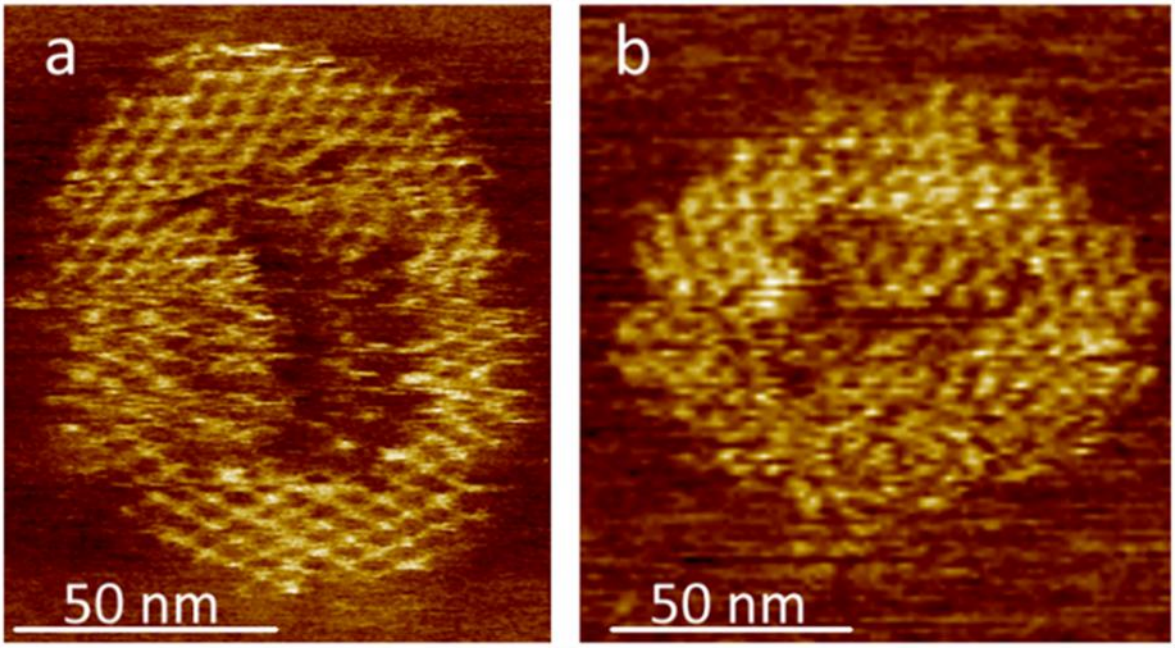

Figure 3.2 High resolution AFM images of DNA origami circular shape where are visible the inter-helical crossovers (every ~11 nm for 32 bp). In image (a) is also visible the distortion provided by the AFM tip: during the scanning (from bottom to top of the image) the central part is damaged and the axis is tilted at the origami top.

3.3 Nano-actuation detection techniques: transmission electron microscopy

The transmission electron microscopy is the main characterization technique of nano-material structures due to its sub-nm resolution. The accelerated electrons (50-200 kV) go through the sample due to their high energy. The different electron-density of the sample generates areas where electrons are transmitted in large or small quantity. The electrons are collected and amplified by detector and the image is then reconstructed. The electrons high energy allows a consistent penetration in the metal providing high resolution imaging of gold nanoparticles. We are able to distinguish not only the borders but even the NP facets and atomic planes (Figure 3.3). Although the great resolution, TEM technique, similarly to SEM needs vacuum condition that prevent the investigation of biological sample in their liquid phase. The biological sample has to be fixed and stained with heavy atoms compounds (OsO_4, $UO_2(CH_3COO)_2$,...) to increase its electron density contrast. For this reasons the TEM is an optimal technique to image metal nanoparticles gap due to the high resolution, but is not

suitable to see a conformational change like in the case of a 3D DNA origami actuation. In spite of the latter, is widely used to image hybrid DNA origami linked to NP structures after a DNA staining to contrast the origami. This strategy does not allow to analyze the 3D origami conformational changes but the addressing of NP on the origami platform is quite well appreciable (Figure 5.24).

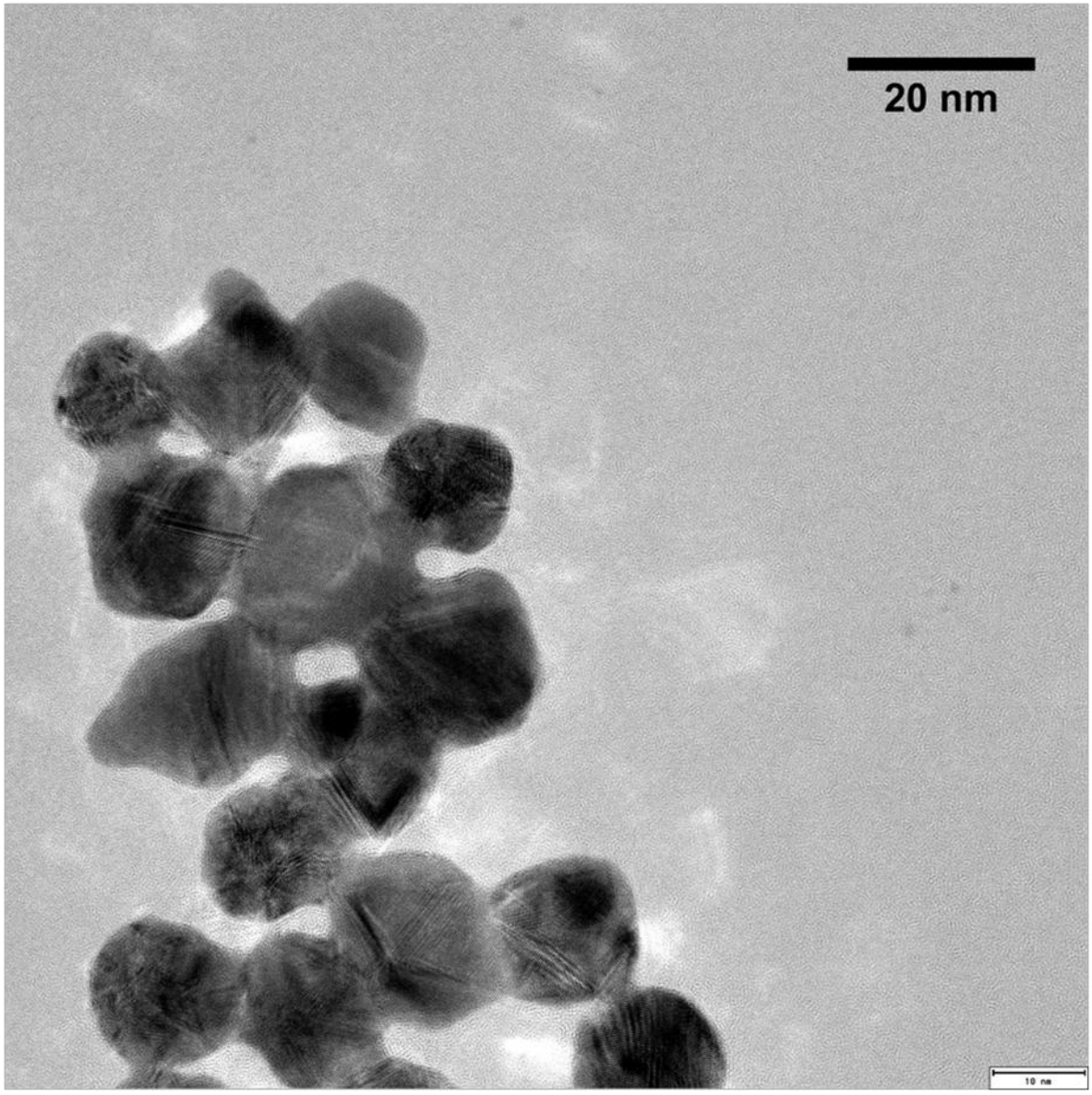

Figure 3.3 High resolution TEM image of gold nanoparticles of ~10 nm diameter. In some of them are clearly visible the gold atoms planes (black lines) alternate to white lines produced by electrons that do not interact with atoms.

In order to overcome the 3 dimensional problem with TEM imaging a quite novel strategy is to use the Cryo-TEM configuration where the sample is firstly frozen in its biological buffer and then imaged with different 3D angles. In this way biological flexibility of the sample is literally "frozen" in that particular moment and the dimensions in 3D space are comparable

with the liquid phase ones. Taking a series of images of a number of equivalent origami frozen in different positions is equivalent to take a series of sequential snapshot of the motion of an individual origami, thus information of the dynamics can be recovered. This strategy can largely help in the reconstruction of real dimensions during an actuation conformational change like instantaneous picture frame of the process.

3.4 Nano-actuation detection techniques: FRET

One of the most used techniques to unravel molecular changes is the Förster Resonance Energy Transfer (FRET). This technique is based on the mechanism of energy transfer from a light-sensitive molecule (or chromophores) which emits at short wavelength and is called *donor* and a second chromophore which emits at longer wavelength and is called *acceptor*. The transfer efficacy depends on the donor-acceptor distance and is typically in the range of few nm. When the two fluorosphores area very close, all the energy is transferred from the donor to the acceptor and the first is actually quenched. The distance at which the efficiency is 50%, or, in other terms, both the donor and the acceptor emit light with the same intensity is called Förster radius. More in detail, after light irradiation the donor molecule is in its electronic excited state and normally, it will return in its non-excited state with a radiative process where it emits photons with less energy than the incoming ones due to the relaxation effect. If the acceptor molecule is placed close to the excited donor may be possible a transfer of energy to the acceptor through a non-radiative dipole-dipole coupling. The subsequent return to non excited state provides the acceptor emission after the relaxation effect (Figure 3.4).

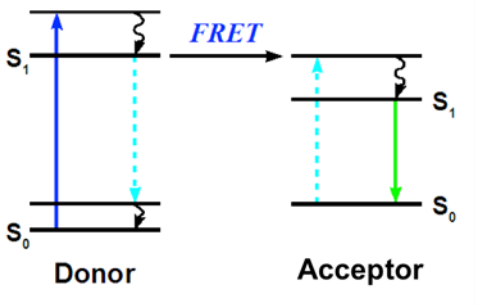

Figure 3.4 Representation of the FRET mechanisms by the electronic states of the donor and acceptor chromophores molecules. S_0 is the non excited state and S_1 is excited state of the molecules. The continue and dotted arrows represent radiative and non-radiative phenomenon relatively, while the black curved arrows represent the relaxation effect.

The efficiency of the energy transfer is inversely proportional to the sixth power of the distance between donor and acceptor, for this reason FRET is highly sensitive to sub-

nanometer distance modulations. The Förster radius (R_0), is specific to the couple of chromophores and it ranges between 2 to 8-10 nm (Figure 3.5). Having said that, in order to form a FRET couple the chromophores should have an overlap between the donor emission and the acceptor excitation bands to allow the energy transfer.

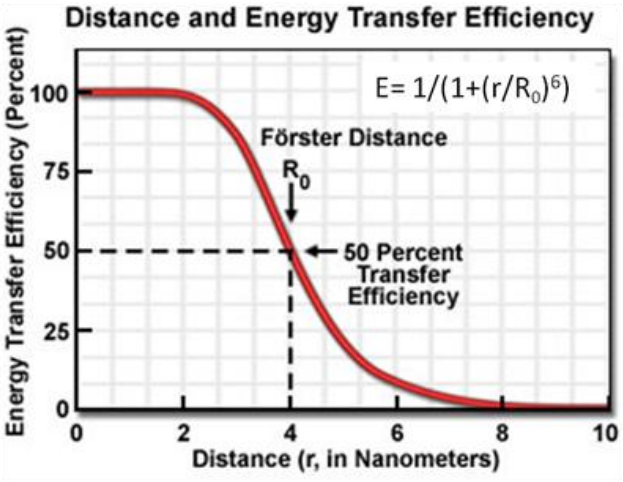

Figure 3.5 FRET efficiency versus gap distance in nanometers graph. The Förster radius (R_0) is at the 50% of efficiency. The efficiency formula is written in the graph where "r" is the real gap distance and R_0 the Förster radius.

The FRET technique is widely used in biology to detect molecular binding because, selectively to the gap distance, we can have different emission in case of binding. Irradiating at wavelength of donor's excitation we can collect donor's emission if there is no binding and acceptor's emission in case of binding of the two molecules. In spite of its high sensitivity the application of this technique has also two severe limitations. The first is the photobleaching effect that is a photochemical destruction of the dye molecule during the time of exposure to light irradiation; this problem can affect the long time experiments like time-lapse monitoring[54]. The second is the extremely narrow dynamic range: the modulation of energy transfer is limited to few nanometer around R_0, thus, the FRET is not suitable for applications that demand to detect changes in long distances range.

3.5 Nano-actuation detection techniques: Surface Plasmon Resonance

In the nanometer distance detection of architectural changes Surface Plasmon Resonance (SPR) technique is a valid alternative to FRET. This technique is based on the particular properties of conductive electrons in metal surface. At interface of metal surfaces the incident light can stimulate the collective oscillation of conduction-band electrons named plasmon waves; the plasmon excitation efficiency is maximal in when the incoming light frequency

equals the natural frequency of the collective surface oscillations (plasmons) of the free electrons at the Fermi level.

The SPR effect is based on the propagation of the plasmonic waves confined on the metal surface. These waves, called polaritons, are confined at the boundary between metal and the dielectric medium and have a propagation direction parallel to the metal/dielectric interface. For this reason they are very sensitive to any changes of the dielectric properties at the surface, such as following the deposition of organic material. The incident light generates at metal/dielectric interface an evanescent plasmon wave with a cross section that increases with the roughness of the bulk metal surface. In the case of metal nanoparticle these collective oscillation are confined on the limited surface of the particle and they exhibit enhanced near-field at the resonant condition. This field is highly localized on the nanoparticle surface and decays rapidly in the dielectric medium away from nanoparticle: it is known as Localized Surface Plasmon Resonance (LSPR)[55]. The LSPR frequency depends strongly on the composition, size and shape of nanoparticle. Furthermore the combination of more nanoparticles can provide an even higher field enhancement at specific inter-particles points, named "hot spots" which have been exploited for biosensing and SERS enhancing[56].

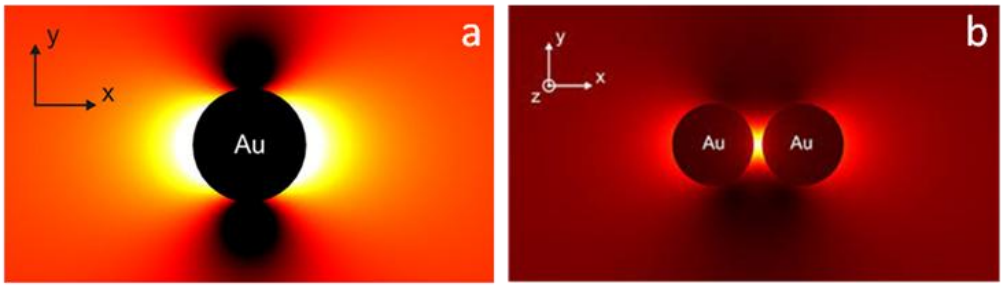

Figure 3.6 Representations of EM field intensity on (a) ideal gold nanosphere due to the its LSPR with polarized incident light. (b) In the case of nanospheres dimer the LSPR can create an hot spot in the gap between them.

Among the few materials that exhibit interesting plasmonic properties, gold was choose for two additional important properties: its inertness – gold is not easily corroded, does not oxidizes and maintain its properties in air and in water; its functionalization ability – the only exception to gold inertness is represented by the Au-S interaction which is exploited to decorate Au surfaces with a large number of organic molecules. For these reasons, Au is the most used metal to create plasmonic architectures with nanoparticles in order to enhance near-field properties for bio-detection. Starting to a simple dimer of gold nanospheres a large

variety of AuNP have been created[38]. The DNA nanotechnology and in particular DNA origami is an optimal strategy to assemble NPs in novel plasmonic architectures.

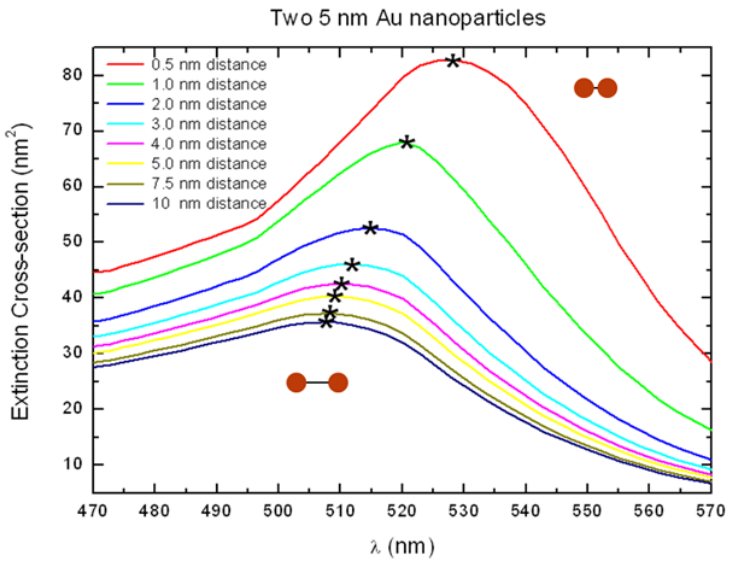

Figure 3.7 Graph that represents the plasmon ruler concept between two 5 nm gold nanoparticles. The plasmon resonance peak position is shifted depending on the increasing of the inter-particle gap.

The plasmonic near-field properties of AuNP dimer can be exploited also to measure the gap between two or more Au nanostructures. The resonance peak wavelength of a AuNP dimer is red shifted from the single nanoparticle situation because of the interaction of the two LSPR near-field. Based on this concept, it can be created a sort of plasmonic ruler between two AuNP only analyzing the relative shift of their plasmon resonance peak. In specific, subsequent to a decrease of the inter-particle gap we have an increase of red shift and *vice-versa*. Depending on the particle size and shape the detectable gap distance range can reach tens of nanometers.

The LSPR of nanoparticles can be a valid alternative to FRET technique in bio-molecular sensing for two main reasons. Firstly, since dye molecules are not involved, the LSPR is not affected by degradation during the time overcoming the problem of photobleaching effect in FRET measurements. Secondly, adjusting the size and shape of metal nanoparticles, the detectable range of distance is considerable higher than the few nm range of FRET, providing a longer distances analytical tool. Moreover the plasmonic properties of nanoparticles like LSPR are absolute in value and so, the relative spectral shift do not depend on the quantity and/or intensity of the near-field events. On the contrary, FRET efficiency depends strongly on the intensity of the emitted light that in turn, depend on the quantity of the emitting molecules.

Chapter 4

Materials and Methods

4.1 DNA origami design

The design of DNA origami structures can be performed by using few available software that calculate the spacing of the double helix and the place where it is possible to form DX crossovers. Usually, they also provide a graphical overview of the 3D structural assembly. The most used are SARSE-DNA origami, NanoEngineer 1 and CaDNAno. SARSE has been developed by Ebbe Andersen and colleagues in Aarhus, it is a free download software and presents an user friendly interface and a 3D generator. The editing and automatic folding with staple strands present some complexity and problems[57]. NanoEngineer 1 is an open source software to construct DNA folding designs, is not user friendly and quite time consuming because the crossover require to be added manually one by one. Shih and colleagues developed CaDNAno that is an open source design software based on the finite elements analysis performed by CanDo (Computer-Aided eNgineering for Dna Origami) previous developed by Mark Bathe from MIT[58]. The latter is the most used software to create DNA origami because its interface is simple and the process of folding is complete and automatic; there are two version: "squared" and "honeycomb" depending on the type of the lattice involved. The second version of CaDNAno is based on the Autocad Maya© platform and can create clear 3D graphical helices representations (Figure 4.3)[59]. In this project I used CaDNAno to design both the rectangular shape (Figure 4.2) and the asymmetrical hatch (Figure 4.1)[53]. Once the DNA origami design is complete, the staples are defined. The staple/scaffold crossovers are placed properly and the scaffold sequence can be chosen and inserted in the design. In this way all the staples sequences can be generated and listed. In the case of the most common circular M13 phage scaffold the available length is 7249 nts but also linear or synthetic scaffolds can be used depending on the requirements.

The origami structure can now be obtained by a simple self assembly process where the scaffold and staples strands are mixed together in a buffered solution allowing them to anneal. Usually the staples are mixed in excess (10-100 times) with respect to the scaffold and the buffer used is commonly composed by Tris (40 mM), acetic acid (20 mM), EDTA (2 mM), and $MgCl_2$ (12.5 mM) forming the 1X TAE/ Mg^{2+}. Mg^{2+} is essential to ensure the correct folding of multiple crossovers because it neutralizes and stabilizes the negatively-charged phosphodiesters by bridging them together. Moreover Mg^{2+} provides a good sticking *via* salt bridge to the mica substrate important in atomic force microscopy imaging.

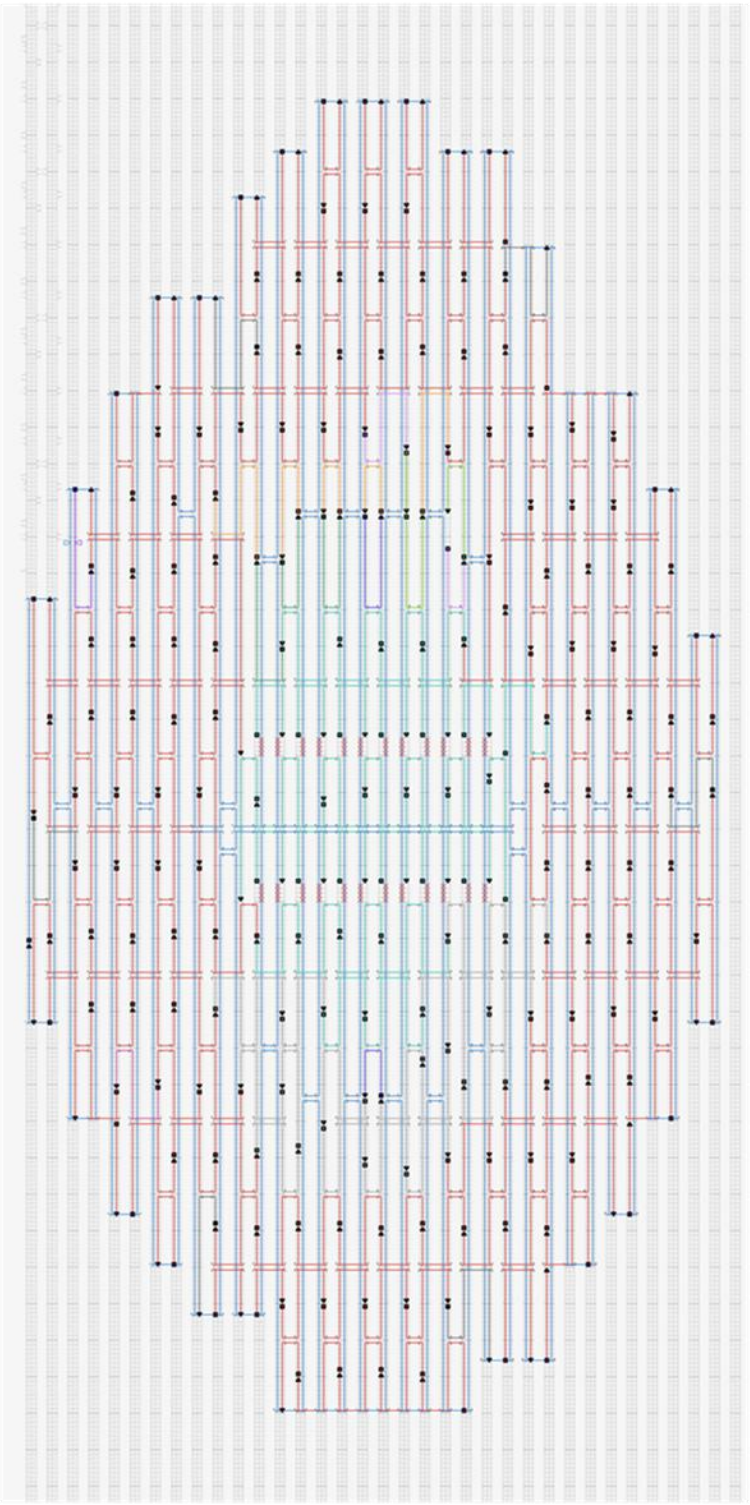

Figure 4.1 Asymmetric hatch DNA origami design obtained with caDNAno software package. The scaffold strand (in blue) is folded with the staple strands starting from the first row on the top. In pink and light green are highlighted the catchers staples, while in pink are the modified staple to close one flap.

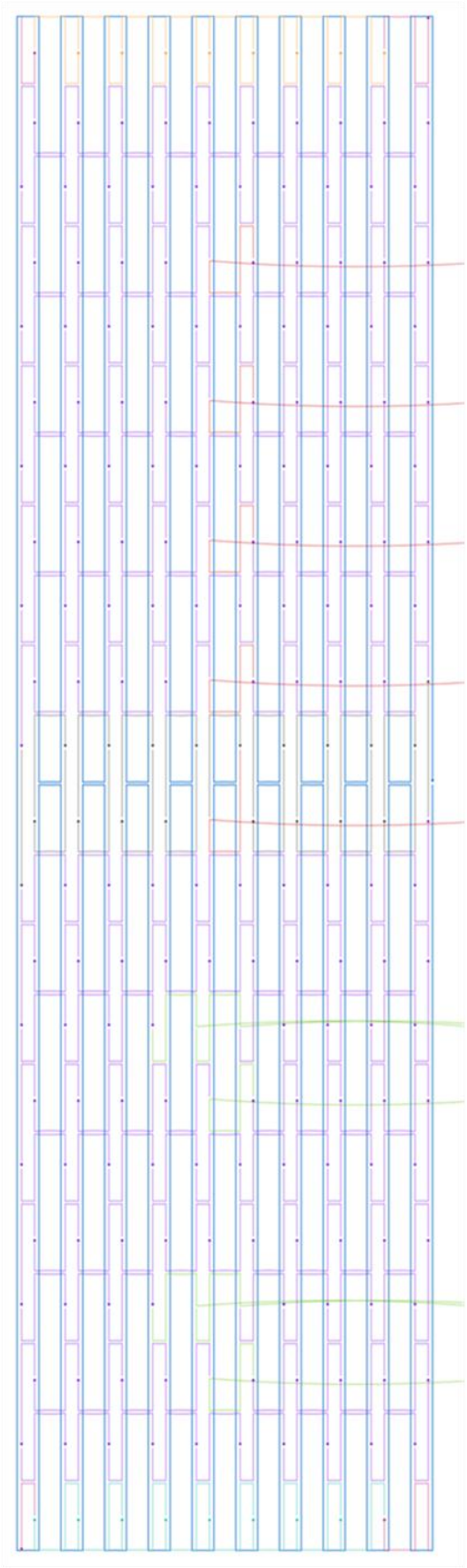

Figure 4.2 Rectangular DNA origami design obtained with caDNAno software package. The green and red are catchers strands for NP and NR.

The solution is heated to 90° in order to denature the DNA strands and then they are hybridized by a slowly cooling to room temperature (RT)[15].

The cooling process can vary depending on the complexity of the design and can be carry on with a simple thermocycler. In particular the more complex is the structure, the slower will be the cooling process, and this is particularly important for 3D structures.

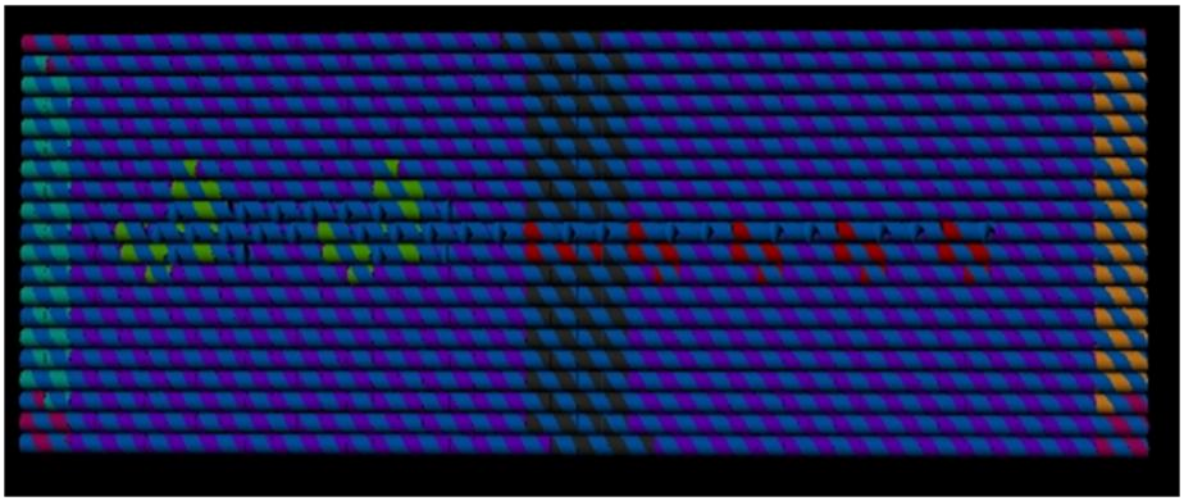

Figure 4.3 Top view of 3D graphics of rectangular DNA origami design obtained with caDNAno software package. The green and red are catchers strands for NP and NR. The black are staples involved in the seam.

The success in the creation of a complex 3D DNA origami structures rely not only on a careful design but also on an extremely long cooling process after the de-hybridization of all the DNA mixture. It has been proved that a specific cation (Na^+/Mg^{2+}) concentration and a very slow process are fundamental to produce properly folded large and complex structures. The Mg^{2+} concentrations can vary from 10 mM to 16 mM and the cooling process can last up to 173 hours[18].

Folded constructs were purified from the excess of staple strands using Amicon Ultra 0.5 ml 100 kDa (Millipore, Massachusetts) filters, adjusting the protocol supplied by the constructor. Briefly, 2x TAEM solution was added in the same amount of sample volume; capped Amicon Ultra were centrifuged four times for 1.5 minutes at 14000 g. Concentrated samples were eluted spinning the inverted filters in a clean vial at 2000 g for 3 minutes.

The probe, target and competitor sequences were built using the rules of no self-annealing, no loops in each sequence, no strong dimers and 50% GC, that were checked using the on-line tools of IDT's Oligo Analyzer® v.3.1 (Figure 4.4)[60]. An exception was made for the target as it includes a 18 bp GC clamp (C120).

When used for actuation, the target was added in a 100:1 concentration relative to the probe and let react for one hour at room temperature. In order to demonstrate the reversibility of the origami actuation, the origami was first actuated by adding a not perfectly probe matching (S64) target, in a 100:1 concentration relative to the probe; then the origami initial configuration was re/established by adding the competitor in a 10:1 concentration relative to the target[60].

"PROBE"	5'- CGATCCGACCTTCCTCCCTTGTGGTGAAGGTTTCCACACCTCAC TGAATTGTCTTTGAACGACAGTTCGAGCTTGTTGTGTTTGAAAC TGATTTCCTAAGGCAGCTTCCCGGGCTCGCAG-3'	120 nts
"C120"	5'- GGGCGGGGCGGGGGCGCGGCCTTAGGAAATCAGTTTCAAACAC AACAAGCTCGAACTGTCGTTCAAAGACAATTCAGTGAGGTGTG GAAACCTTCACCACAACGCGCCCCCGCCCCGCCC-3'	120 nts
"L84"	5'- GCCTTAGGAAATCAGTTTCAAACACAACAAGCTCGAACTGTCG TTCAAAGACAATTCAGTGAGGTGTGGAAACCTTCACCACAA-3'	84 nts
"S64"	5'- CAAAAGGAAGCATTTGACAGATACGCAGAACTTGTCTGTCACA ATACTTT CCAGACAATGCGAC-3'	64 nts
"C64"	5'- GTCGCATTGTCTGGAAAGTATTGTGACAGACAAGTTCTGCGTAT CTGTCAAATGCTTCCTTTTG-3'	64 nts

Figure 4.4 Sequences of the probe, targets and competitor used for the DNA origami actuation.

4.2 Nanoparticles synthesis

Unless otherwise specified, chemicals and reagents were purchased from Sigma-Aldrich. The 3' thiol-capped DNA oligonucleotides were purchased with HPLC purification from Sigma-Aldrich. The gel filtration columns used to desalt DNA solution from DTT were illustra™ NAP5 and NAP10 Columns from GE-Healthcare. Syringe nylon filters (0.22 μm cut-off) were purchased from Teknokroma. The gold colloids used for dimers creation were synthesized following a revised version of the Turkevich method[61]: a 150 mL of sodium citrate (2.2 mM) solution was heated up to the boiling point, under continuous stirring and without refluxing system. Then 1 mL of $HAuCl_4 \cdot 3\ H_2O$ (25.4 mM) was added and the solution was kept stirring for 5 minutes until the color change from light grey to ruby red. The solution was left cooling down to RT and filtered with 0.22 μm syringe filters (Teknokroma) before use. AuNP concentration was determined by UV-Vis spectroscopy assuming an

extinction coefficient of 1.57 x 10^9 M^{-1} cm^{-1} at 520 nm. The average particle diameter measured from SEM analysis is 17.3 ± 2.5 nm.

4.3 Nanoparticles DNA functionalization and dimers creation

Au nanoparticles were functionalized following several steps. First a coating with BSPP (Bis(p-sulfonatophenyl) phenylphosphine dihydrate dipotassium salt) was carried on following published procedures[62-64]. Briefly 36 mL of colloids solution are left to incubate over night with 14.4 mg of BSPP. Then the particles are centrifuged to remove supernatant before being rinsed, concentrated and resuspended in 2.5 mM BSPP in approx. 2 mL. Second, since the commercial DNA oligoucleotides are protected with disulfide bond, before use, they were reduced with DTT (0.37 M) in a solution with NaCl (0.3 M) and sodium phosphate buffer (0.01 M NaH2PO4/Na2HPO4, pH 7.04) for at least 2 h of incubation. After filtration with NAP5/10 columns the oligonucleotides are mixed with colloids solution (final concentrations ~0.33 nM AuNP, ~2 μM oligonucleotide). After 24 h sodium phosphate buffer (10 mM) was added and the solution was incubate over night. In a subsequent salt-ageing process, NaCl solution was added to reach the concentration of 0.1 M in 6 steps during 48 h. To remove free oligonucleotides that didn't react, the solution was centrifuged (8 min at 10000 x g) and the supernatant was removed. The dark red precipitate was redispersed in buffer (TAE 1X, 0.1 M NaCl) and stored at 4°C.

In order to create dimer I developed two alternative methods (described in chapter 5): called "aggregation" and "disaggregation" method. In the "aggregation", the solution of NP (20 nm, TedPella Inc.) functionalized with DNA oligonucleotide and the solution of NP functionalized with the complementary DNA oligonucleotide were processed separately[65]. In both solutions NP and unreacted free oligonucleotides were separated by centrifugation (8 min at 10000 x g) and supernatant oligonucleotides were partially removed. The remaining solutions were resuspended and mixed with 50:50 volume ratio. The total removal of oligonucleotides yield instead large aggregates. DNA hybridization was promoted heating up the solution for 45 minutes at 50 C and left cooling to RT over night in a tube rotator (Stuart) agitation.

In the "disaggregation" method I followed the same procedure described above, but in both solutions unreacted free oligonucleotides were totally removed by 3 centrifugation steps (8 min at 10000 x g). The resulting NP solutions were resuspended and mixed with 50:50 volume ratio resulting in fast aggregation of large NP clusters. One or both DNA complementary oligonucleotide were added with variable molar concentrations. Then the solution was heated up for 45 minutes at 50 C and left cooling to RT for at least 1h.

4.4 Nanorods synthesis

In order to create nanorods (NRs) suitable for placing on the rectangular DNA origami I tried to synthesize NR 60 nm long and 20 nm large. I chose a new method with a good possible tuning of the NR dimension using additives[66]. First, I prepared a seed solution in which 5mL of 0,5 mM $HAuCl_4$ were mixed under vigorous stirring with 5mL of 0,2M CTAB. Then I added 1mL of 6mM NaBH4 directly injected in the solution, I stopped the stirring after 2 min (color change from yellow to brownish-yellow) and I left aging for 30 min at RT. Afterward, a growth solution has been prepared: in which I dissolved 2,25g of CTAB and 0,275g of 5-Bromosalicylic Acid in 62,5mL hot H_2O mQ (50°-70°C) in a three necks round bottom flask, then left to cool to 30°C. Then I added given volume of 4mM AgNO3 solution, typical 3 mL, and I left the solution undisturbed for 15 min at 30°C. After I added 62,5mL of 1mM HAuCl4 keeping 15 min in a slow stirring at 30°C. To complete the growth solution I added 0,5mL of 0,064M ascorbic acid stirring vigorously for 30s until the solution became colorless. The growth solution has to be used right after the preparation.

Finally, I mixed 0,2mL of seed solution with the growth solution and then stir for 30s and I left undisturbed at 30°C for 12h for NR growth. After I purified the products by centrifugation at 8500 rpm for 25 min. I removed the supernatant and re-dissolved the precipitate in 10mL of H_20 mQ.

The tuning and control on the dimensions of the NR is possible varying accordingly the volume of 4mM AgNO3 solution and the amount of seed solution when it is mixed with growth solution.

4.5 Nanorods functionalization

For the functionalization of the NR with thiol-capped DNA oligonucleotides, I chose a new method with low pH in order to use less DNA molecules (the NR surface is much larger than NP)[67]. As explained in chapter 5 the low pH forces the CTAB to leave the gold surface exposing the unprotected gold surface. In this way the thiolated DNA has easy and fast access to create the covalent Au-S bond.

First of all, I prepared the NR1 buffer (1X TBE,0.4 M NaCl, 0.02% SDS) adjusting its concentration at 5X and its pH at 2.4. Then, I de-protected and desalted the DNA with same strategy of NP functionalization in order to have 1.5 mL of final volume and a DNA concentration in the order of 1-10uM. Immediately after that, I added 0.5 mL of NR1 5X to reach a pH around 3 in 2.5 mL total solution, because right after, I added 0.5 mL of AuNR purified solution leaving at 24°C in agitation for at least 30 minutes. At this point, we can

centrifuge the solution at 6000 x g for 5 minutes and resuspend it vigorously in 1X TBE, 0.1 M NaCl pH 8 buffer for 3 times, and store at 4°C.

4.6 Electrophoresis

The visualization and separation of NP aggregates was carried on with a electrophoretic analysis in agarose gel 3.6 % (0.5X TBE, pH 8.0, ~ 7 V/cm) for ~15 minutes of run. The visualization and separation of DNA origami and/or NP was carried on with a electrophoretic analysis in agarose gel 1 % (0.5X TBE, pH 8.0, ~ 7 V/cm) for ~30 minutes of run. In every gel pocket 17 μL of sample plus 3 μL of loading buffer (10mM Tris, 60mM EDTA, 60% Glycerin, pH 7.6) were loaded. The DNA staining was assured from addition of 1X of GelRed™.

4.6 Extraction and purification of nanoparticles and/or DNA origami from agarose gel

After the agarose gel electrophoresis the nanoparticles bands and/or DNA origami can be extracted and purified from the excess of buffer. I used D-Tube Dialyzers devices purchased from Merck-Millipore and used following the manufacturer's protocol, this ensured the highest purity of the extracted sample. Basically, I cut the band of interest and placed inside the tubes with buffer. These tubes have a nitrocellulose membrane window that allows the ongoing of the electrophoretic run inside them. In such a way the NP/DNA origami continue the electrophoretic run and exit the gel band going inside the tube buffer. The solution so obtained can be centrifuged (8 min at 16000 x g) and the pellet can be re-suspended in ~ 20 μL for the subsequent use.

4.7 DNA origami AFM characterization

In the AFM characterization the DNA origami samples were dispersed on a freshly cleaved mica surface in a saline buffer (125 mM MgCl2, 400 mM Tris-HCl, 10 mM EDTA, 20 mM NaCl, pH 8.0). The large concentration of positive ions, mainly $Mg2^{+}$ has the functionality of screening the negative charges present at the mica surface and on the external structure of the dsDNA, allowing the adhesion of the origami to the mica surface. Samples were let sediment for at least five minutes and were never rinsed or dried. The AFM images have been recorded using either a JPK Nanowizard II, a VEECO Multimode with Nanoscope V control or an Asylum MFP3D AFM system. All the AFM instruments where operated in liquid in non-contact mode. I used Olympus OMCL-TR400PSA tips with a force constant of 0.08 N/m and a resonance frequency of 34kHz, in air.

4.8 DNA origami SEM characterization

The DNA origami with and without nanoparticles was also analyzed by the SEM. A clean piece of silicon with a layer of silicon oxide of 200 nm was previously treated with oxygen plasma to make the surface more hydrophilic and then a droplet (5 μL) of purified DNA origami solution was left to adsorb for 7 minutes and washed with water to remove salt crystals. After drying, the sample was imaged with SUPRA 40 (Zeiss) scanning electron microscope at 4 kV.

4.9 DNA origami TEM characterization

The rectangular DNA origami with and without nanoparticles was also analyzed by the TEM. A copper grid (TedPella Inc.) with a layer of carbon film was previously treated with oxygen plasma to make the surface more hydrophilic and then a droplet (5 μL) of purified DNA origami solution was left to adsorb for 5-10 minutes and washed with water to remove salt crystals. A solution of OsO_4 has been used to stain the organic DNA material. After drying and gentle washing, the sample was imaged at 80 kV.

4.10 Direct gel absorption measurements and data analysis

UV-Vis characterization of the plasmonic shift is discussed in chapter 5; however the used method and data fitting is following described in details.

UV-Vis characterization was performed on inverted optical microscope (Axiovert 200, Zeiss) in transmitted light illumination (HAL 100 illuminator, Zeiss) coupling a microscope with 750 mm long spectrometer (Shamrock SR-750, Andor Technology plc.). The agarose gel resulting from the electrophoretic procedure with distinguishable bands was placed onto clean glass coverslip that was mounted on XY sample stage. The light transmitted through the sample was collected by 100x immersion objective (NA 1.45, α Plan-FLUAR, Zeiss), directed into a spectrometer, split by a diffractive grating of 600 lines/mm, and finally analyzed using TE-cooled EMCCD (Newton DU971-UVB, Andor Technology plc.). The raw extinction spectra are plotted using the equation:

$$E = (I_0 - I_i)/(I_0 - I_{bg}) \quad (1)$$

where I_i is the corresponding intensity of light passed through each band, and I_0 is the intensity of light passed through the clean gel in a position without origami. I_{bg} is a background dark signal of CCD. At least 5 different positions along each band were characterized and finally averaged[60].

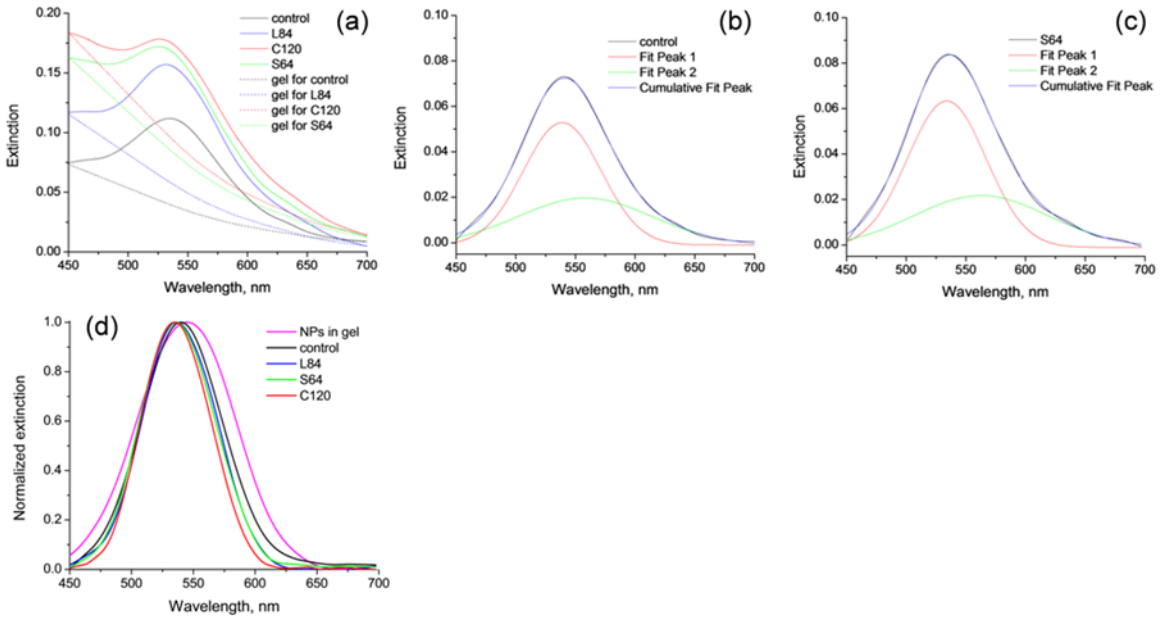

Figure 4.5 (a) The raw extinction spectra of lane 3-6 displayed in Figure 5.28 together with corresponding gel thickness corrected backgrounds. (b,c) An example of fitting procedure for control origami (b) closed configuration, and (c) actuated open structure with two Gaussian functions in the range of 450-700 nm. (d) The extinction spectra after background subtraction and normalization procedures.

The resulting spectra show a peak in the range of 525-535 nm which is attributed to the LSPR in single gold NPs or dimers. The spectra also demonstrate a different extinction at low wavelengths complicating an estimation of LSPR position. Since the gel density, gel hydration and AuNP size in each series of experiment are supposed to be constant the difference in the extinction is caused by a variable gel thickness in a position of the lanes. To determine the LSPR position we applied two steps procedure. At first step, the gel thickness corrected background was plotted for each spectrum (Figure 4.5a) and then subtracted. Second, the resulted spectra were fitted with two Gaussian functions in the range of 500-600 nm considering i) LSPR in spherical gold NPs at about 530 nm[68], and ii) an additional peak in the range of 560-600 nm. The last one is caused either by a non-sphericity of gold NPs[69] or possible plasmon coupling effect[55], which are inseparable in our case. An example of such fitting for closed and open origami is shown in Figure 4.5b-c. This allowed to determine the LSPR positions for three series of experiments resulting in 6.0±1.0 nm, 5.7±0.5 nm, and 3.6±0.7 nm blue shifts in respect to the control sample for C120, S64, and L84 targets respectively, and summarize the data in the box plot displayed in the inset of Figure 5.29. For comparison Figure 5.29 is re-plotted after background subtraction and normalization. The figure shows the broadening of LSPR peak in case of closed origami or highly packed NPs in

gel due to plasmon coupling effect (dimer effect) and highlights that the determination of actual extinction peak position requires the fitting procedure[60].

4.11 Nanoparticles dark field optical visualization

The nanoparticles dimer have shifted plasmon resonance respect to the single NP configuration. The resonance difference can be registered also by the wavelength of the scattered light. For this reason I tried to visualize NP dimer using dark field microscopy. In this particular inverted optical microscope configuration all the incoming light is focused by the high numerical aperture (NA) objective on the sample but only the light scattered with high angle is collected by the same objective and transferred to the camera. In this way the most rough objects on the sample (like NP on a flat surface) are the only visible ones. Coupling the tube lens exit with the entrance slit of a 300 mm spectrophotometer we can analyze the wavelength of light coming from specific part of the sample and we can compare different spectra from selected areas.

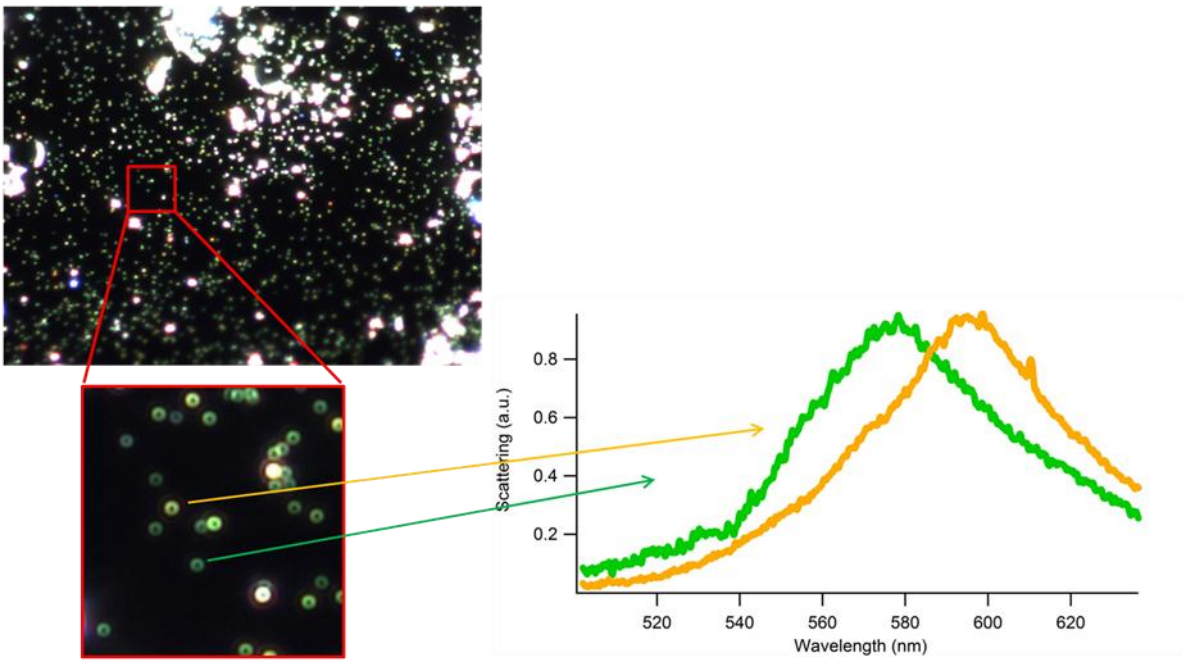

Figure 4.6 Example of dark field imaging of the NP aggregates solution. In the zoomed image the different scattered light wavelength (color) coming from different aggregates can be appreciated. The latter is confirmed by the spectra reported in the graph.

The NP solution, typically 5-10 μL, is left to deposit on a clean piece of silicon, then washed and dried. The area presents lighting dots that can be analyzed in wavelength (Figure 4.6). The main advantage of this technique is that I can investigate and recognize the plasmon resonance of individual NP dimer or aggregates purifying the solution from the abundant residual of single AuNP. In Figure 4.6 is presented an example of different plasmon

resonance acquired from different NP structures. The analyzed gold NPs are 60 nm in diameter and unfortunately it has been seen that moving to 20 nm the intensity of the scattered light dropped below the system noise and it was not possible to apply this approach to the origami decorated with 20 nm AuNP. Due to the optical detection limit, to have correspondence with the real NP structure is necessary to imaged the same NP aggregates by SEM or TEM.

Chapter 5

Results and Discussion

Project Rationale

The objective of my PhD project was based on the application of a movable DNA origami to create a continue and reversible tunable plasmonic architecture. More in detail, I aimed at tuning the plasmon resonance between two gold nanoparticles. The motivation behind this idea was threefold: the AuNP pair can be seen as a Plasmon ruler tightly linked to the DNA origami structure, that can be used to monitor and quantify the motion of the DNA origami upon actuation. On the other hand, the DNA origami can be seen as an actuator that can be operate to tune the inter-particle distance, providing a spectral response univocally linked to the state of the origami itself: in this way the origami-AuNP hybrid structure can be operated as a biological sensor, that transduces a molecular recognition event into an optical shift. Finally the inter-particle distance can be tuned to switch on and off a Raman sensitive hot spot, thus creating a tunable SERS substrate.

The starting point of my project was the DNA origami hatch developed in our laboratory that already included an effective actuation mechanism triggered by specific stimulus. However the analysis of the system status was limited to the recognition of the ON/OFF transition. The FRET system was able to distinguish only two states OPEN/CLOSED and real information about movement amplitude, angles and forces that are playing during the actuation were still missing. This condition was sufficient to assure a bio-detection of DNA/RNA strands but it was not sufficient to explain in detail the target-actuator interaction. One of the goal of this project is to understand the differences in the structural displacement between various target sequences and the actuator. In particular I wanted to investigate the distances, angles and forces provided by different targets and how this can affect the opening of the hatch architecture.

Since the actuation flap displacement could reach tens of nanometer distances the FRET technique was not suitable for the purpose. Thus, in order to have a continuous informative tool with a stable signal and wider distance range of sensitivity I chose to use LSPR technique to overcome these few but basilar limitations to reach the information required. I implemented a plasmonic architecture using two gold nanoparticles on the existing DNA origami structure, one on flap edge and the other on the external ring in the place of the two donor and acceptor FRET molecules. After the target addition and so, the actuation the distance between the two

AuNPs should change and the LSPR should change accordingly. Setting up a direct absorption analysis I would be able to register the LSPR shift between the different states of the origami actuation generated by different DNA targets additions. The creation of this hybrid structure allows to have a continuous and reversible tuning of the LSPR between gold nanoparticles using a DNA origami platform. Nevertheless the engineering of the DNA targets strands could give a good control on different LSPR tuning never reached before.

Moreover, the analysis of fixed AuNPs positions using the addressable precision of the DNA origami assembly can provide a correlation between inter-particle gap distance and the registered LSPR shift. This is fundamental to construct a calibration for a plasmonic ruler exploiting DNA origami that can be used to measure not only linear distances in various DNA origami actuations structures but also distances in 3D architectural positions.

Once developed the plasmonic architectural tool I can employ the hybrid structure to detect DNA target strands with direct plasmonic analysis, and furthermore, I could modify the actuator to detect other molecules of research interest as proteins or aptamers.

5.1 Gold nanoparticles: nanospheres synthesis and characterization

In order to decorate DNA nanostructures with AuNP a few accessory methods are required: gold colloid synthesis, AuNP surface functionalization and the control of NP-NP interaction. The synthesis of gold colloid in particular, can in principle be overcame purchasing commercial solution, which are available on the market. However a detailed control of the synthesis offer a larger degree of freedom in term of AuNP size, shape and passivation. Indeed the synthesis of nanorods is also reported, although they did not find application in the our DNA origami structures, so far. Additional details of the different processes are presented in chapter 4.

The gold nanospheres used in this project are in the range of 10-20 nm of diameter. Since, at the beginning, to develop and optimize a AuNPs functionalization protocol several attempts were needed, the synthesis of large quantity of gold colloids was necessary. I decided to create AuNP around 20 nm diameter to match technical requirements for the DNA origami dimensions. Firstly I used the classical gold colloids synthesis with sodium citrate as reducing agent and CTAB (cetyltetrimethylammonium bromide) as surfactant to reduce NP-NP electrostatic interactions. The size of particles is controlled by the reducing agent concentration while CTAB surfactant cover the gold surface playing an important role in the shape elongation of the gold nano-object. After the synthesis the nanoparticles were imaged at Scanning Electron Microscope (SEM) to characterize the size and shape uniformity. Following this synthesis protocol I obtained large poly-dispersion in size and shape due probably to the weak control of reaction temperature that combined with CTAB, generates several shapes like spheres, triangles, and rods with different sizes (Figure 5.1). Furthermore, the nanoparticles size range obtained, as Figure 5.1 shows, was larger than the expected 20nm. In the gold nanoparticles functionalization procedures, especially in those based on thiol-gold interaction, the reactive molecules have to interact with the naked gold surface replacing by affinity any other adsorbed molecules. It has been reported that CTAB molecules are difficult to replace only by affinity thus, preventing the controlled formation of a well defined molecular functionalization. To overcome this problem the functionalization procedures reported in literature that employ CTAB require a strong acid pH to force, by electrostatic interactions, CTAB molecules to leave the gold surface exposing it to reactive molecules[67].

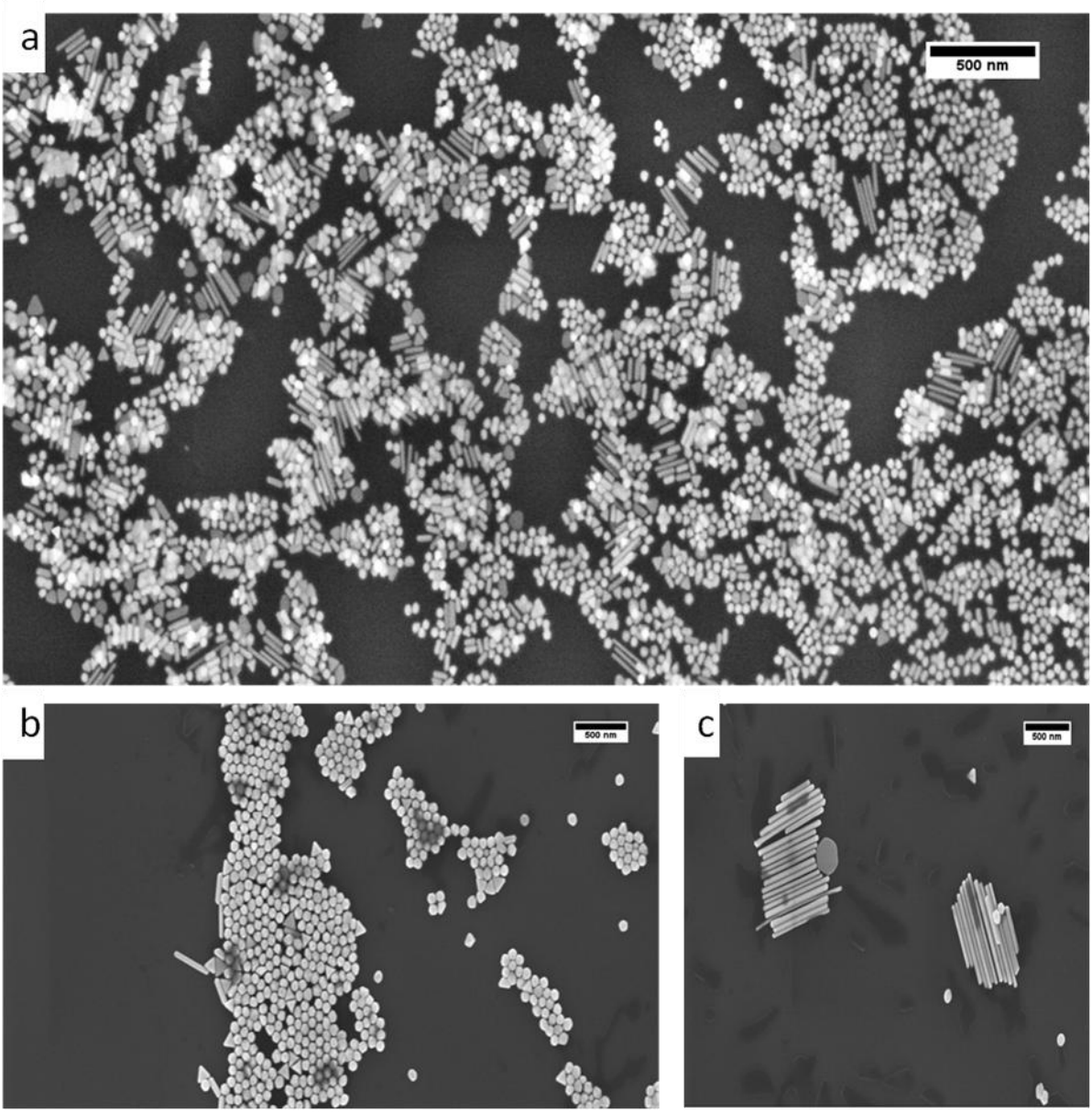

Figure 5.1 SEM images of gold nanoparticles of different synthesis with CTAB as surfactant. The size is larger than the expected 20 nm diameter and the shape is not under control. (a,b) Mixture of nanospheres, nanotriangles and nanorods without selectivity in size and shape. (c) Zoomed image of long nanorods.

In CTAB containing functionalization procedures the very low pH used can hydrolyze phosphodiester backbone of DNA and so, fast buffer neutralization is needed. These multiple passages between acidic and neutral conditions affect the long-term stability of DNA covered NP. Therefore, for my purposes, a strong acidic condition is not favorable. Additionally, in the synthesis of small gold nanospheres the reducing agent is sufficient to stabilize the colloids and so, the use of surfactants is not absolutely needed.

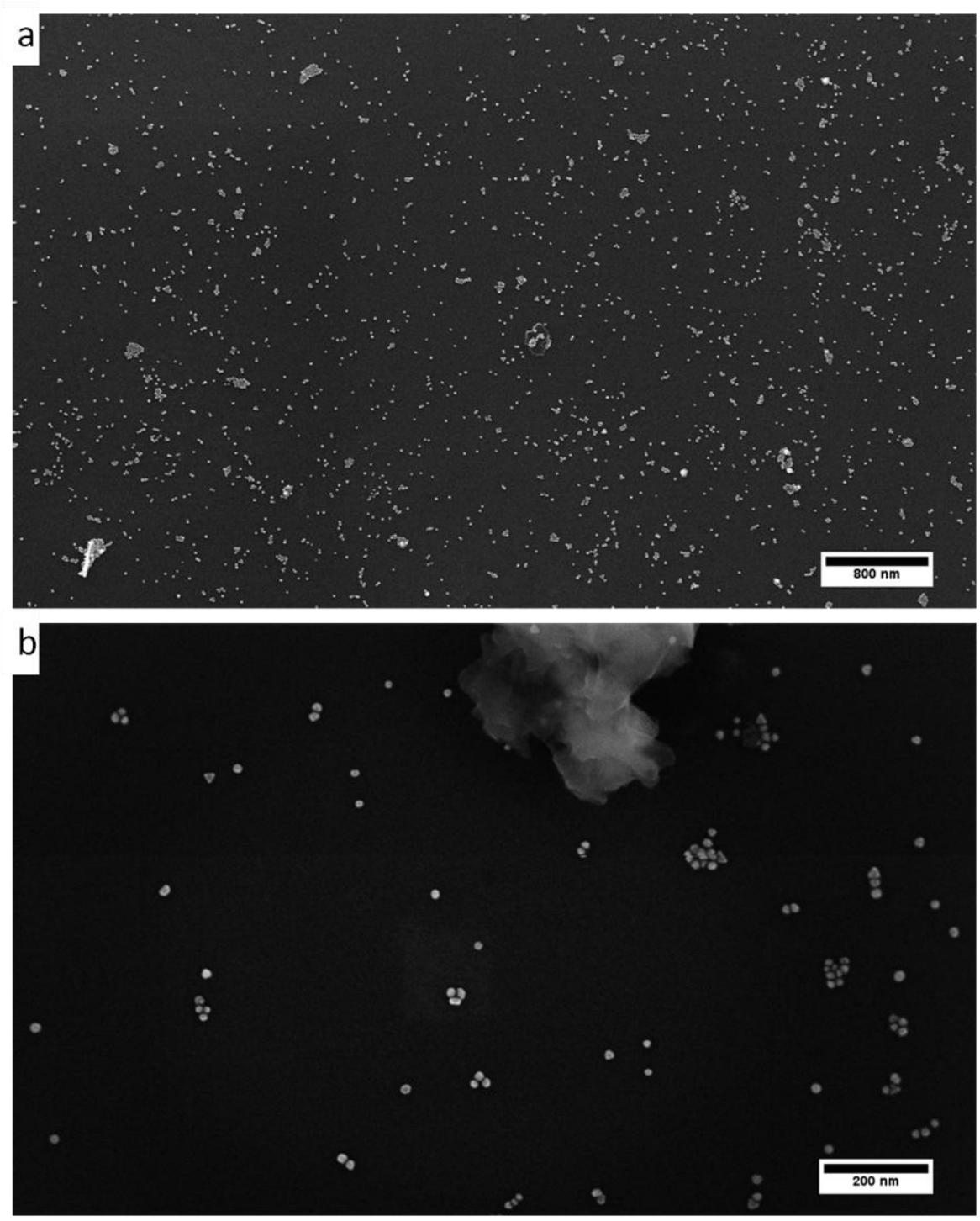

Figure 5.2 SEM images of gold nanoparticles of different synthesis without CTAB as surfactant. The average diameter is 17.3 ± 2.5 nm and no differences in shape were registered. (b) Although small aggregates, due to drying process, a majority of single NP are visible.

A good candidate is a revised Turkevich synthesis method[70] in which sodium citrate is the reducing agent but no surfactant are employed. Basically, a sodium citrate solution is heated up to the boiling point, under continuous stirring and without re-fluxing system. Then, a

$HAuCl_4$ solution is added and the formation of gold ions aggregates is displayed by the color change from light grey to ruby red. The solution is then cooled to room temperature (RT) and filtrated. The gold nanoparticles obtained were good in shape and presented a more homogeneous size dispersion (Figure 5.2). I evaluated the size distribution by spectroscopy and SEM statistical analysis founding 17.3 ± 2.5 nm average diameter.

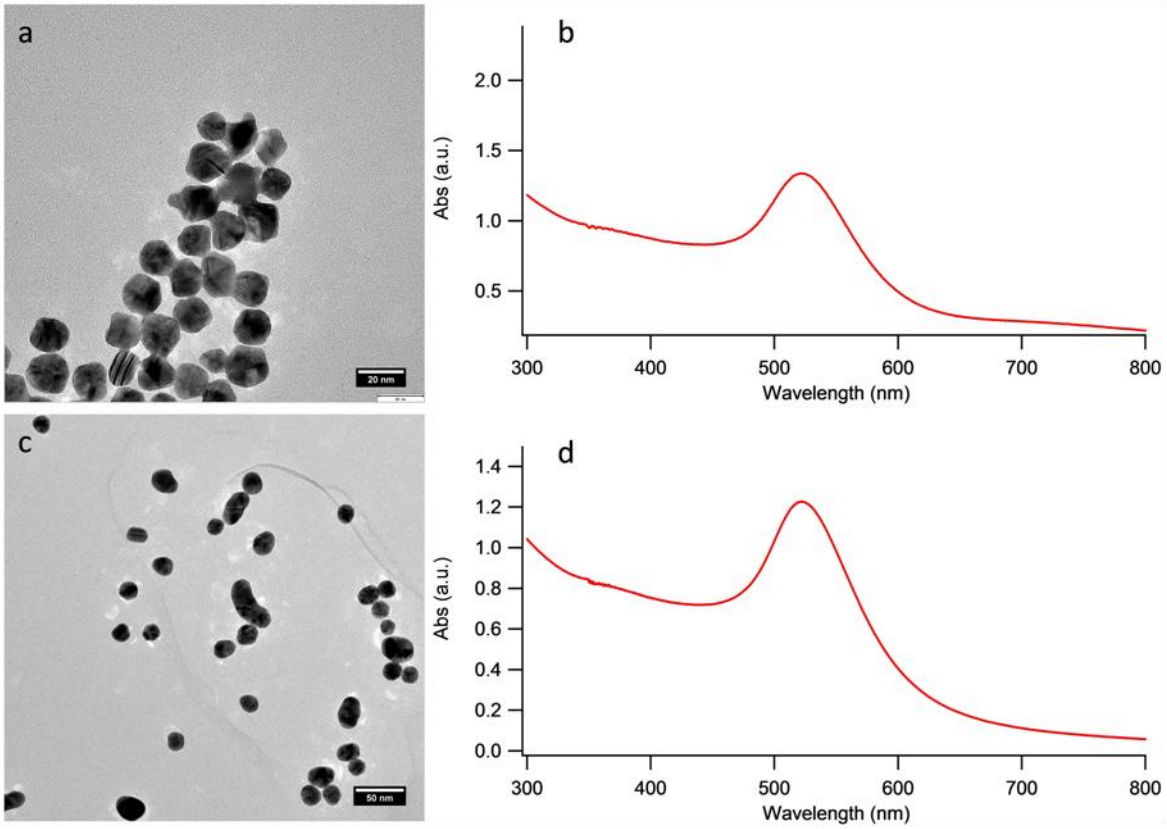

Figure 5.3 (a,c) TEM images of 20 nm gold nanoparticles synthesis. (a,b) Using high $HAuCl_4$/citrate ratio fused NP were obtained and absorption spectrum was too broad denoting large dispersion; while lowering the ratio (c,d) well separated NP were obtained with sharper absorption spectrum.

During the first part of this project these gold NP with 17 nm diameter, were employed in DNA functionalization to create dimers. Later, during my research period abroad at the Karlsruhe Institute of Technology[71], I took the opportunity offered by the long term experience of my hosts, to create precise plasmonic architecture with two NP and one nanorod (NR) to specifically enhance hot spot plasmonic properties. There I approached a synthesis protocol to synthesize exactly 20 nm gold NP with sodium citrate (details in chapter 4). The ratio between $HAuCl_4$ and sodium citrate was adjusted time by time to obtain the desired NP dimensions analyzing their morphology with transmission electron microscope (TEM) and correlating it with absorbance spectrum (Figure 5.3).

The procedure was optimized producing good dispersion in diameter, but a considerable size variability was still present comparing several synthesis attempts of same protocol. Since to get a precise LSPR shift in response to distance changes a standardization of NP dimension is highly required, in the DNA origami NP linking experiments I decided to use commercial available 20 nm gold NP to have the sharpest size dispersion possible. Figure 5.4 is representative of the high shape and size uniformity of the commercial gold nanospheres . The latter are coming from sodium citrate synthesis without any other surfactant molecule assuring good substrate for DNA functionalization.

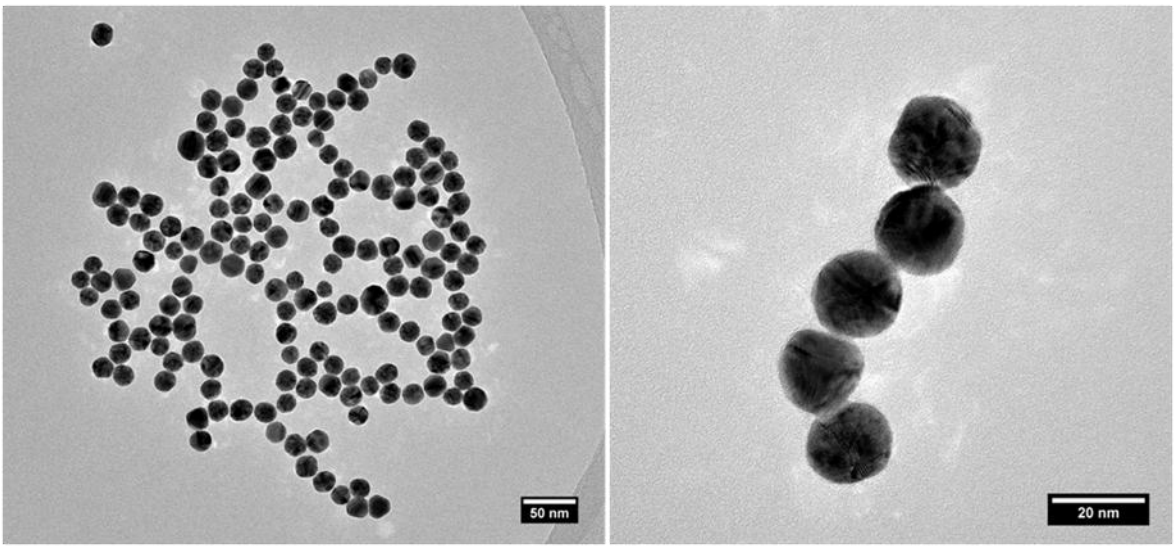

Figure 5.4 TEM images of 20 nm commercial gold nanoparticles. The NP are well separated and highly uniform in shape and size.

5.2 Gold nanoparticles: nanorods synthesis and characterization

During my research period at KIT I tried to functionalize DNA origami with precise assembly of nanoparticles to create a LSPR hot spot able of high enhancement. One of the main applications of this structure was the calibration of the LSPR ruler and the characterization of different plasmonic architecture such as a line composed by two NP and one NR. Despite I didn't finish the hybrid structure because of the lack of time, I synthesized gold nanorod following clear published method[66]. The key principle to obtain gold nanorod is the asymmetric elongation of gold seeds generates by CTAB molecules covering of the two long sides. Following this method I could tune the NR ratio between long and short side by changing the reagents volumes to reach the desired NR dimensions. In Figure 5.5 two different conditions are displayed. In figure 5.5a the used reducing agent/gold ratio was not suitable to create uniform nanorods. In figure 5.5b, instead, I was able to obtain straight rods

with the requested width but slightly higher length. This was the best condition available compatible with the plasmonic design for 2nd harmonic generation: indeed in this application the an accurate control of the rod diameter was more important than the control of the length . The use of CTAB molecules to synthesize NR re-proposed the problem of gold surface accessibility forcing to use different methods than classical DNA functionalization procedure. This problem and the use of acidic pH in DNA functionalization method is discussed in the chapter 4.

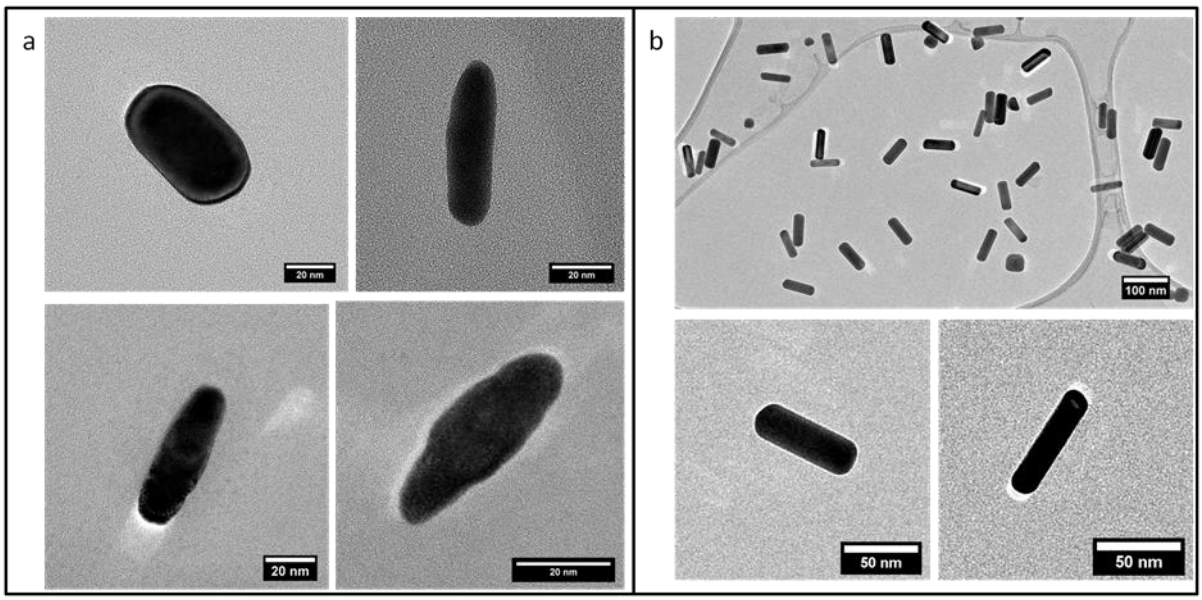

Figure 5.5 TEM images of gold nanorods different synthesis attempts. (a) The shape is not uniform and the sides are not close to desired dimensions, while (b) with different reagents volumes a good NR ratio and shape uniformity was obtained in addition to acceptable sides dimensions.

5.3 Gold nanospheres functionalization

The implementation of the two gold NP on the DNA origami is based on the classical functionalization with a ssDNA complementary to the respective catcher strand protruding out of the DNA origami surface. The success of a good covering of the gold nanospheres is dependent on the type of bond and on how the reactive molecules arrange themselves on the surface. The molecule surface density is tightly correlated with their disposition on the surface mostly because the stacking interaction along the molecular chains can increase a lot with higher concentration. On the contrary a low number of molecules could generates a large non-homogeneity on the surface that prevent the correct stand up position leaving most molecules laying down[72]. This effect confers an higher flexibility of the attached molecules leaving large portions of gold surface exposed and available for electrostatic interactions such as, for

example with the ions contained in the buffer solution. In this case, since the gold surface is negatively charged it tends to generate aggregation between NP because of the formation of an electrostatic salt bridge between exposed gold surface portions. In other words the functionalization procedure has to provide a sufficient number of molecules attached on the surface to allow the NP to be electrostatic stable in buffered ionic solutions like physiological media.

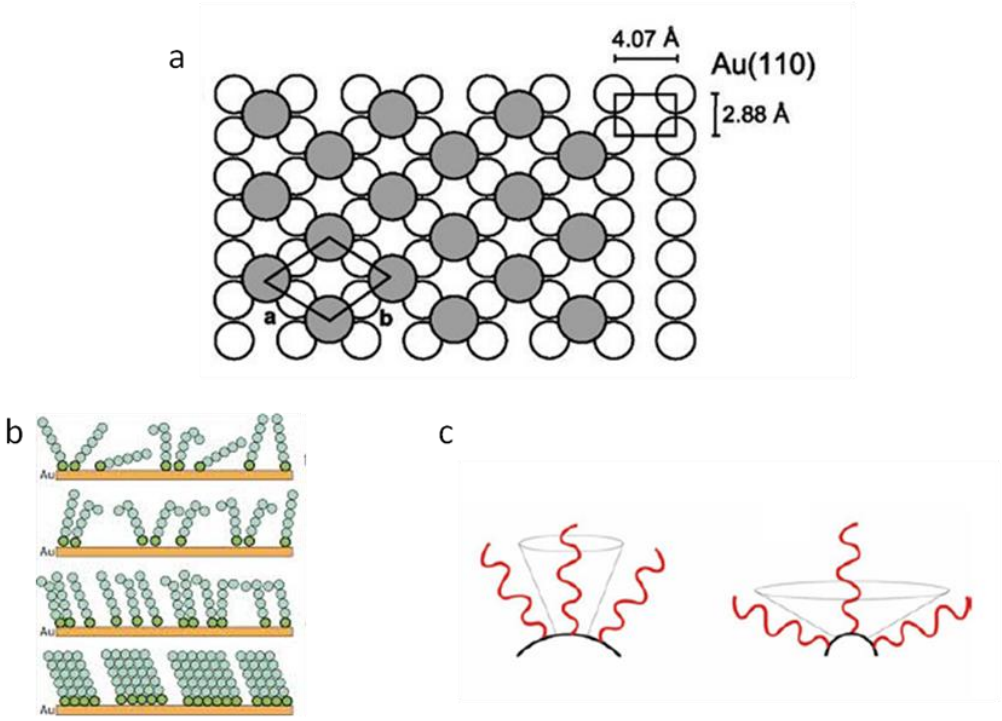

Figure 5.6 (a) Schematic representation of sulfur atoms coordination on a gold atoms layer. One sulfur is coordinated with 4 gold atoms cell on Au (110) surface. (b) The concentration of reactive molecules drives degree of ordered structure in the formation of planar SAM but in the case of spherical surface (c) the radius of curvature gives space and the flexibility of reactive molecule is increased.

The most used type of functionalization of gold surfaces makes use of a thiol reactive group at one extremity of the molecular chain. It has been shown that the sulfur atom strongly interact with gold atoms on the surface. In particular the sulfur interacts with a cell of four gold atoms providing a bond strength quite close to a covalent bond one[32]. A lot of examples of Self-Assembled Monolayers (SAM) are reported in literature where thiol modified molecules that react with gold planar surfaces are used to create a monolayer with a controlled degree of order[73]. On a spherical surface the arrangements of the molecules is different because of the radius of curvature that determines the angle between molecular chains affects the stacking interactions (Figure 5.6). Moreover, in order to passivate the gold colloids after sodium citrate synthesis, BSPP (Bis(p-sulfonatophenyl) phenylphosphine dihydrate dipotassium salt) should

be used since it can be easily replaced on the Au surface by thiol reactive groups. For this reasons, although is a well known and characterized technique, the functionalization of gold NP with DNA is a delicate process where tiny changes in the protocols could compromise dramatically its success.

I used commercial ssDNA modified with thiol reactive group at one extremity. The disulfide bond (oxidation of two thiol groups that bind together) is thermodynamically favorite in solution. Thus, to prevent premature disulfide bond formation in solution between the DNA strands that will prevent the interaction with gold surface, the thiol group is synthesized with a protective chemical "cap" making the extremity not reactive. The thiol-capped DNA sequences has to be de-protected just before the interaction with gold surface. The reduction reaction to break disulfide bonds can be carried on with several reducing molecules. I chose the dithiothreitol (DTT) because, as widely reported in literature[74], it is able to reduce the disulfide bond producing two -SH (thiol) terminations. Right after DTT de-protection, the DNA molecules were mixed with a proper ratio with gold colloids previously coated with BSPP. In principle, the higher is the DNA/NP ratio the better are covered the NP but to deal with a reasonable and cost effective amount of DNA I tested several different ratios finding a good covering and stability of the NP for [DNA] = 4000-6000. The stability of the DNA-AuNP link is assured by a salt-ageing process in which the NP are kept stirred and a small salt (NaCl) amounts are added step by step to reach 0.1 M concentration gradually.

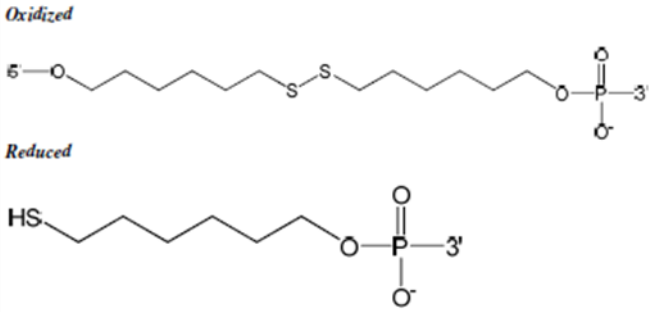

Figure 5.7 Chemical formula of the "capping" before and after reduction reaction to protect thiol group keeping it in not reactive form.

In this way the ionic charge does not change dramatically fast and the DNA strands have the time to gather all the counter ions needed to be stable in stacking interactions. If the salt ageing process is not enough there are other strategies to allow a good stabilization of the coating molecules, one of them is to use a second reactive molecule that is smaller than the previous one and so it can easily intercalate between the longer chains conferring them higher packing. In my first experiments I used a short poly-ethylenglycole metilated at one end (mPEG) to be not reactive at the surface. Although the great NP good dispersion using

mPEG, I chose to do not use it because of the very good results obtained optimizing the salt ageing process and the DNA/NP ratio.

Once functionalized the NP following the optimized protocol (details in chapter 4) the solution stability was checked visually controlling the color that should remain ruby red color during agarose gel electrophoresis. If the NP are stable in buffered media like the running buffer of gel electrophoresis they enter in the gel producing a clear red colored band. On the contrary, if they are not stable enough the NP do not enter in the gel rather form a distorted black band suggesting a large aggregation in presence of ionic charges; this effect is well represented in Figure 5.8.

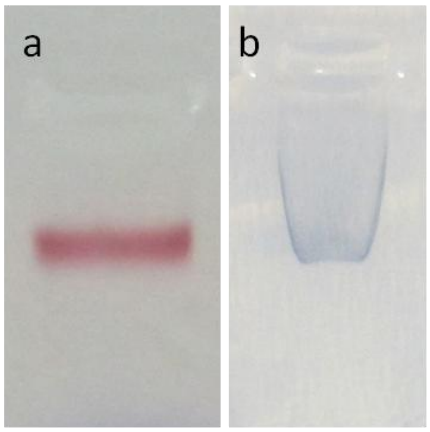

Figure 5.8 (a) Example of clear red band produced when not aggregated gold NP are flown through the gel: a correct run progresses in the line. (b) Representative line in which the gold NP are aggregated during the run progress providing black color and distorted flow shape.

5.4 Gold nanospheres dimer: aggregation and disaggregation methods

The dimeric configuration of gold nanoparticles was a basic concept for implementation of distance detection on the DNA origami using plasmon resonance distance correlation. Thus, I focused my research firstly to create dimers of gold NP functionalized with short DNA oligonucleotides[65]. Thiolated DNA oligonucleotides can be used to cover the gold nanoparticle surfaces, assembling them in a precise structural way with different aggregation orders. In literature there are many examples of the formation of aggregates of two or more nanoparticles using DNA self assembly strategies, different nanoparticles diameter (6 nm to 30 nm) and DNA lengths variable from 20 nts to 100 nts[62, 75, 76]. In this process, which is one of the main building blocks for further engineering of nanoparticle arbitrary structures, one of

the most difficult challenges is the high yield selective formation of two nanoparticle aggregates (dimers).

In the following, I reported on the efficient gold nanoparticles dimer formation using 17 nm gold nanoparticles (AuNPs) and short DNA oligonucleotides with three different sequence length: 11, 16 and 21 nts, through two alternative methods based on the DNA-induced aggregation and disaggregation (both represented in Figure 5.9), and on a fine tuning of the complementary ssDNA self-passivation.

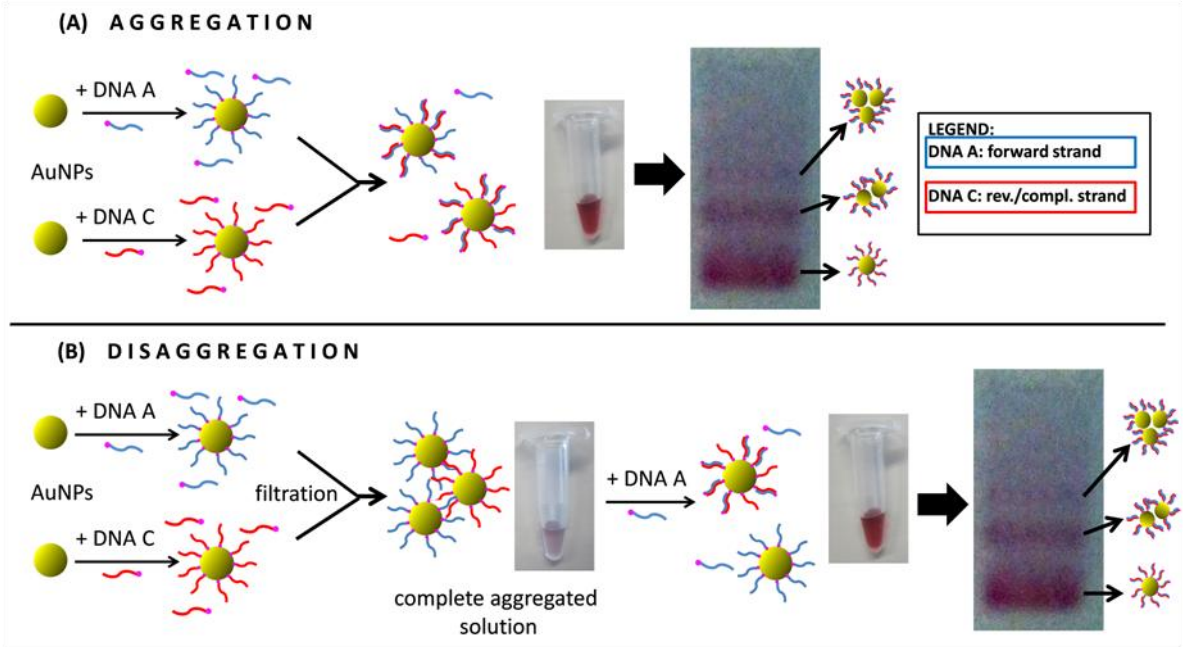

Figure 5.9 Schematic representation of the two methods for dimers production, where two separate NPs colloidal solutions are functionalized with thiolated DNA oligonucleotide "DNA-A" and with its complementary "DNA-C", respectively. (A) Aggregation: the excess DNA oligos are only partially removed; upon mixing the two solutions the residual strands present in one solution partially hybridize the complementary DNA linked to the NPs surface formed in the second solution; by a proper tuning, only few non-hybridized DNA are left on NP resulting in few NP aggregates. (B) Disaggregation: excess DNA is fully removed from both DNA-A and DNA-C solutions; upon mixing the two solutions large NP aggregates are precipitated; and adding a controllable amount of "DNA-A" the aggregate size is reduced to few NP aggregates.

The dimer formation was investigated by UV-visible (UV-vis) spectroscopy, by gel electrophoresis, and by scanning electron microscopy (SEM); solution stability, concentration, dispersion and dimers formation yield is analyzed as a function of the protocol parameters and in particular of the free DNA concentration used to hybridize the ssDNA present in excess on AuNP surface, thus controlling the NPs reactivity. I prepared two sets of AuNPs functionalized with thiol-capped DNA oligonucleotides: one with the primary sequence and the other one with its fully complementary sequence; they are shown in Figure 5.9 as "DNA-A" and "DNA-C". In DNA functionalization of colloid the sequence length,

usually employed to avoid nonspecific hybridization, is at least 15 nts, and at least 12 nts are used to assure a stable hybridization process[77]. I tested the direct aggregation method with three different short sequence lengths: 11, 16 and 21 nts. The dimer formation was demonstrated with all the three DNA sequence lengths[65].

However, the 11 nts sequence, being shorter, is expected to exhibit the highest plasmonic response, therefore in the following I will focus on this latter strand. Two separate colloidal solutions were prepared by adding the colloidal solutions described above with DNA-A and DNA-C respectively; in this method I used a large DNA/AuNP molar ratio (6000 to 1), so that a large DNA excess amount remained unbound in solution. Excess DNA molecules are more reactive than NPs bound DNA, because either of larger diffusion coefficient (approximately two order of magnitude) and of the larger number of configurations accessible. Therefore, upon mixing the two solutions, unbound DNA-A hybridize with AuNP bound DNA-C, and vice versa leading to a complete passivation of both functionalized nanoparticles and little or no dimer formation is observed. To increase the dimer formation yield, a centrifugal step should be performed to remove the free DNA before mixing the two NPs sets.

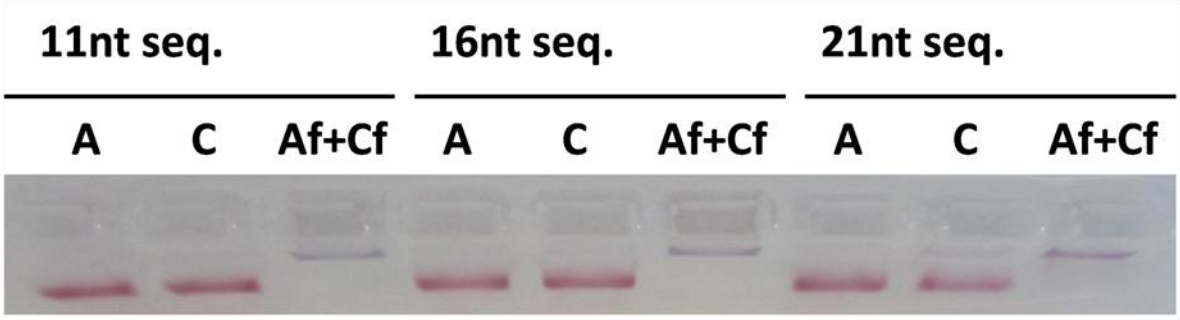

Figure 5.10 Agarose gel characterization of the functionalized NPs with the three different DNA lengths (11, 16, 21 nts) where "A" and "C" stand for DNA-A and DNA-C coated NPs respectively; otherwise "Af + Cf" stands for a mixed solution of both NPs sets after a complete purification from free DNA strands. All the samples "A" and "C" run into the gel and present a narrow and compact red band: the NPs are stable and run individually. All "Af + Cf" samples are aggregated in the pocket and they do not enter in the gel. Longer sequence runs slightly slow than shorter one.

I performed gel electrophoresis analysis to check the complete DNA coating of the gold colloids and their stability in high electrolyte solution: the results are shown in Figure 5.10 for the three different sequences. AuNPs coated with DNA enter in the gel, forming a clear compact and uniform red band. The individual run denotes an optimal stability and DNA coverage of the spheres. On the contrary, when DNA-A and DNA-C colloidal solutions are first purified from unbound DNA (by 3 centrifugal steps) and then mixed together,

nanoparticle aggregates do not enter in the gel, ("Af + Cf" lines, Figure 5.10) indicating that, as expected, the mutual hybridization of NP-bound DNA-A and DNA-C.

To obtain AuNP dimers in a controlled way, I investigated an intermediate situation, removing only a fraction of unbound DNA strands from DNA-A and DNA-C gold colloid solutions, before mixing. Typically, after one centrifugal step I partially removed the supernatant (~75%). After resuspension, I mixed the two solutions (DNA-A and DNA-C) and heated up at 50°C to promote the hybridization. Then I analyzed the resulting samples by gel electrophoresis showing the formation of several equi-spaced bands that I attributed to the formation of few nanoparticles aggregates. In particular I attributed the lowest and most intense band to single particles, the second band to dimers, and the third band to trimers (Figure 5.11). The bands intensity analysis denotes a dimer yield of 21.5%. Moreover, in the absence of the purification step to remove the free DNA, the mixed NPs sample runs compact and uniform without any different bands formation ("A + C", Figure 5.11). This latter proves that all the NP-bound DNA-A and DNA-C molecules from one colloidal solution hybridized with unbound complementary sequences present in the complementary colloidal solution.

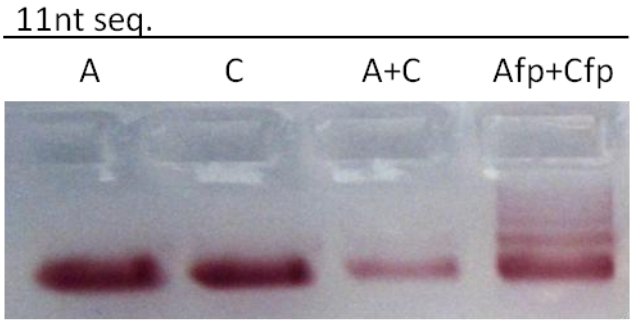

Figure 5.11 Agarose gel of the 11 nts sequence sample that shows the run of "A" and "C" referred to DNA-A and DNA-C solutions. In "A + C" unbound DNA was not removed; in "Afp + Cfp" unbound DNA was partially removed.

To better understand and characterize the NPs coating and NP dimers formation, I studied the plasmonic resonance by UV-vis absorption. Typically the volume of the mixed solution was too small for normal spectrophotometer cuvettes therefore I performed the analysis directly through the agarose gel. In this way a better defined band selection was achieved. In Figure 5.12a is reported a simulation that follows multiple scattering principles explained by Garcia de Abajo in 1999 or more general Mie theory with some approximations in dielectric function of the gold-gel composite[78, 79]. The simulation shows a red-shift of the plasmon peaks both for increasing of dielectric function environment and for the onset of particle-particle interaction of AuNP dimer. Core-shell model of single NP (black curve, Figure 5.12a) is in a good agreement with effective medium approximation (EMA) (magenta curve, Figure 5.12a).

EMA is used as well to calculate the absorption spectra of NPs dimers in agarose gel (blue curve, Figure 5.12b) with the same effective dielectric permittivity of $\varepsilon_5 = 0.65\ \varepsilon_3 + 0.35\ \varepsilon_4$ presented in a simple form. The gel absorption experimental data are shown in Figure 5.12b; the observed red-shift of the plasmon peaks are in agreement with simulations. This is due to the increase of dielectric function of dsDNA with respect to ssDNA in the single NPs case and to the NPs proximity in the dimer case. Since the length of dsDNA should be ~30% shorter than ssDNA[80], I remark an increase of absorption in the long-wavelength range, not only in dimers band (second band of "Afp + Cfp" referred to the blue curve, Figure 5.12b), but also in dsDNA single NPs band (first band of "Afp + Cfp" referred to the black curve, Figure 5.12b).

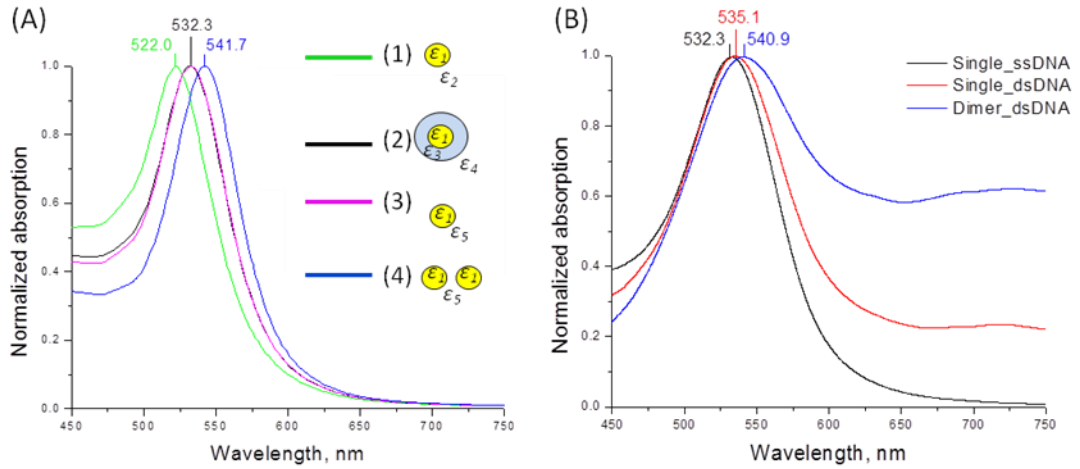

Figure 5.12 (A) Simulated light absorption spectra of (1) gold NPs in aqueous medium (ε_2=1.769), (2) DNA-functionalized (11 nts, 3 nm shell thickness, ε_3=2.450) gold NPs in 3.6% agarose gel (ε_4=1.796), (3) single gold NPs and (4) gold dimers in effective medium with ε_5=2.220. The EMA (effective medium approximation) was calculated as 65% of DNA and 35% of agarose gel. (B) Experimental direct from gel absorption spectra of the "A" and "Afp+Cfp" different bands (Figure 5.11). In particular black curve is referred to "A" band, red curve is referred to first and blue to the second band of "Afp+Cfp". The second band (blue curve) corresponds to the dimers structures.

Furthermore I analyzed the samples by scanning electron microscopy (SEM) to characterize the population distribution of each band. To this purpose, I electro-eluted the NPs from the gel, dispersed on the surface of a silicon wafer and imaged. The morphological investigation indicates a predominant presence of single NPs, NPs dimers and NPs trimers, respectively in the first, second and third band (Figure 5.13). Moreover in the latter, trimers appear randomly shaped and not only triangular, as is in the case of surface force driven aggregation (Figure 5.13).

The reproducibility of direct aggregation method, was however, rather poor. The results of repeated experiments showed an inconstancy of the outcomes, that ranged between mostly aggregated samples without dimer formation, and high yield of dimer production. Following the residual concentration of free DNA oligonucleotides after hybridization with gel-red DNA staining, I observed a significant correlation between dimer formation and residual unbound DNA concentration. In particular, I observed that a certain amount of free DNA strands is needed to provide a good dimer yield, amount, however, difficult to quantify with gel-red staining.

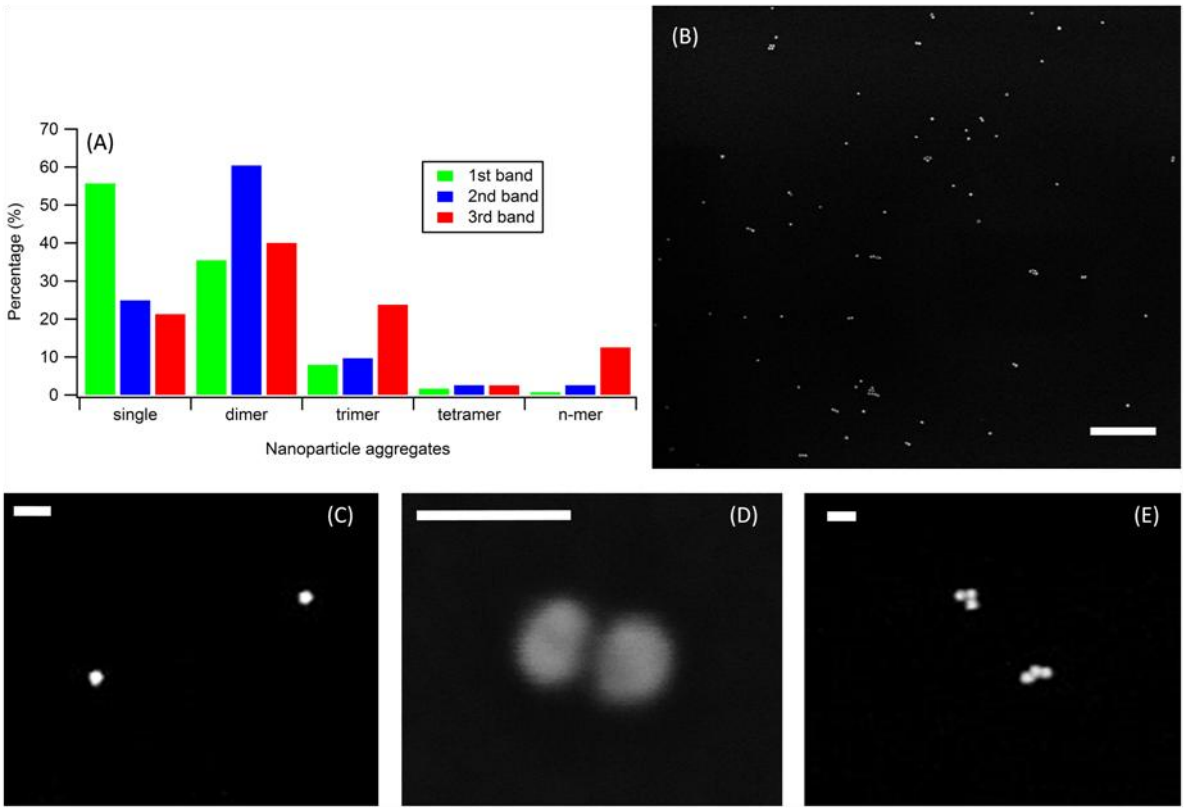

Figure 5.13 (A) Graph that shows the statistical distribution of single/dimer/trimer/tetramer and nmer (>4) in the different bands. The calculated percentage of events regards the electro-eluted solution from the agarose gel of the first, second and third band. It's evident a correlation between first, second and third band with one two and three NP aggregates respectively. Representative SEM micrographs of the solution with all the aggregates species (B), scale bar 300 nm. SEM micrographs of monomer (C), dimer (D), and trimer (E) NP aggregates, scale bars 40 nm.

In general, the optimal condition for a reproducible formation of dimers is that only one DNA molecule is activated for each AuNP. Two or more DNA molecules would lead to the formation of large aggregates. Since each AuNP of 17nm in size may accommodate about 1000 molecules, this implies that 99.9% should be passivated by further unbound DNA hybridization. It is clear that small deviation from the proper unbound DNA concentration

may significantly move the equilibrium toward aggregation or pure single particle. Since in this protocol, the passivation is obtained using the residual concentration of unbound DNA after centrifugation, and supernatant removal and since this amount is operator dependent, it can hardly be used as a given parameter, in a protocol. Improvements may be obtained by first removing completely the supernatant and then, adding a precise value of complementary unbound DNA sequence, but also in this case, the requirement of a complete removal of supernatant may be a source of non reproducibility. I have obtained a much more precise control of dimer formation by first aggregating AuNP in large cluster and then inducing a controlled disaggregation by adding DNA complementary strands. In detail, I removed the unbound DNA-A and DNA-B oligonucleotides in the two solutions, carrying on two or three centrifugal steps removing the supernatant at the end as for the experiments shown in Figure 5.10. The complete removing of residual unbound DNA was confirmed by the absence of DNA gel staining in the electrophoresis analysis. So, I obtained full aggregation upon mixing the two solutions, with clear transparent aspect as shown in the inset of Figure 5.9b. The aggregated solution is extremely stable and can remain unalterated for months at room temperature, moreover, residual free DNA strands may be easily removed by further centrifugation at this stage, making the unbound DNA purification a non-critical protocol step.

At this point, in order to disaggregate the solution and create single NP, or dimer, or other aggregates I added a calibrated amount of both complementary DNA[65]. I heated up the solution to 50°C for 45 minutes and left cooling down to RT: as a result it recovered the typical ruby red colour. In Figure 5.14 is represented the agarose gel electrophoretic analysis of the functionalized NPs with 11 nts DNA sequence. I prepared the "Af+Cf" solutions (Figure 5.14a) mixing the DNA-A and DNA-C bound NP colloid solutions purified from unbound DNA strands. This leads, as already mentioned, to the precipitation of large aggregates, confirmed by the absence of bands in the "Af+Cf" pocket (Figure 5.14a). On the contrary, in the "extra 1-2-3" samples, after the purification step, I added DNA-A, DNA-C and both respectively. In all the last three pockets at least 4 different small NPs aggregates were separated ("extra 1-2-3" lines in Figure 5.14a). In absence of extra DNA, the NPs do not resuspend in solution and remain aggregated. The addition of one or two unbound DNA sequence, promotes a controlled disaggregation and the formation of few NP aggregates. By comparing the latter gel bands with those on un-mixed colloid solutions which are formed by single AuNP, I were able to identify up to four bands as originating from single particles, AuNP dimers, trimers and tetramers. Then, I carried on an analysis of the bands intensity to

investigate the effect of unbound DNA on AuNP n-mers formation. The first band relative to single NP, is increasing in intensity in "extra3" sample. On the contrary, the signal above the third band, which is attributed to n-mers with n>3, decreases drastically when both ssDNA sequences are introduced together (Figure 5.14b). This analysis suggests that the presence of only one DNA sequence is sufficient to create dimer NPs but larger nanoaggregates are also formed. Adding both the DNA oligonucleotide sequences the population of larger aggregates decreases in favour to the mono-dimer and trimer groups of NPs (black and red curve, Figure 5.14b). Although the third band slightly decreases with both DNA strands (blue curve, Figure 5.14b) the second band (dimeric aggregates) increases in presence of both sequences highlighting a dimer yield of 22.7%. If the same experiments are performed without any thermal annealing, the sample remains in its aggregated form and do not enter in the gel. This suggests that the disaggregation process and the subsequent dimer formation follow the hybridization between complementary strands promoted by annealing.

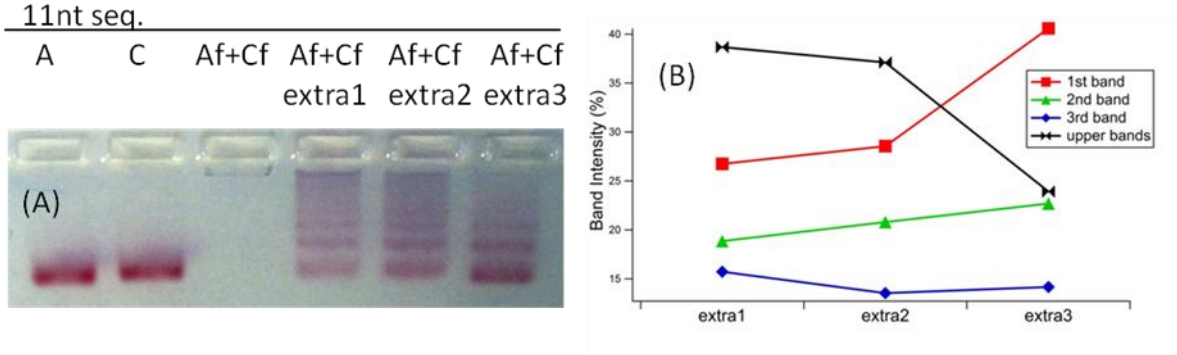

Figure 5.14 (A) Agarose gel analysis of the 11 nts sequence sample. "A": DNA-A coated single AuNP; "C": DNA-C coated single AuNP; "Af+Cf" mixture of DNA-A and DNA-C coated AuNP colloid solution, from which unbound DNA has been removed by centrifugation; "extra 1, 2, 3": same as "Af+Cf" in which a controlled amount of DNA-A; DNA-C and DNA-A + DNA-C has been added. It is clear the formation of discrete bands only in presence of extra DNA. (B) Analysis of percentage of bands intensity of "extra1", "extra2" and "extra3" lines, that put in evidence the inverse correlation between first and upper bands (red and black curves), and the linear increasing of second band (green curve). The 100% is calculated from all the cumulative bands intensity of one line.

Furthermore, in order to investigate thoroughly the correlation between the extra DNA concentration and the dimer formation efficiency, I tested the disaggregation method with different concentrations of DNA-A sequence added. In Figure 5.15 it is shown the analysis of 11 nts sequence "Af+Cf" samples with different concentration ratios of added DNA-A. In particular 0/0,5/1/2,5/5/10 times respect to the initial DNA concentration used in the functionalization reaction volume (~2 μM) ("Af+Cf extra1", 0/0,5/1/2,5/5/10 lines Figure 5.14a). It is noticeable both that in every "Af+Cf" samples with extra DNA there is formation of bands, and that the intensity of each band changes with DNA-A concentration. I calculated

the band intensity to clarify this correlation (Figure 5.15d). Firstly, I notice that each band reaches its maximum (black rectangles, Figure 5.15d) for different extra DNA-A concentration. While the first band is continuously increasing with increased DNA, the trimer and the n-mers bands have the highest yield with 2.5X ratio, and finally the dimer band reaches its maximum with 5X ratio with a yield of 26.5 % of the total amount of AuNP concurring to the reaction, which exceeds of about 2% the highest yield value reported so far in literature[81]. This, suggests that there is a critical concentration of the extra DNA in which, partial NP surface passivation provides highest dimer yield. A further SEM characterization, confirmed the homogeneity of the population within band with isolated NPs (first band) and dimers (second band), as underlined in the representative SEM images shown in Figure 5.15b and 5.15c respectively.

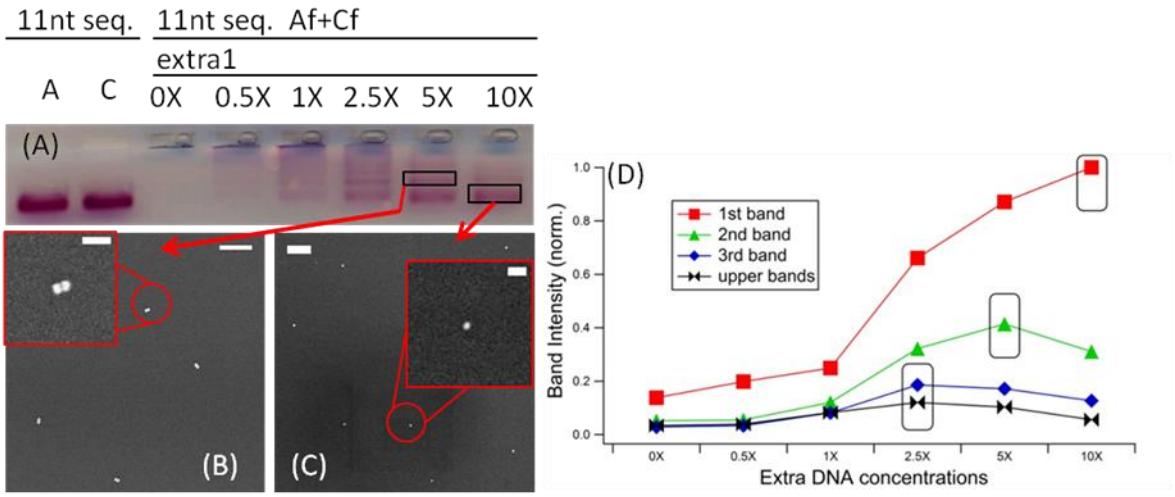

Figure 5.15 (A) Agarose gel analysis of 11 nts sequence sample where "A" and "C" stand for DNA-A and DNA-C coated NPs respectively; and the "Af+Cf extra1" sample to which was added DNA-A in different concentrations: 0/0,5/1/2,5/5/10 times respect to the initial DNA molarity (~2uM). The concentration of NPs is equal in all the "Af+Cf extra1" lines. The formation of discrete bands is highlighted only in the presence of extra DNA and the intensity changes on varying the ratios. (B) SEM images that represent the NP nanoaggregates population of the second and (C) first band in which it was found majority of dimers and singles NP respectively, scale bars 200 nm (insets 50 nm). (D) Analysis of the intensity of the bands in normalized values: the black rectangles underline the maximum of each different band at the various extra DNA ratios.

Regarding these experiments I can affirm that I developed a protocol for the formation of gold nanoparticles dimer with extremely high efficiency[65]. I produced stable and discrete mono-di-trimer nanoaggregates in high electrolyte solution using DNA hybridization technology to create well functionalized nanoparticles, with short DNA oligonucleotide sequences reaching optimal results also with only 11 nts length. I performed this system both via direct aggregation, both via post-process disaggregation of the functionalized gold nanoparticles.

Through the disaggregation method I set up a reproducible and controlled protocol that allows to understand the aggregates formation trend in a passivation self assembly process, reaching the maximum NP dimer yield (26.5%)[65]. This last condition could provide the basis for the creation of plasmon architecture on DNA origami opening the possibility of optical detection and distance measuring through LSPR shift investigations.

5.5 Development of a movable actuator DNA nanostructure: DNA origami hatch

My research activity was then focused on the development of a DNA origami movable structure based on a revertible actuator. To this purpose I designed and characterized a circular hatch-like origami shape able to switch between closed and open state after the addition of specific DNA target[53]. The structure consists of an external ring with a 100 nm diameter and an internal disk with ~50 nm diameter that are linked together at the center of the shape. The origami design of the internal disk has two parallel lines along the central axis that confer higher flexibility to the two semi-halves of the disk. These lines consists of a four scaffold nucleotides unpaired with staples sequences that generate a flexible single strand portion making possible the flipping of the semi-halves. Since across the internal disk is linked a 120 nts ssDNA named "actuator", after the addition of a complementary strand named "target" their hybridization shortening produces a pulling force that is able to raise up the two semi-halves like two "wings" of an hatch (Figure 5.16).

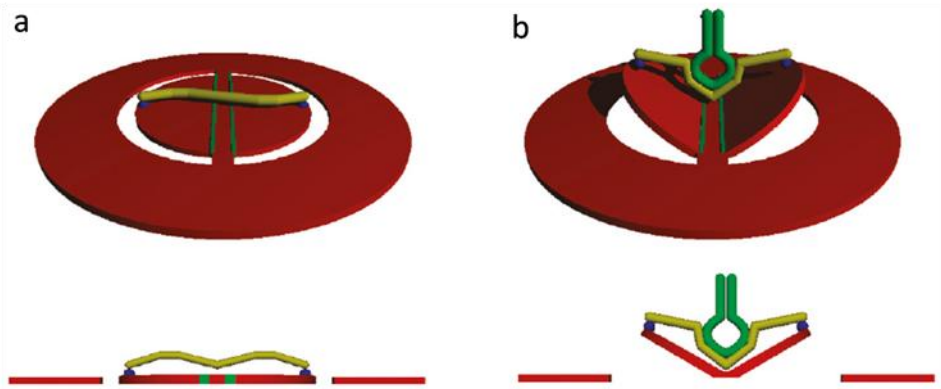

Figure 5.16 (a) Sketch of the hatch DNA origami structure with lateral and top view in which are visible the internal disk and the external ring and their separation is emphasized. The two green lines represent the single strand portion that confer flexibility to the two semi-halves. (b) After the target hybridization (green hairpin) with the actuator strand (yellow) the raising up of the two "wings" is possible.

The sequence used as target has a central part fully complementary to the actuator and 18 bp portion of CG clamp giving it an hairpin structure; in this way the shortening upon the tight target-actuator hybridization produces a considerable pulling force exerted on the wings that open the structure. The simple base pairing mechanism to open the hatch structure was exploited also to make the movement reversible inserting a first target partially complementary with the actuator and subsequently adding a fully complementary single strand named "competitor". Moreover the movement actuation can be detected by FRET analysis thanks to the insertion of a fluorophore at the wing-tip and a quencher molecule at its proximity on the external ring modifying two staples strands. In this way a fluorescent signal is generated in open position and is quenched in closed state generating an ON/OFF signal as a consequence of the target hybridization (Figure 5.17). In fact, one of the possible applications is to create an hybrid sensor structure placing the hatch circular structure on a rounded pore of a solid state membrane, in order to have a selective passage of molecules triggered by the target recognition[53].

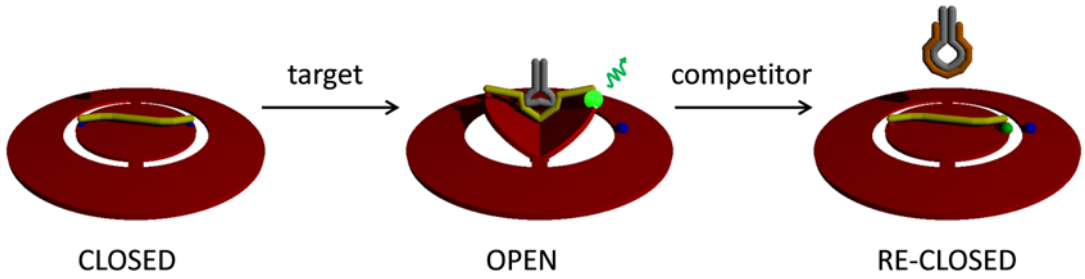

Figure 5.17 Sketch of the hatch DNA origami structure with reversible movement technology. The addition of a partially complementary target (grey) opens the structure and the subsequent fully complementary competitor cancel the target action and re-close the structure. The signal of the fluorophore (green sphere) is visible on the open state and quenched on the closed position.

The hatch structure has been tested with different DNA/RNA target sequence to analyze the possible detections of viral and plant RNA sequences. In addition, linear fully and partially complementary target sequence have been tested to investigate the different ability to raise up the wings but since we can get only ON/OFF information using FRET characterization, the precise dynamic scale of the opening remain unpredictable.

5.6 DNA origami as nanoactuators: development and characterization

The good result in gold NP functionalization and gold NP dimers creation and purification allowed me to focus my research on the creation of a plasmonic - DNA origami hybrid in which the nanoactuator system approach was used to tune the plasmonic response. First of all I characterized and demonstrated the design of self-assembled DNA-origami nanostructures capable of an autonomous switchable motion and with an unique addressable change of conformation and shape in response to environmental stimuli provided by the operator. The mechanical motion of this DNA origami nanostructure is fully reversible, making use of the simple and well known rules of base-pairing between different nucleic acids strands. The estimated total diameter of ~100 nm, consisting of an internal disk of an estimated total diameter of ~60 nm and an external ring, of ~20 nm (shown schematically in Figure 5.16). In order to secure flexibility to the two semi-halves of the internal disk and thus allow them to bend relative to the plane of the ring, the DNA was left single stranded for a length of four nucleotides in each row of the internal disk in positions aligned to a row perpendicular to the bending axis of the flaps.

I confirmed this structure morphology with AFM, that directly revealed the formation of isolated DNA origami nanostructures, with average diameter of 97 ± 6 nm and average height of 2.1 ± 0.2 nm[53]. No double layers existed (Figure 5.18a), but a significant portion of origami nanostructures appeared to be connected on their side, in couples (Figure 5.18b), probably, due to blunt ends' interactions forces between the same edges. A detailed analysis on more than 2000 nanostructures revealed that 75±2% of the disks adopted the designed shape while 25±2% of the disks were incomplete, missing often the internal disk or part of the external ring (Figure 5.18d).

In order to control the motion of the DNA origami flaps, two oligonucleotides of the internal disk were substituted with longer oligonucleotides with sticky ends protruding on the upper face of the disk, on the edges of the two opposite movable flaps. This modification allowed for linking, in the self-assembly step, of the "probe", a single stranded DNA molecule designed to be 120 nts long with the ends complementary to the above mentioned sticky ends. Moreover the probe was constructed to be fully complementary to an hairpin DNA target, as depicted in Figure 5.16. The hybridization between the target and the probe originates a tensile force on the internal disk changing its conformation by moving the wing edges toward each other. The modification induced by the probe-target hybridization in the origami structure has been observed by AFM as shown in Figure 5.19a and 5.19b, where two

openings separated by a ridge could be directly identified in real space, as expected from flap movement.

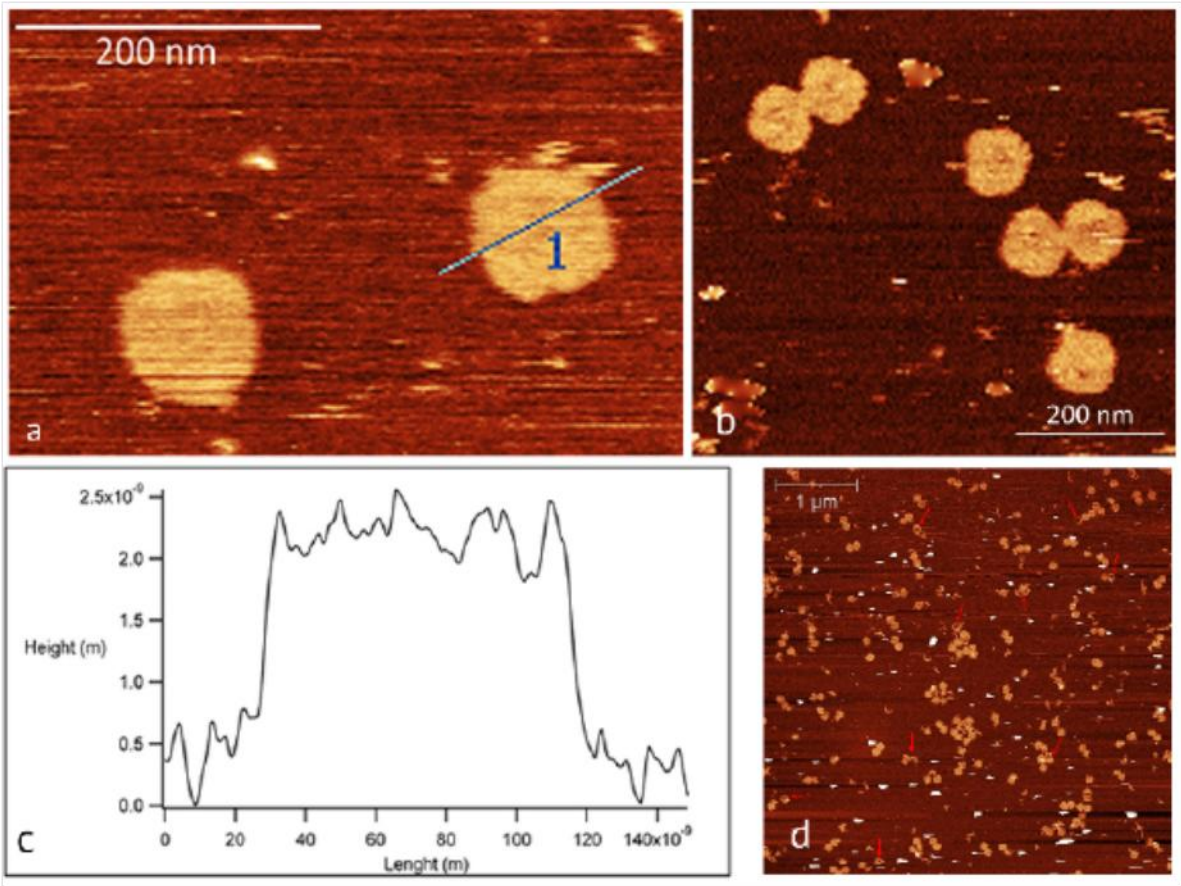

Figure 5.18 AFM imaging of DNA origami hatch structure. (a) AFM image in tapping mode in liquid of two well-formed closed DNA origami and (c) height profile of the structure, referred to the line 1 in the AFM image. The profile analysis highlights the correspondence of the self-assembled nanostructure with the design dimensions: height around 2 nm and diameter around 100 nm. (b) AFM image of well formed origami pairs originating from lateral blunt ends interaction. There is no opening between the inner disk and the outer ring. (d) Low-resolution AFM image showing incomplete DNA origami (red arrows), missing the internal disk and part of the external ring.

I investigated the efficiency of the actuation by recording a number of AFM images and counting the number of reacted versus non reacted origami nanostructures. When the target was added to buffer-suspended origami, i.e. before the deposition on the substrate, 86 ± 6% of the structures reacted with the target and changed conformation. When the origami was first deposited on the substrate and then exposed to the target solution, however only 48 ± 15% of the origami structures were found to be opened. Since, in order to successfully hybridize with the target, the origami should lie on the substrate surface face-up, the two data are consistent; the small difference between the observed (48%) and the expected (one half of 86%), although within a statistical error, may be explained with a orientation preference when the

origami are deposited on mica. My observations indicate that the actuation force is large enough to overcome the electrostatic and van der Waals interactions between the DNA origami actuator and the substrate, as well as the stacking between the internal disk and the external ring, demonstrating the applicability of the actuator strategy for integration of DNA origami nanosystems[53].

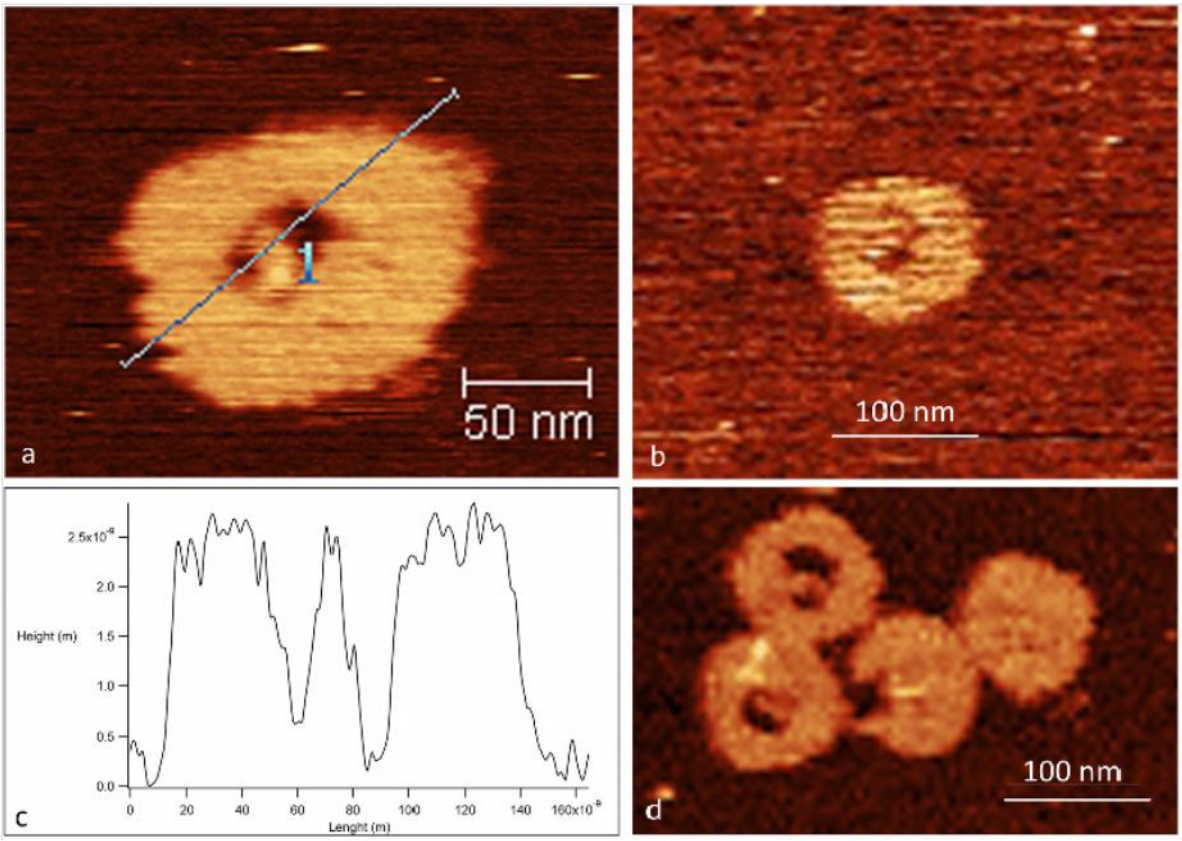

Figure 5.19 AFM imaging of DNA origami structures after hybridization with a complementary target. (a, b, d) AFM images of well formed origami. Two openings are evident. (c) Height profile of the structure, referred to the line 1 in the AFM image in (a), highlighting that the opening of the nanostructure reaches the substrates as expected for a complete opening.

To integrate a further degree of flexibility and making the flap movement of the DNA origami actuator reversible, probe/target pairs that were not fully complementary were used as above mentioned and showed in Figure 5.17[53]. The reverse actuation was performed by decomposing the probe/target hybrid by adding an excess amount of an additional oligonucleotide named "competitor", which was fully complementary to the target, as above summarized in Figure 5.17. A fast and qualitative method based on insertion of a FRET couple in the structure was introduced to monitor the conformation changes of the DNA origami associated with flap motion following the target addition.

The DNA origami hatch design was further modified to investigate better the flap DNA actuation. One of the two semi-halves was linked with staples strand making the opening

asymmetric and the flexible line was shifted producing slightly longer movable flap (Figure 5.20)[82]. I used this asymmetric hatch design to implement plasmonic architecture for tuning the LSPR between two gold NP, but a complete description of this argument will be thoroughly exposed in the paragraph 5.6.

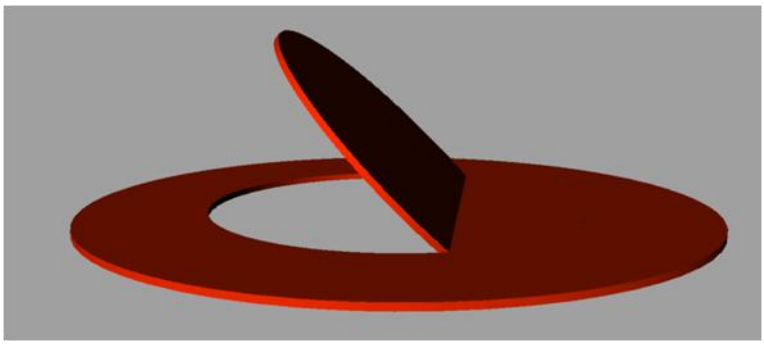

Figure 5.20 Drawing of the asymmetric design of DNA origami hatch. The only one movable flap is longer.

The workability of the flap actuator system was investigated also in a 3D DNA origami structure. The flap developed above was reduced in size and implemented in a 3D origami nano-robot. The latter had estimated dimensions of 14 nm × 14 nm × 48 nm. The volume of the inside cavity (8 nm × 8 nm × 44 nm) was estimated to be 3 zeptoliters. The flap dimensions were 9 nm × 5 nm, and the distance between the anchored probe tails was 28 nm. The overall efficiency of the synthesis and purification process was estimated to be 21% by measurement of the optical density of the recovered DNA nanostructure that, according to subsequent agarose gel and AFM visualization, resulted intact and without excess staple strand contamination. TEM and AFM images (Figure 5.21) confirmed the correct formation of the 3D DNA origami and the average value of the nano-object was calculated on 1500 nanostructures. Their length resulted 55 ± 9 with AFM and 40 ± 7 nm with TEM, i.e. smaller than predicted, in agreement with previous observations of Sander and Golas[83] who visualized a DNA box using conventional negative staining and TEM instead of AFM and Cryo-EM used by Andersen et al.[46] and reported that negative staining and air drying resulted in an apparent shrinkage of the hollow DNA box. The DNA nanorobot was assembled, purified and subjected to FRET measurements to confirm the flap opening following target addition. In the absence of the target (closed state), the fluorophore and the quencher were in close proximity resulting in a low FRET emission, as demonstrated by a low fluorescent signal intensity. A significant increase of the fluorescent intensity could be detected, demonstrating flap motion

determining the consequent FRET pair separation, after 1 h incubation at room temperature in the presence of the target[82].

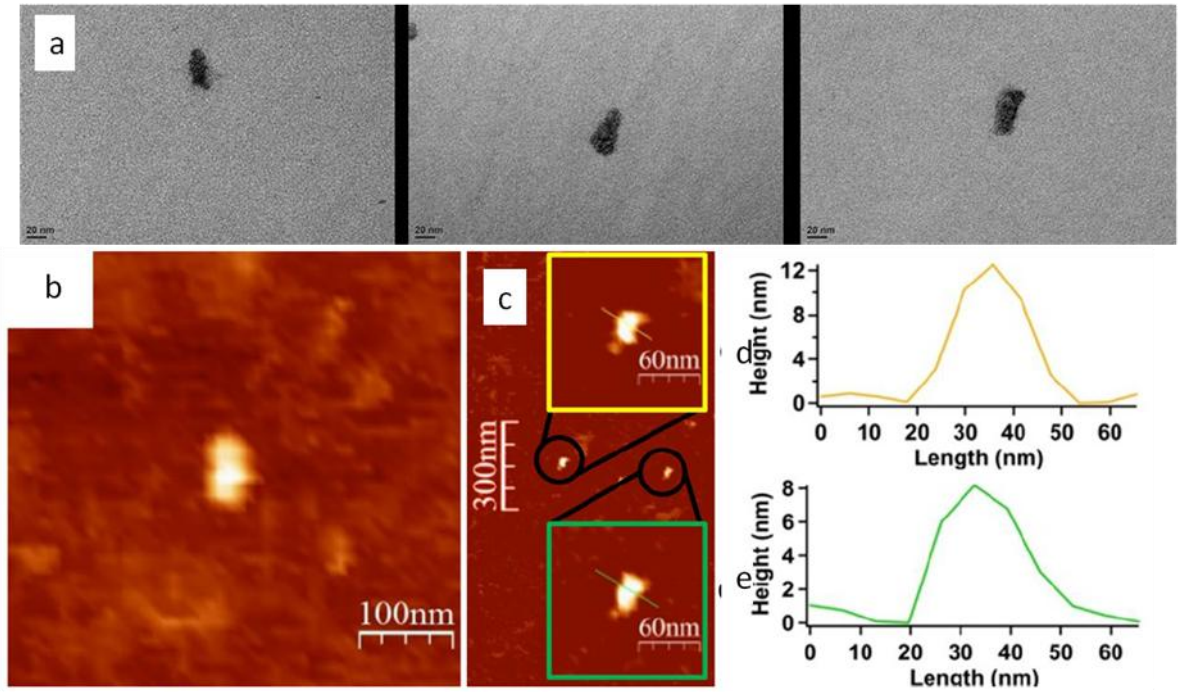

Figure 5.21 (a) TEM images of the 3D DNA origami nanorobot. (b,c) AFM image of the nanorobot structure. (d, e) Height profile analysis of two different structures underlined in the zoomed insets of image: the profile (d) is referred to the top inset, the profile (e) is referred to the bottom inset. The maximum height difference could be attributed to the pushing effect of the AFM tip.

This flap actuator technology was implemented in the DNA nano-robot as "door" to expose specifically a cargo molecule in order to have specific reaction in open state. A DNAzyme cargo was linked in the cylindrical DNA origami equipped with a flap described above. The cargo was the 20 nts long hemin-binding sequence PS2.M[84]. After the addition of the DNA target and movement of the flap in an open position, the PS2.M protruding stretch was pulled out of the cylinder and exposed to the external solution. The incorporation of hemin via the formation of intra-molecular guanine quadruplexes defined a cofactor-utilizing nucleic acid that catalyzes oxidative chemistries. To confirm the occurrence of the process, was used a colorimetric assay based on the catalyzed oxidation of ABTS 2− by H_2O_2 and an assay based on the generation of chemiluminescence in the presence of luminol/ H_2O_2[82].

5.7 DNA origami as architectural scaffold for plasmon resonance tuning

As described in previous chapters the main purpose of this project is to take advantage of DNA origami actuation to create particular plasmon architectures in order to succeed in tuning the LSPR properties and detecting distances in response to structural conformational changes.

First of all I used a prototype DNA origami to test the gold NP decoration in order to optimize all the procedures before using the real actuator design. I designed, with previous described software, a rectangular 2D origami in which I inserted two NP binding sites. Each of this site is composed by three DNA staple strands protruding out as catchers for complementary counterpart on the functionalized NP. In addition, I wanted to investigated the linking of a gold nanorod (previously functionalized) thus, I inserted five similar catcher strands along the hypothetical axis of the rod. In Figure 5.22 is well sketched the configuration on the rectangular origami.

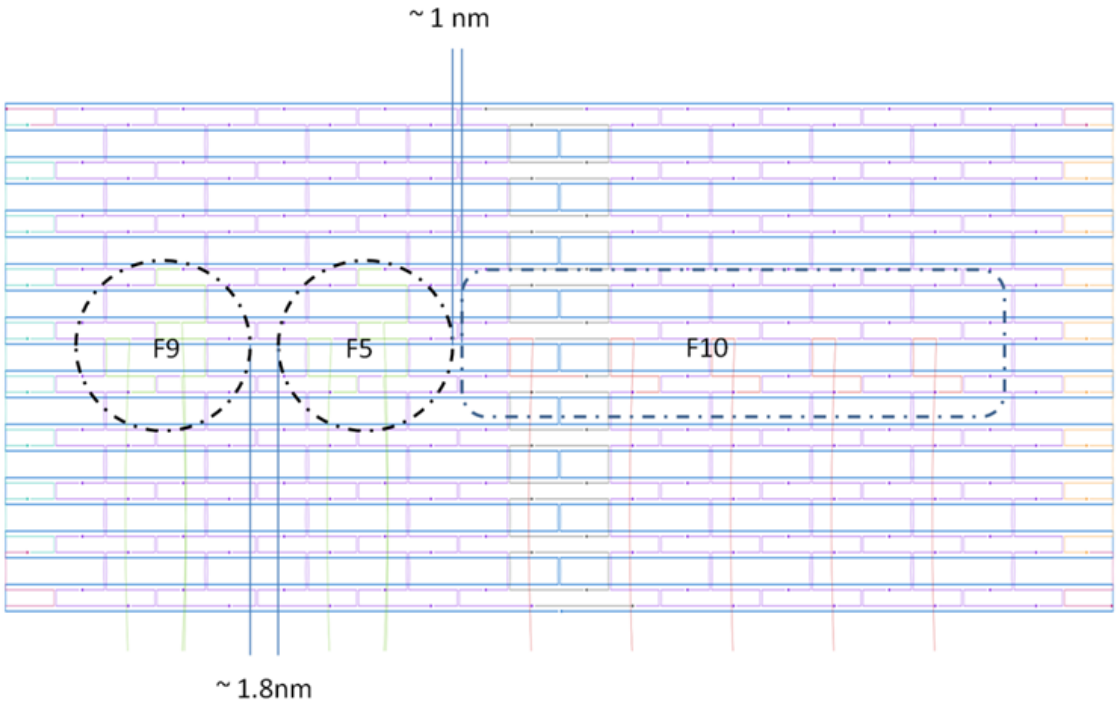

Figure 5.22 Sketch of the two NP and one NR on the rectangular origami. The caDNAno design represents the scaffold (in blue) and staples strands (colored). I drew the putative positions and dimensions of the gold particles in correspondence of the catchers positions.

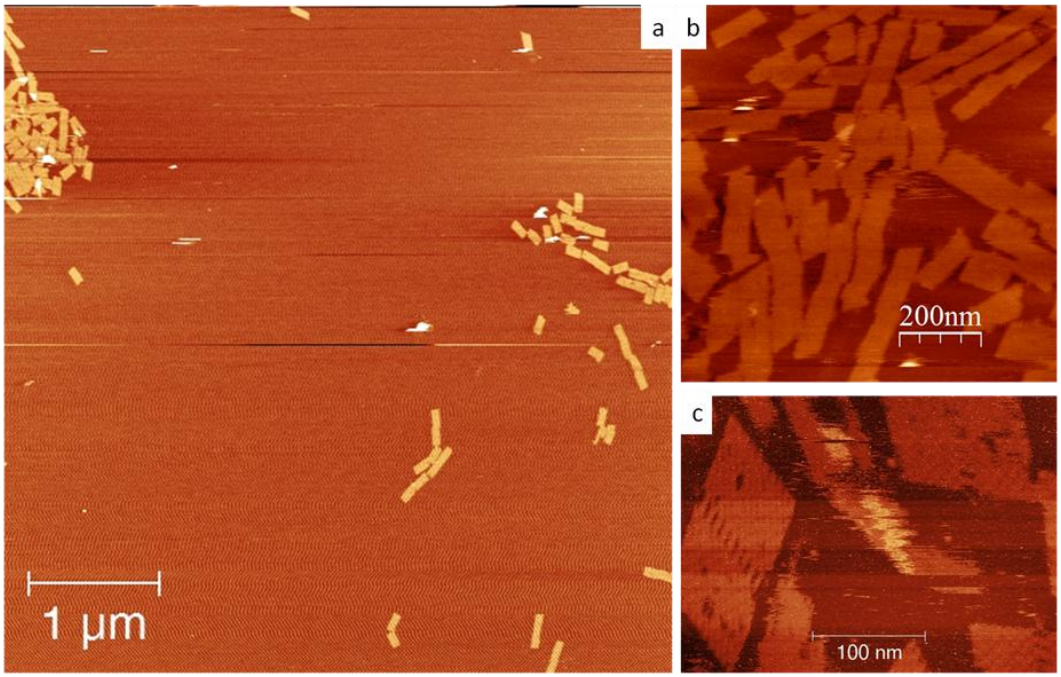

Figure 5.23 AFM images of the rectangular DNA origami. (a-b) The stacking interactions between isolated rectangles are clearly visible and form little modular chains of rectangles. (c) High resolution AFM image where the internal seam along the middle axis and the double crossovers are visible.

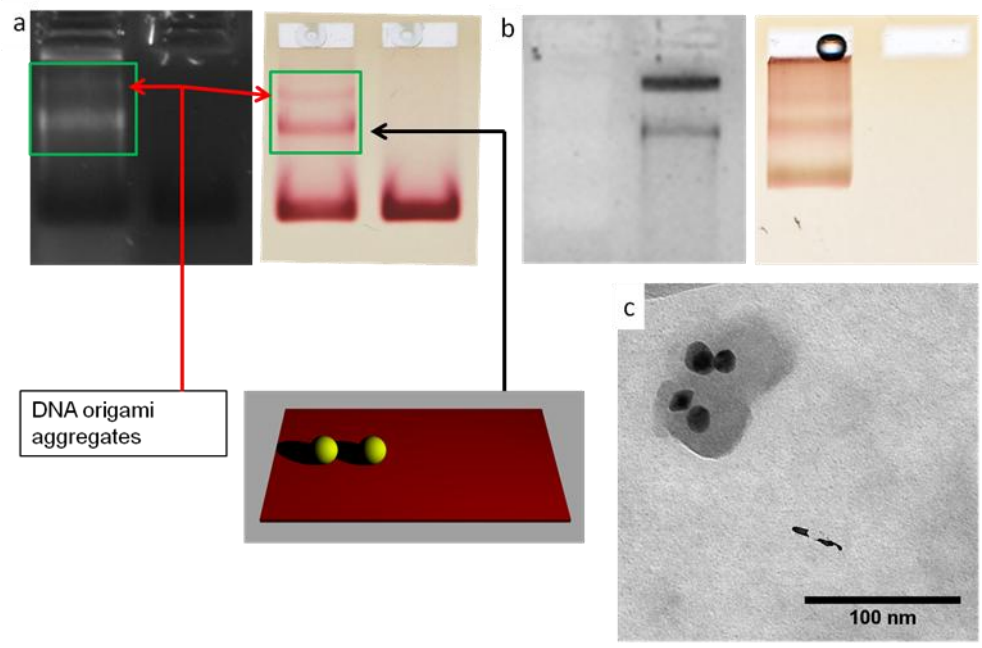

Figure 5.24 Agarose gel panels with UV and white light image of the same lines. (a) The origami linked to NP band is clearly visible. (b) The linking between NR and origami is correspondent to the origami DNA staining band, in this case the NR quenched completely the emission of DNA "cancelling" (lighter background) the band in the left line. (c) TEM image of DNA origami rectangle with two NP matching the design positions.

Afterwards, I successfully characterized the rectangular origami with AFM (Figure 5.23) highlighting known stacking interactions between several origami. I incubated them with functionalized gold nanospheres and nanorods (put in excess) analyzing the formation of specific bands with agarose gel electrophoresis. The Figure 5.24a-b shows clearly the formation of upstream band in correspondence of the linking between origami and NP and NR respectively. It is also appreciable the upper band of DNA origami aggregates confirmed by AFM characterization. The UV light image of the same gel highlights the DNA staining allowing to appreciate the clear correspondence between the specific bands of hybrid structures with the band of DNA origami. The rectangular origami with NP was also characterized at TEM after the extraction from the gel. The Figure 5.24c shows the linking of two NP on top of two rectangles and denotes the matching of the NP positions with the design construction.

Once I optimized the protocol to link NP on the DNA origami rectangle I moved on the principal structure. I wanted to create the DNA-NP hybrid structure using the asymmetric hatch structure, previously described.

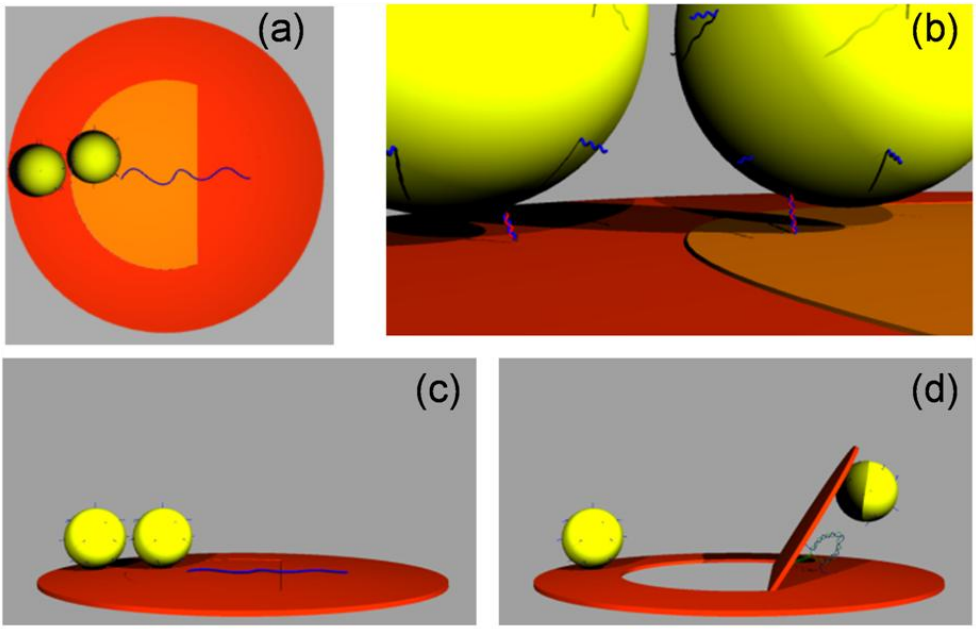

Figure 5.25 Schematic representations of the DNA origami circular shape and linked gold nanoparticles hybrid structure. (a) Top view of the disc shape with the nanoparticles position according to the design, the ssDNA probe is schematized in blue and the flap portion is highlighted in orange. (b) Zoomed view of the linking zone between the two DNA coated NPs and the DNA origami: one on the external ring and the other (right) on the flap region. (c) The non actuated hybrid structure presents a close nanoparticles pair. (d) Example of hatch opening angle after the hybridization with the target.

The design allows to link two gold NP at the same place of the FRET acceptor/donor couple in order to have distance displacement during the actuation. In order to decorate the DNA

origami hatch structure, I functionalized 20 nm gold colloids (Ted Pella Inc.) with thiol-capped DNA oligonucleotides following above described procedure[60]. To arrange one NP on the external ring and one on the edge of the internal flap (Figure 5.25a-b). Two scaffold-sequence portions were left free to hybridize with the NP linked oligonucleotides. In this way two 20 nm gold NP were placed in contact with each other when the hatch is closed as shown in Figure 5.25a-b-c. As in the previous report, the target-probe hybridization reduces the end-to-end distance of about ~30% thus generating an actuation tension that opens the hatch. The opening width – or angle – depends on the specific hybridization path and on the target sequence. Using this closing/opening principle, the precise tuning of the optical properties of DNA-plasmonic constructs could be obtained. In order to produce different opening angles I tested two fully complementary targets: a linear sequence 84 nts long (L84), and an hairpin sequence 120 nts long which includes in the central part the same sequence of the L84 target (C120); and a partially complementary linear target 64 nts long (S64) (details in chapter 4).

I verified the DNA origami formation by atomic force microscopy, revealing a compact circular shape corresponding to the initial design. As the previous symmetric design the circular shape presented sometimes a dimerization due to the blunt ends stacking interactions in specific positions as it shown in Figure 5.26[60].

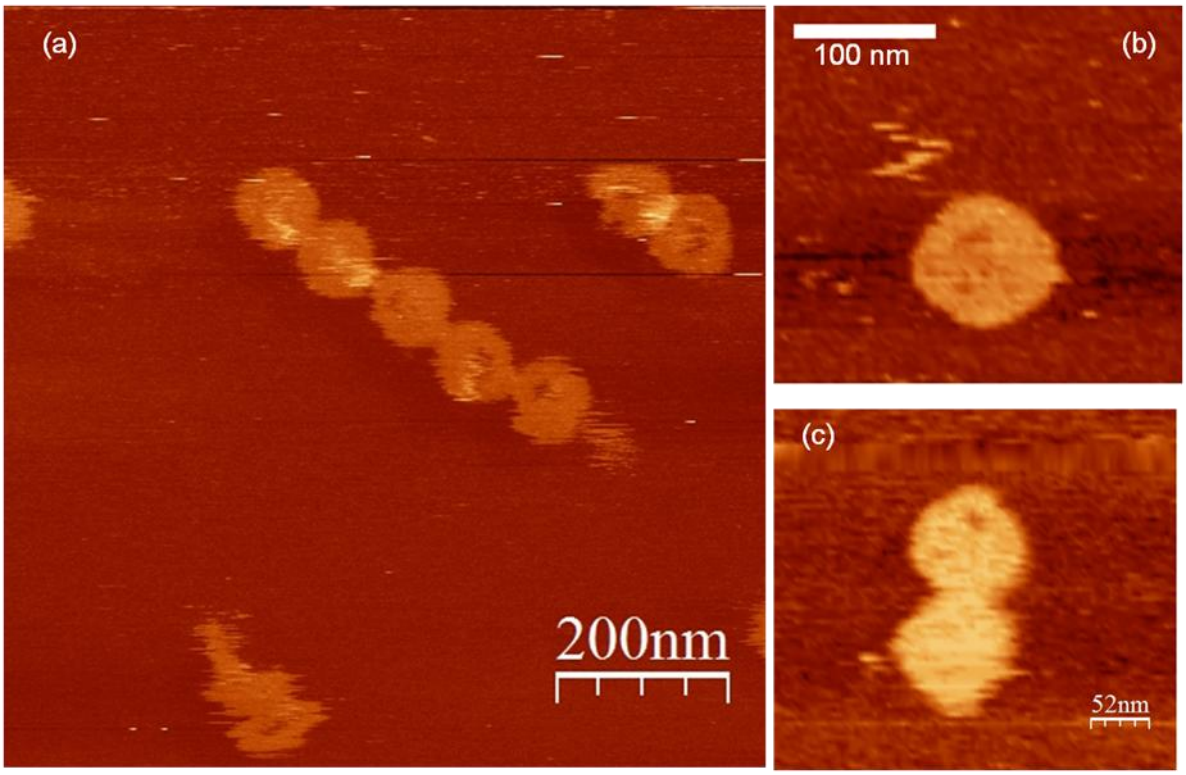

Figure 5.26 AFM representative images of the DNA origami hatch with asymmetric design. (a) The circle shape design tends to aggregate in dimers because of the stacking interaction at the edges. (b-c) High resolution AFM images to better see the single and dimer structure.

Additionally, in order to demonstrate the complete workability of the DNA origami actuation, I investigated the reversibility of the asymmetric open of the hatch playing with the different complementarity of the target sequences. The strategy is the same of previous reversible actuation report[53] where a not fully complementary target is firstly involved. Since is the only one not fully complementary with the probe, in this case I used the S64 DNA target in connection with a new DNA competitor sequence called C64. The latter is fully complementary with the S64 target thus, by higher affinity hybridize and replace it from the actuator probe. The removal of the S64 target trigger the re-closure of the system. I characterized the reversible process firstly by AFM on the DNA origami hatch without NP on it[60]. The Figure 5.27 shows a clear demonstration of this effect, in fact in presence of no target addition the origami is closed (Figure 5.27a) and no apertures are visible in the middle of the structure, while after S64 target addition we can see clear holes in the middle produced by the AFM tip invasion and pushing of the bended flap (Figure 5.27b). On the other, after the addition of C64 (put in excess) the re-closure of the internal flap is appreciable in Figure 5.27c.

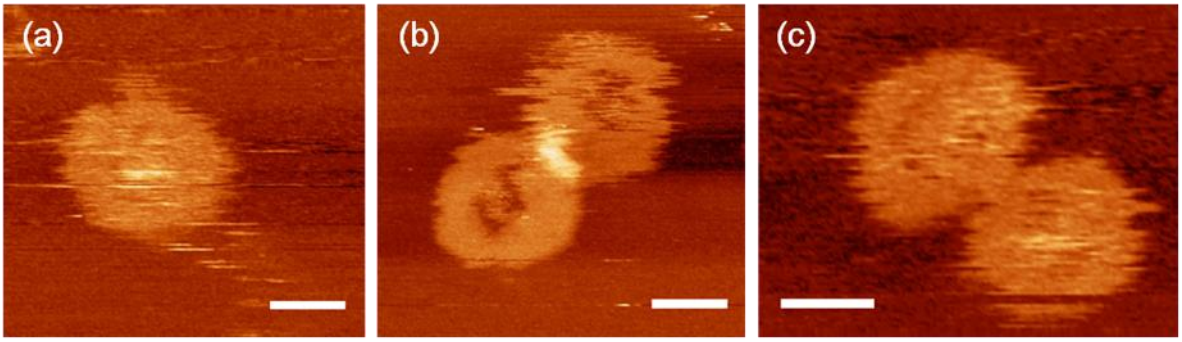

Figure 5.27 AFM zoomed images of the DNA origami structures without gold NPs showing the reversibility of the hatch system using S64 target (scale bars: 50 nm). The origami is closed subsequently to (a) no target addition, (b) open after S64 addition and (c) re-closed after C64 addition.

At this point I used the 20 nm gold NP functionalized with the staple strands able to link the scaffold in specific points of the DNA origami hatch. I incubated overnight the two parts with a specific ratio of 2-3 NP per binding site on the origami. This time is needed to allow a good interaction between the DNA strands. The presence of hybridized AuNPs on the DNA origami was confirmed by gel electrophoresis. Both visible (for AuNP) and UV (for DNA stained with GelRed™) images of the same gel were taken and the band positions were compared. In this way I was able to uniquely associate a band corresponding to AuNP decorated DNA-origami (Figure 5.28). The UV image relative to DNA staining is aligned to the white light image where the contrast is provided by the gold NP plasmonic absorption.

The first and second wells were filled with the scaffold sequence (M13mp18) and the DNA origami respectively, which show a signal only in the UV section, since there are no AuNP to provide a contrast in the visible absorbance region. The correctly folded DNA origami migrates slower than the linear scaffold (Figure 5.28, lane 2) and it is used as reference for the other lanes. The DNA origami incubated with NPs is included in all of the remaining lanes (Figure 5.28, lanes 3-6), which differ only in target sequence. In detail, the lane 3 is used as a control and no DNA target is added, while the targets C120, L84 and S64 are added to lanes 4, 5 and 6, respectively. The targets are usually mixed in excess (2 μL of 8 μM), to induce complete hybridization to DNA origami, and the unbound DNA oligonucleotides, which migrate faster in gel, form broad downstream bands visible only in the UV images. In the case of C120 target, the excess DNA moves slightly slower within gel due to the longer sequence (Figure 5.28, lane 4).

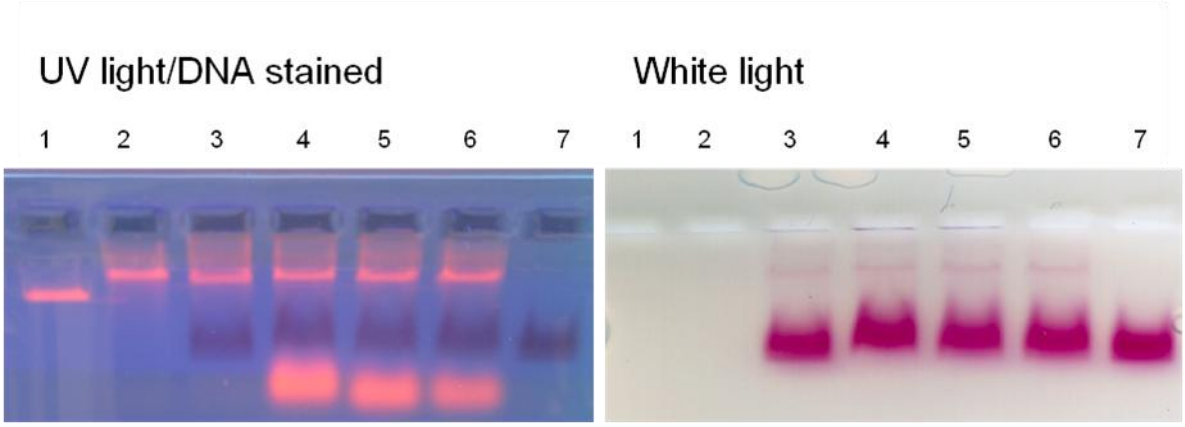

Figure 5.28 UV fluorescence (left section) and white light (right section) images of electrophoretic migration of DNA with and without AuNP. Lane 1: M13mp18 (scaffold) DNA control. Lane 2: DNA origami with no AuNP functionalization. Lane 3-6: DNA origami functionalized with nanoparticles and hybridized to: no target (control, lane 3), target C120 (lane 4), target L84 (lane 5) and target S64 (lane 6). A light red-colored band in white light picture indicates the linking between nanoparticles and DNA origami. The presence of the target strand excess is highlighted by the bottom intense DNA band in lines 4-6; while the specificity of the origami-NP linking is assured by the absence of red NP band when no origami is added (line 7).

The match between the DNA origami band and a light red-colored band obtained under white light indicates the linking between NPs and DNA origami. The excess of unbound NPs can be observed as the broad red band in all the lanes and is negative upon DNA staining. I observed no difference in the bands position between the control and the three DNA target-actuated constructs. The structural differences induced by the target hybridization are not large enough to produce an appreciable electrophoretic migration delay. A few weak, slowly moving bands can be observed that are attributed to the formation of DNA origami superstructures (dimers,

tetramers, etc.) as it was also confirmed by AFM and SEM characterization (Figure 5.26 and 5.30). As evidence of the specificity of the bonding there the red slightly NP band is not present when no origami is added (Figure 5.28, line 7)[60].

I recorded the extinction spectra for each structure directly on the separated gel bands to minimize cross band contamination, gel extraction induced damage, and complex re-concentration procedures. I displayed the raw spectra in Figure 5.29 together with the extinction spectra of DNA coated gold NPs in gel and water. We have to note that NPs in gel form highly packed aggregates and this, together with higher dielectric permittivity of gel, results in significant red shift of LSPR peak and its broadening due to a plasmon coupling effect in respect to origami with gold NPs[55].

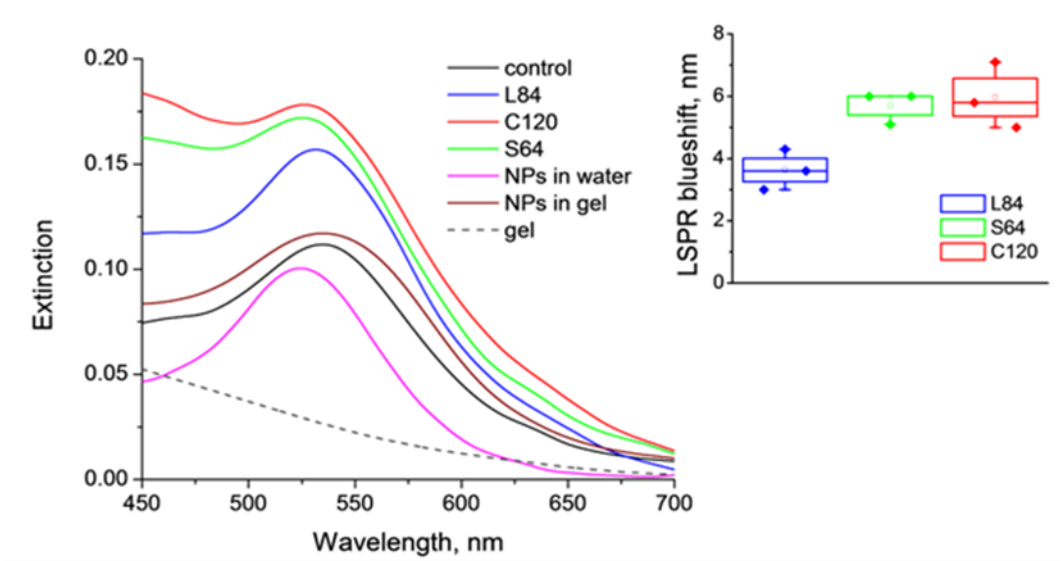

Figure 5.29 Raw UV-Vis extinction spectra from the origami bands described in Figure 5.23: a blue shift is visible for all the targets in respect to the control. In the inset the box plots of the three targets relative shifts repeated three times are reported. The LSPR positions were determined after fitting procedure described.

All the three targets induced a blue shift and a narrowing of the spectra with respect to the control, however the spectra differ significantly in the background contribution, which I attributed to gel thickness variability. I replicated the experiments 3 times with different origami synthesis. I consistently observed an LSPR blue shift although absolute values were slightly different. To discard the background contribution and compare the results of different experiments I applied the fitting procedure described in details in chapter 4. The C120 and S64 target sequences produce a relative blue shift of ~6 nm, while the L84 target provided only ~4 nm (Figure 5.29, inset). The relative shift depends only on the NP separation controlled by the addition of the three targets, since all the other contributions, namely gel density, gel hydration and NP size[55], are common to all experiments. The large shift provided

by S64 and C120 is consistent with the competitors design, and in particular with the reduced length of the S64 sequence and the hairpin structure of the C120 in contrast with the full linear structure of the L84 target[85]. Since the probe sequences can be arbitrary varied, the plasmonic resonance can be tuned continuously from the fully closed to the fully opened configuration: three points along this range are exemplified here. The measurement of the plasmon resonance shift can be used to deduce the actual opening angle for each configuration.

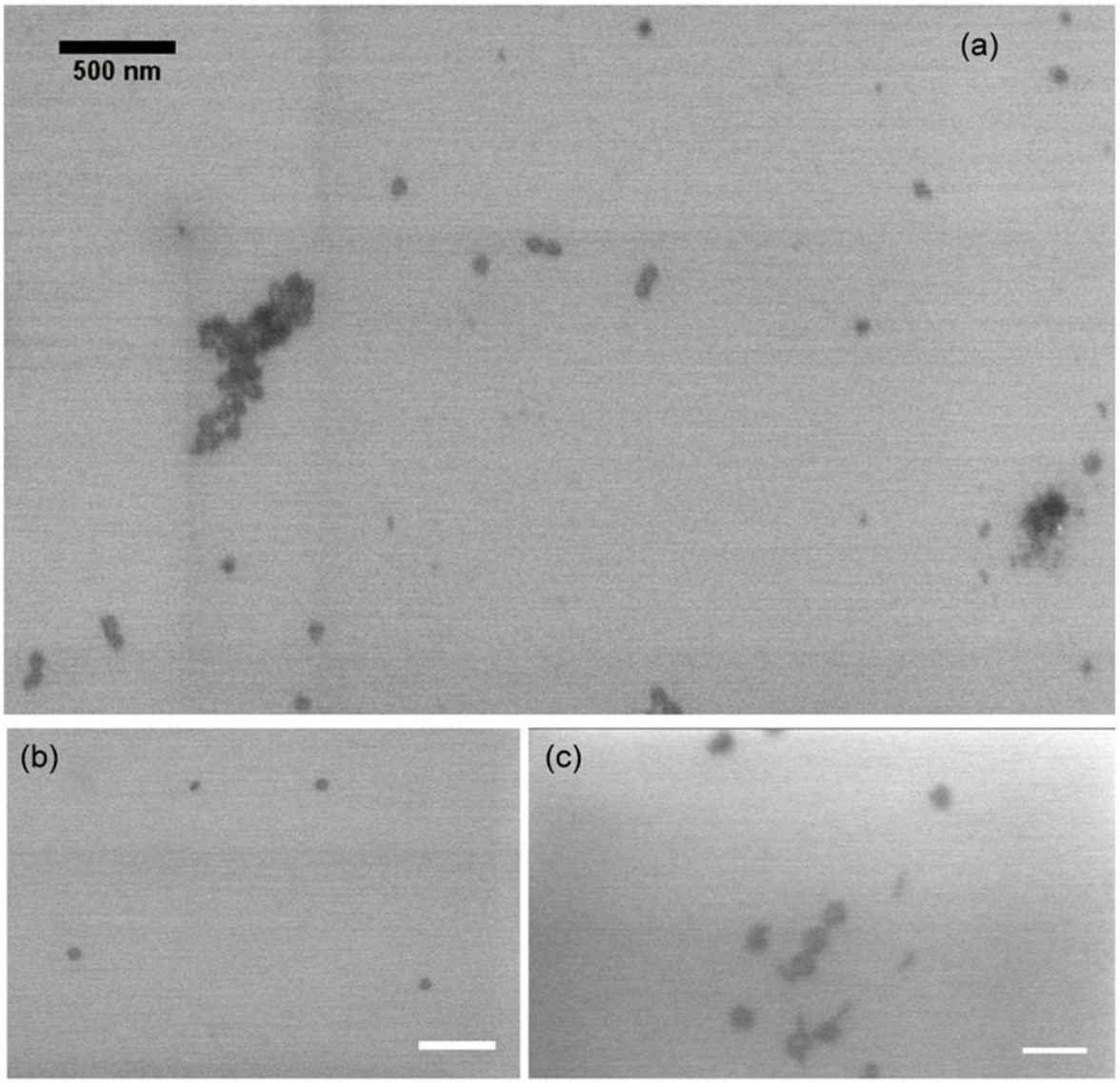

Figure 5.30 Asymmetric open hatch DNA origami imaged by SEM. Dimerization is visible like in the AFM characterization.

Moreover, I confirmed the presence of two gold NP on the origami with characterization by SEM on the sample extracted from the bands of Figure 5.28 gel experiment. In particular, I analyzed firstly the DNA origami hatch without NP to compare it as control (Figure 5.30),

and then I analyzed the DNA origami with NP on top to check the efficiency and architecture of the NP linking (Figure 5.31)[60].

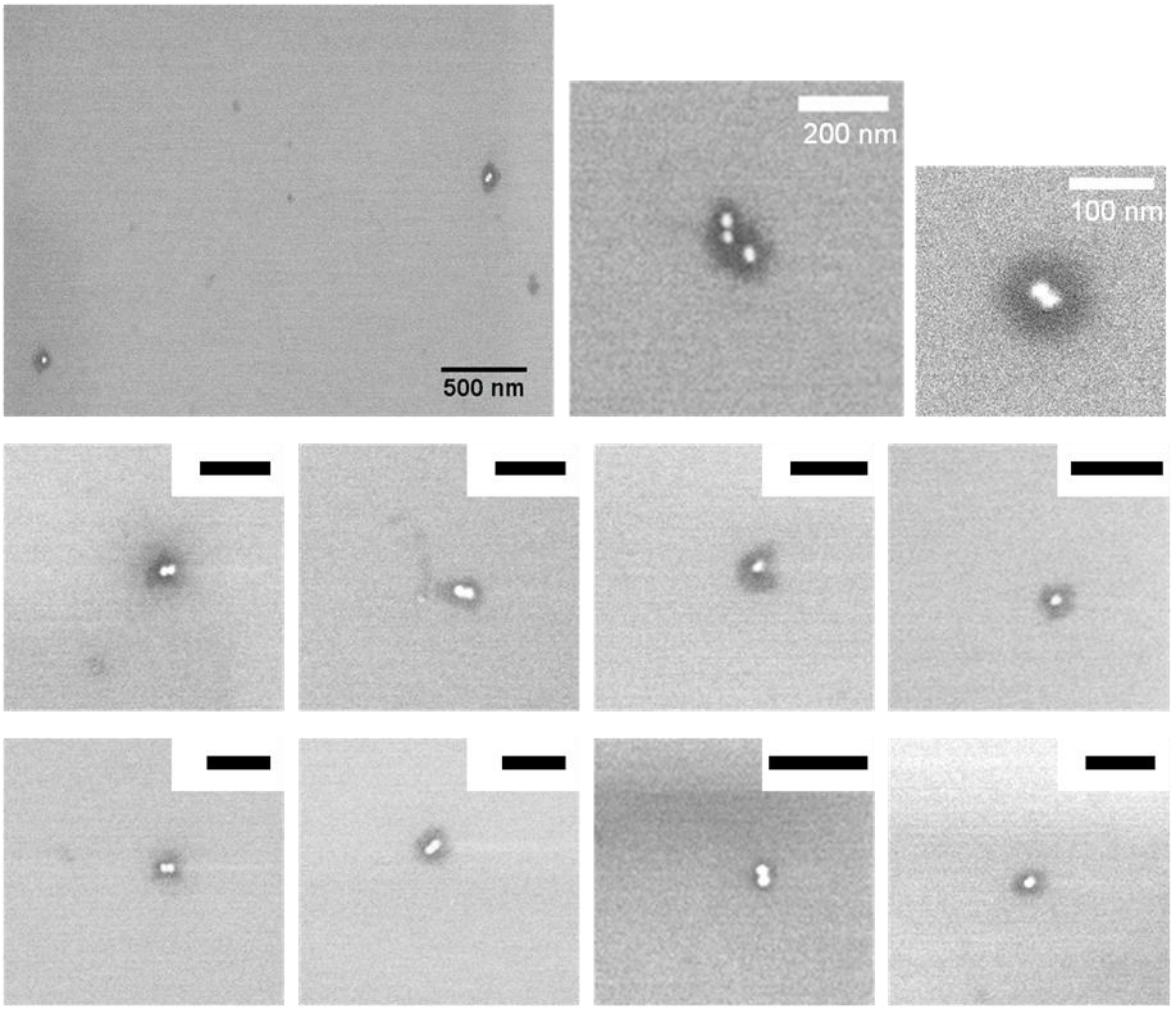

Figure 5.31 SEM images of the DNA origami with nanoparticles extracted from the gel band. There are both single both double nanoparticles placed on the DNA disc structures (200 nm black scale bars).

Afterwards, I investigated the reversibility of the LSPR tuning by UV-Vis spectroscopy after decorating the origami with the AuNP. To this purpose, following the same procedure that I used to demonstrate the reversibility of the asymmetric open with S64 target (described above) I incubated the origami+NP hybrid structure with S64 target and then with the competitor C64 in excess. Then, I analyzed these sample with agarose gel analysis to let forming the bands of specific linking. Finally I recorded the raw spectra directly from the gel bands of before and after addition the S64 target, and then after addition of the C64 competitor and the results are displayed in Figure 5.32. The target induces a blue shift of 4 nm; the addition of the competitor reduces - but do not cancel - the shift to 2 nm. This only

partial flap re-closure with respect to situation observed by AFM imaging could be originated by a modification of the origami mechanical properties due to the AuNP-induced mass and surface increase.

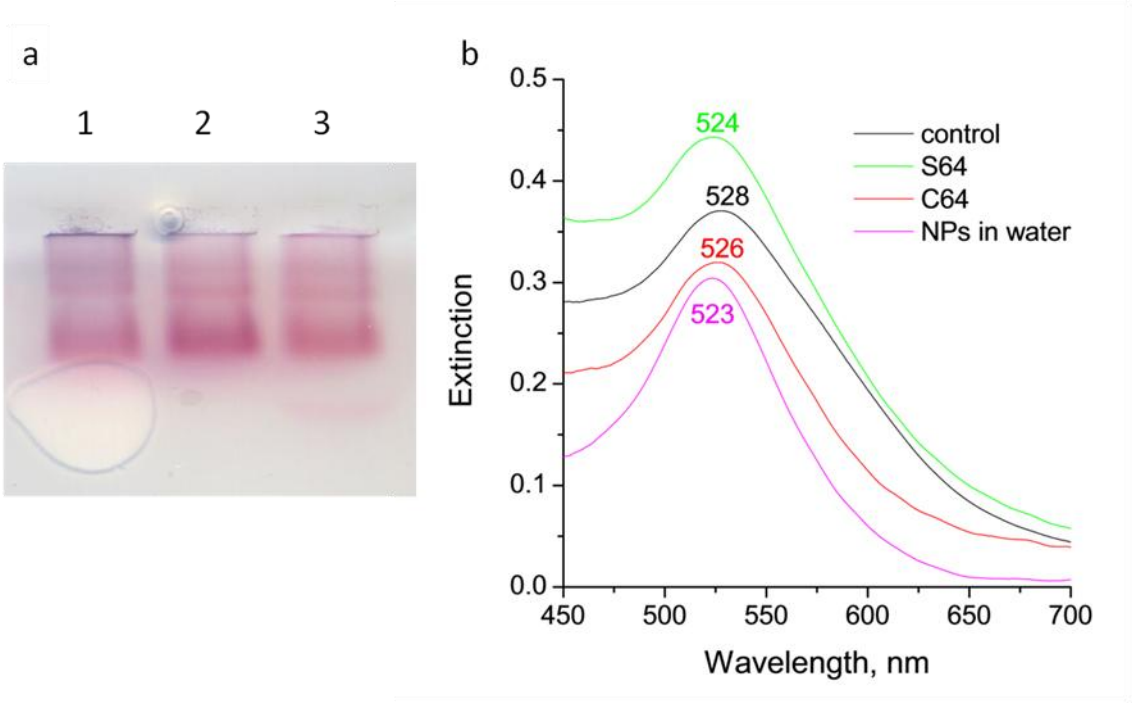

Figure 5.32 (a) Agarose gel analysis of the reversibility of the asymmetric hatch origami with NP. The origami+NP is incubated with no target (line 1), with S64 target (line 2) and with S64+C64 (line 3). There are no appreciable differences in the gel but from the correspondent raw spectra (b) is visible that the blue shift of 4 nm provided by the S64 target is then, reduce - but do not cancelled - to 2 nm by the addition of the competitor.

Chapter 6

Conclusions and future perspectives

In my PhD three years project, I performed successful experiments focused mainly on the DNA nanotechnology as a tool for nano-bio-objects construction and gold particles functionalization. Progressively, I combined the LSPR properties of gold particles with DNA origami structure in order to create hybrid systems. This combination has allowed me to open up innovative architectural features for plasmon resonance tuning with the perspective to use them as starting point for bio-detection.

I developed a protocol for the formation of gold nanoparticles dimer, as plasmonic hot spots, with the highest efficiency so far reported in literature. Using DNA hybridization technology to create well functionalized nanoparticles, I produced stable and discrete mono-di-trimer nanoaggregates in high electrolyte solution; with short DNA oligonucleotide sequences reaching optimal results also with only 11 nts length. The system was performed both via direct aggregation, both via post-process disaggregation of the functionalized gold nanoparticles. Through the disaggregation method I set up a reproducible and controlled protocol that allowed me to understand the aggregates formation trend in a passivation self assembly process, reaching the maximum NP dimer yield (26.5%) reported in literature. This novel approach may open possibility to have a controlled NP dimer production also with very short nucleotides DNA sequence and thus, with really short inter-particles distance. This last condition could lead to improvements in the creation of plasmon/optical detection nano-mechanical devices. Thus, regarding my project purposes, this was a fundamental intermediate milestone in the way to the creation of more complex plasmonic architectures.

Studying and developing DNA origami actuation systems I was able to combine them with functionalized gold nanoparticles. In this way, I exploited DNA origami architecture to tune the plasmon resonance between two gold nanospheres. The particular actuation mechanism design has allowed me to produce a continuous, or analog, tuning of the interparticles distance in aqueous solution. The resulting resonance blue shifts and narrowing of LSPR peaks were observed in three different configurations. The actuation mechanism, based on hybridization with ssDNA targets, opens a wide range of possibilities for the fine manipulation of angles and dynamics between nanostructured components, depending on the secondary structure of the DNA filament. The proposed design is suitable to investigate DNA hybridization configurations, or could be used as tunable plasmonic platform for enhanced Raman

applications. Moreover, using the inter-particles distance and plasmon resonance dependence a sort of plasmon ruler can be achieved as precise investigation tool for molecular conformational studies.

In future, I will optimize the Dark field UV-VIS spectroscopy to overcome the present limitation and measure the plasmon resonance shift directly in solution and on individual nanoparticles. In this way, the AuNP size broadening will be no longer an issue, several different actuator will be tested on the very same DNA origami structure and the reproducibility will reach the high level requested in a biosensor production. Additionally using liquid phase the handling and the implementation of the sample in a detection automatic system will provide faster measurement. The DNA origami platform can will be also used to immobilize the gold nanoparticles in fixed positions and known distances in order to provide a proper calibration to the LSPR shifts (which indeed are influenced also by the presence of the origami, so that the available AuNp-DNA-AuNP dimer measurements cannot be used to this purpose) and thus, interpret properly the plasmonic shift induced by DNA origami actuation for different actuators architecture.

Finally single particle Cryo-TEM imaging will be performed at the Molecular Foundry in Berkeley, through an approved user project, to investigate the thermal fluctuations and the thermodynamic distribution of the DNA origami configuration depending on the different actuator architecture.

References

1 J. A. Alberts B., Lewis J., Raff M., Reberts K., and Walter P., *Molecular Biology of the Cell*, Garland Science, 2008.

2 S. Neidle, **Principles of Nucleic Acid Structure**, Academic Press, 2007.

3 Y. Zhang and N. C. Seeman, **Construction of a DNA-Truncated Octahedron**, *J. Am. Chem. Soc.*, 1994, **116**, 1661-1669.

4 Y. Li, Y. D. Tseng, S. Y. Kwon, L. d'Espaux, J. S. Bunch, P. L. McEuen and D. Luo, **Controlled assembly of dendrimer-like DNA**, *Nat Mater*, 2004, **3**, 38-42.

5 R. Holliday, **Induced mitotic crossing-over in relation to genetic replication in synchronously dividing cells of Ustilago maydis**, *Genetics Research*, 1965, **6**, 104-120.

6 J. H. Chen, N. R. Kallenbach and N. C. Seeman, **A specific quadrilateral synthesized from DNA branched junctions**, *J. Am. Chem. Soc.*, 1989, **111**, 6402-6407.

7 J. Chen and N. C. Seeman, **Synthesis from DNA of a molecule with the connectivity of a cube**, *Nature*, 1991, **350**, 631-633.

8 C. S. Nadrian, W. Hui, Y. Xiaoping, L. Furong, M. Chengde, S. Weiqiong, W. Lisa, S. Zhiyong, S. Ruojie, Y. Hao, W. Man Hoi, S.-A. Phiset, L. Bing, Q. Hangxia, L. Xiaojun, Q. Jing, D. Shou Ming, Z. Yuwen, E. M. John, F. Tsu-Ju, W. Yinli and C. Junghuei, **New motifs in DNA nanotechnology**, *Nanotechnology*, 1998, **9**, 257.

9 X. Li, X. Yang, J. Qi and N. C. Seeman, **Antiparallel DNA Double Crossover Molecules As Components for Nanoconstruction**, *J. Am. Chem. Soc.*, 1996, **118**, 6131-6140.

10 T. H. LaBean, H. Yan, J. Kopatsch, F. Liu, E. Winfree, J. H. Reif and N. C. Seeman, **Construction, Analysis, Ligation, and Self-Assembly of DNA Triple Crossover Complexes**, *J. Am. Chem. Soc.*, 2000, **122**, 1848-1860.

11 S. H. Park, C. Pistol, S. J. Ahn, J. H. Reif, A. R. Lebeck, C. Dwyer and T. H. LaBean, **Finite-Size, Fully Addressable DNA Tile Lattices Formed by Hierarchical Assembly Procedures**, *Angew. Chem. Int. Ed.*, 2006, **45**, 735-739.

12 K. Lund, Y. Liu, S. Lindsay and H. Yan, **Self-Assembling a Molecular Pegboard**, *J. Am. Chem. Soc.*, 2005, **127**, 17606-17607.

13 Y. Liu, Y. Ke and H. Yan, **Self-Assembly of Symmetric Finite-Size DNA Nanoarrays**, *J. Am. Chem. Soc.*, 2005, **127**, 17140-17141.

14 P. W. Rothemund, **Folding DNA to create nanoscale shapes and patterns**, *Nature*, 2006, **440**, 297-302.

15 A. Kuzuya and M. Komiyama, **DNA origami: fold, stick, and beyond**, *Nanoscale*, 2010, **2**, 310-322.

16 Y. Ke, S. M. Douglas, M. Liu, J. Sharma, A. Cheng, A. Leung, Y. Liu, W. M. Shih and H. Yan, **Multilayer DNA origami packed on a square lattice**, *J. Am. Chem. Soc.*, 2009, **131**, 15903-15908.

17 H. Dietz, S. M. Douglas and W. M. Shih, **Folding DNA into twisted and curved nanoscale shapes**, *Science*, 2009, **325**, 725-730.

18 S. M. Douglas, H. Dietz, T. Liedl, B. Hogberg, F. Graf and W. M. Shih, **Self-assembly of DNA into nanoscale three-dimensional shapes**, *Nature*, 2009, **459**, 414-418.

19 D. Han, S. Pal, J. Nangreave, Z. Deng, Y. Liu and H. Yan, **DNA origami with complex curvatures in three-dimensional space**, *Science*, 2011, **332**, 342-346.
20 Y. Ke, S. Lindsay, Y. Chang, Y. Liu and H. Yan, **Self-assembled water-soluble nucleic acid probe tiles for label-free RNA hybridization assays**, *Science*, 2008, **319**, 180-183.
21 R. Chhabra, J. Sharma, Y. Ke, Y. Liu, S. Rinker, S. Lindsay and H. Yan, **Spatially addressable multiprotein nanoarrays templated by aptamer-tagged DNA nanoarchitectures**, *J. Am. Chem. Soc.*, 2007, **129**, 10304-10305.
22 R. P. Goodman, C. M. Erben, J. Malo, W. M. Ho, M. L. McKee, A. N. Kapanidis and A. J. Turberfield, **A facile method for reversibly linking a recombinant protein to DNA**, *ChemBioChem*, 2009, **10**, 1551-1557.
23 W. Shen, H. Zhong, D. Neff and M. L. Norton, **NTA directed protein nanopatterning on DNA Origami nanoconstructs**, *J. Am. Chem. Soc.*, 2009, **131**, 6660-6661.
24 Y. He, Y. Tian, A. E. Ribbe and C. Mao, **Antibody Nanoarrays with a Pitch of ~20 Nanometers**, *J. Am. Chem. Soc.*, 2006, **128**, 12664-12665.
25 B. A. R. Williams, K. Lund, Y. Liu, H. Yan and J. C. Chaput, **Self-Assembled Peptide Nanoarrays: An Approach to Studying Protein–Protein Interactions**, *Angew. Chem. Int. Ed.*, 2007, **46**, 3051-3054.
26 B. Sacca, R. Meyer, M. Erkelenz, K. Kiko, A. Arndt, H. Schroeder, K. S. Rabe and C. M. Niemeyer, **Orthogonal protein decoration of DNA origami**, *Angew. Chem. Int. Ed. Engl.*, 2010, **49**, 9378-9383.
27 A. Kuzuya, M. Kimura, K. Numajiri, N. Koshi, T. Ohnishi, F. Okada and M. Komiyama, **Precisely programmed and robust 2D streptavidin nanoarrays by using periodical nanometer-scale wells embedded in DNA origami assembly**, *ChemBioChem*, 2009, **10**, 1811-1815.
28 N. V. Voigt, T. Torring, A. Rotaru, M. F. Jacobsen, J. B. Ravnsbaek, R. Subramani, W. Mamdouh, J. Kjems, A. Mokhir, F. Besenbacher and K. V. Gothelf, **Single-molecule chemical reactions on DNA origami**, *Nat. Nanotechnol.*, 2010, **5**, 200-203.
29 A. Kuzyk, B. Yurke, J. J. Toppari, V. Linko and P. Torma, **Dielectrophoretic trapping of DNA origami**, *Small*, 2008, **4**, 447-450.
30 A. E. Gerdon, S. S. Oh, K. Hsieh, Y. Ke, H. Yan and H. T. Soh, **Controlled delivery of DNA origami on patterned surfaces**, *Small*, 2009, **5**, 1942-1946.
31 R. J. Kershner, L. D. Bozano, C. M. Micheel, A. M. Hung, A. R. Fornof, J. N. Cha, C. T. Rettner, M. Bersani, J. Frommer, P. W. Rothemund and G. M. Wallraff, **Placement and orientation of individual DNA shapes on lithographically patterned surfaces**, *Nat. Nanotechnol.*, 2009, **4**, 557-561.
32 Y. Xue, X. Li, H. Li and W. Zhang, **Quantifying thiol–gold interactions towards the efficient strength control**, *Nat. Commun.*, 2014, **5**.
33 J. Sharma, R. Chhabra, C. S. Andersen, K. V. Gothelf, H. Yan and Y. Liu, **Toward reliable gold nanoparticle patterning on self-assembled DNA nanoscaffold**, *J. Am. Chem. Soc.*, 2008, **130**, 7820-7821.
34 Z. Zhao, E. L. Jacovetty, Y. Liu and H. Yan, **Encapsulation of Gold Nanoparticles in a DNA Origami Cage**, *Angew. Chem. Int. Ed.*, 2011, **50**, 2041-2044.
35 B. Ding, Z. Deng, H. Yan, S. Cabrini, R. N. Zuckermann and J. Bokor, **Gold nanoparticle self-similar chain structure organized by DNA origami**, *J. Am. Chem. Soc.*, 2010, **132**, 3248-3249.
36 S. Pal, Z. Deng, B. Ding, H. Yan and Y. Liu, **DNA-Origami-Directed Self-Assembly of Discrete Silver-Nanoparticle Architectures**, *Angew. Chem. Int. Ed.*, 2010, **49**, 2700-2704.

37 S. Pal, Z. Deng, H. Wang, S. Zou, Y. Liu and H. Yan, **DNA Directed Self-Assembly of Anisotropic Plasmonic Nanostructures**, *J. Am. Chem. Soc.*, 2011, **133**, 17606-17609.
38 Z.-G. Wang, C. Song and B. Ding, **Functional DNA Nanostructures for Photonic and Biomedical Applications**, *Small*, 2013, **9**, 2210-2222.
39 G. P. Acuna, F. M. Moller, P. Holzmeister, S. Beater, B. Lalkens and P. Tinnefeld, **Fluorescence enhancement at docking sites of DNA-directed self-assembled nanoantennas**, *Science*, 2012, **338**, 506-510.
40 V. V. Thacker, L. O. Herrmann, D. O. Sigle, T. Zhang, T. Liedl, J. J. Baumberg and U. F. Keyser, **DNA origami based assembly of gold nanoparticle dimers for surface-enhanced Raman scattering**, *Nat. Commun.*, 2014, **5**.
41 C. Noguez and I. L. Garzon, **Optically active metal nanoparticles**, *Chem. Soc. Rev.*, 2009, **38**, 757-771.
42 X. Shen, A. Asenjo-Garcia, Q. Liu, Q. Jiang, F. J. Garcia de Abajo, N. Liu and B. Ding, **Three-dimensional plasmonic chiral tetramers assembled by DNA origami**, *Nano Lett*, 2013, **13**, 2128-2133.
43 X. Shen, C. Song, J. Wang, D. Shi, Z. Wang, N. Liu and B. Ding, **Rolling up gold nanoparticle-dressed DNA origami into three-dimensional plasmonic chiral nanostructures**, *J. Am. Chem. Soc.*, 2012, **134**, 146-149.
44 A. Kuzyk, R. Schreiber, Z. Fan, G. Pardatscher, E. M. Roller, A. Hogele, F. C. Simmel, A. O. Govorov and T. Liedl, **DNA-based self-assembly of chiral plasmonic nanostructures with tailored optical response**, *Nature*, 2012, **483**, 311-314.
45 E. S. Andersen, M. Dong, M. M. Nielsen, K. Jahn, A. Lind-Thomsen, W. Mamdouh, K. V. Gothelf, F. Besenbacher and J. Kjems, **DNA origami design of dolphin-shaped structures with flexible tails**, *ACS Nano*, 2008, **2**, 1213-1218.
46 E. S. Andersen, M. Dong, M. M. Nielsen, K. Jahn, R. Subramani, W. Mamdouh, M. M. Golas, B. Sander, H. Stark, C. L. Oliveira, J. S. Pedersen, V. Birkedal, F. Besenbacher, K. V. Gothelf and J. Kjems, **Self-assembly of a nanoscale DNA box with a controllable lid**, *Nature*, 2009, **459**, 73-76.
47 R. M. Zadegan, M. D. E. Jepsen, K. E. Thomsen, A. H. Okholm, D. H. Schaffert, E. S. Andersen, V. Birkedal and J. Kjems, **Construction of a 4 Zeptoliters Switchable 3D DNA Box Origami**, *ACS Nano*, 2012, **6**, 10050-10053.
48 A. Kuzuya, Y. Sakai, T. Yamazaki, Y. Xu and M. Komiyama, **Nanomechanical DNA origami 'single-molecule beacons' directly imaged by atomic force microscopy**, *Nat. Commun.*, 2011, **2**, 449.
49 M. Endo, R. Miyazaki, T. Emura, K. Hidaka and H. Sugiyama, **Transcription Regulation System Mediated by Mechanical Operation of a DNA Nanostructure**, *J. Am. Chem. Soc.*, 2012, **134**, 2852-2855.
50 S. M. Douglas, I. Bachelet and G. M. Church, **A logic-gated nanorobot for targeted transport of molecular payloads**, *Science*, 2012, **335**, 831-834.
51 H. Gu, J. Chao, S. J. Xiao and N. C. Seeman, **A proximity-based programmable DNA nanoscale assembly line**, *Nature*, 2010, **465**, 202-205.
52 Z. Zhang, E. M. Olsen, M. Kryger, N. V. Voigt, T. Tørring, E. Gültekin, M. Nielsen, R. M. Zadegan, E. S. Andersen, M. M. Nielsen, J. Kjems, V. Birkedal and K. V. Gothelf, **A DNA Tile Actuator with Eleven Discrete States**, *Angew. Chem. Int. Ed.*, 2011, **50**, 3983-3987.
53 M. Marini, L. Piantanida, R. Musetti, A. Bek, M. Dong, F. Besenbacher, M. Lazzarino and G. Firrao, **A revertible, autonomous, self-assembled DNA-origami nanoactuator**, *Nano Lett.*, 2011, **11**, 5449-5454.

54 Y. Sun, H. Wallrabe, S.-A. Seo and A. Periasamy, **FRET Microscopy in 2010: The Legacy of Theodor Förster on the 100th Anniversary of his Birth**, *Chemphyschem*, 2011, **12**, 462-474.
55 N. J. Halas, S. Lal, W. S. Chang, S. Link and P. Nordlander, **Plasmons in strongly coupled metallic nanostructures**, *Chem. Rev.*, 2011, **111**, 3913-3961.
56 P. Kühler, E.-M. Roller, R. Schreiber, T. Liedl, T. Lohmüller and J. Feldmann, **Plasmonic DNA-Origami Nanoantennas for Surface-Enhanced Raman Spectroscopy**, *Nano Lett.*, 2014, **14**, 2914-2919.
57 E. S. Andersen, *http://cdna.au.dk/software*.
58 M. Bathe, *http://cando-dna-origami.org/*.
59 S. D. Mark Bathe, *http://cadnano.org/*.
60 L. Piantanida, D. Naumenko, E. Torelli, M. Marini, D. M. Bauer, L. Fruk, G. Firrao and M. Lazzarino, **Plasmon Resonance Tuning Using DNA Origami Actuation**, *Chem. Commun.*, 2015.
61 J. Turkevich, P. C. Stevenson and J. Hillier, **The Formation of Colloidal Gold**, *J. Phys. Chem.*, 1953, **57**, 670-673.
62 D. Zanchet, C. M. Micheel, W. J. Parak, D. Gerion and A. P. Alivisatos, **Electrophoretic Isolation of Discrete Au Nanocrystal/DNA Conjugates**, *Nano Lett.*, 2000, **1**, 32-35.
63 B. M. Reinhard, M. Siu, H. Agarwal, A. P. Alivisatos and J. Liphardt, **Calibration of dynamic molecular rulers based on plasmon coupling between gold nanoparticles**, *Nano Lett.*, 2005, **5**, 2246-2252.
64 D. G. Thompson, R. J. Stokes, R. W. Martin, P. J. Lundahl, K. Faulds and D. Graham, **Synthesis of unique nanostructures with novel optical properties using oligonucleotide mixed-metal nanoparticle conjugates**, *Small*, 2008, **4**, 1054-1057.
65 L. Piantanida, D. Naumenko and M. Lazzarino, **Highly efficient gold nanoparticle dimer formation via DNA hybridization**, *RSC Advances*, 2014, **4**, 15281-15287.
66 X. Ye, L. Jin, H. Caglayan, J. Chen, G. Xing, C. Zheng, V. Doan-Nguyen, Y. Kang, N. Engheta, C. R. Kagan and C. B. Murray, **Improved size-tunable synthesis of monodisperse gold nanorods through the use of aromatic additives**, *ACS Nano*, 2012, **6**, 2804-2817.
67 D. Shi, C. Song, Q. Jiang, Z.-G. Wang and B. Ding, **A facile and efficient method to modify gold nanorods with thiolated DNA at a low pH value**, *Chem. Commun.*, 2013, **49**, 2533-2535.
68 G. Chen, Y. Wang, L. H. Tan, M. Yang, L. S. Tan, Y. Chen and H. Chen, **High-purity separation of gold nanoparticle dimers and trimers**, *J. Am. Chem. Soc.*, 2009, **131**, 4218-4219.
69 D. Liu, C. Li, F. Zhou, T. Zhang, H. Zhang, X. Li, G. Duan, W. Cai and Y. Li, **Rapid Synthesis of Monodisperse Au Nanospheres through a Laser Irradiation - Induced Shape Conversion, Self-Assembly and Their Electromagnetic Coupling SERS Enhancement**, *Sci Rep*, 2015, **5**, 7686.
70 J. Kimling, M. Maier, B. Okenve, V. Kotaidis, H. Ballot and A. Plech, **Turkevich method for gold nanoparticle synthesis revisited**, *J Phys Chem B*, 2006, **110**, 15700-15707.
71 L. Piantanida, *Visiting Researcher Scholarship from the Karlsruhe House of Young Scientists (KHYS) for 3 months.*, 2014.
72 H. Kim, R. P. Carney, J. Reguera, Q. K. Ong, X. Liu and F. Stellacci, **Synthesis and Characterization of Janus Gold Nanoparticles**, *Adv. Mater.*, 2012, **24**, 3857-3863.

73 P. Parisse, A. Vindigni, G. Scoles and L. Casalis, **In Vitro Enzyme Comparative Kinetics: Unwinding of Surface-Bound DNA Nanostructures by RecQ and RecQ1**, *The Journal of Physical Chemistry Letters*, 2012, **3**, 3532-3537.
74 S. Bidault, **Water-Based Assembly and Purification of Plasmon-Coupled Gold Nanoparticle Dimers and Trimers**, *International Journal of Optics*, 2012, **2012**.
75 S. Bidault, F. J. García de Abajo and A. Polman, **Plasmon-Based Nanolenses Assembled on a Well-Defined DNA Template**, *J. Am. Chem. Soc.*, 2008, **130**, 2750-2751.
76 M. P. Busson, B. Rolly, B. Stout, N. Bonod, E. Larquet, A. Polman and S. Bidault, **Optical and Topological Characterization of Gold Nanoparticle Dimers Linked by a Single DNA Double Strand**, *Nano Lett.*, 2011, **11**, 5060-5065.
77 L. Guerrini and D. Graham, **Molecularly-mediated assemblies of plasmonic nanoparticles for Surface-Enhanced Raman Spectroscopy applications**, *Chem. Soc. Rev.*, 2012, **41**, 7085-7107.
78 F. J. García de Abajo, **Multiple scattering of radiation in clusters of dielectrics**, *Phys. Rev. B*, 1999, **60**, 6086-6102.
79 V. Myroshnychenko, J. Rodriguez-Fernandez, I. Pastoriza-Santos, A. M. Funston, C. Novo, P. Mulvaney, L. M. Liz-Marzan and F. J. Garcia de Abajo, **Modelling the optical response of gold nanoparticles**, *Chem. Soc. Rev.*, 2008, **37**, 1792-1805.
80 J. Ambia-Garrido, A. Vainrub and B. M. Pettitt, **A model for structure and thermodynamics of ssDNA and dsDNA near a surface: A coarse grained approach**, *Comput. Phys. Commun.*, 2010, **181**, 2001-2007.
81 T. J. Yim, Y. Wang and X. Zhang, **Synthesis of a gold nanoparticle dimer plasmonic resonator through two-phase-mediated functionalization**, *Nanotechnology*, 2008, **19**, 435605.
82 E. Torelli, M. Marini, S. Palmano, L. Piantanida, C. Polano, A. Scarpellini, M. Lazzarino and G. Firrao, **A DNA origami nanorobot controlled by nucleic acid hybridization**, *Small*, 2014, **10**, 2918-2926.
83 B. Sander and M. M. Golas, **Visualization of bionanostructures using transmission electron microscopical techniques**, *Microsc. Res. Tech.*, 2011, **74**, 642-663.
84 P. Travascio, Y. Li and D. Sen, **DNA-enhanced peroxidase activity of a DNA-aptamer-hemin complex**, *Chem. Biol.*, 1998, **5**, 505-517.
85 R. Vafabakhsh and T. Ha, **Extreme bendability of DNA less than 100 base pairs long revealed by single-molecule cyclization**, *Science*, 2012, **337**, 1097-1101.